

# MACROEVOLUTIONARY DYNAMICS AND DIVERSITY OF COCCOLITHOPHORES ACROSS LONG-TERM COOLING PERIODS OF THE CENOZOIC

by

AMY P. JONES

A thesis submitted to the University of Birmingham for the degree of  
DOCTOR OF PHILOSOPHY

School of Geography, Earth and Environmental Sciences

College of Life and Environmental Sciences

University of Birmingham

June 2021

UNIVERSITY OF  
BIRMINGHAM

**University of Birmingham Research Archive**

**e-theses repository**

This unpublished thesis/dissertation is copyright of the author and/or third parties. The intellectual property rights of the author or third parties in respect of this work are as defined by The Copyright Designs and Patents Act 1988 or as modified by any successor legislation.

Any use made of information contained in this thesis/dissertation must be in accordance with that legislation and must be properly acknowledged. Further distribution or reproduction in any format is prohibited without the permission of the copyright holder.

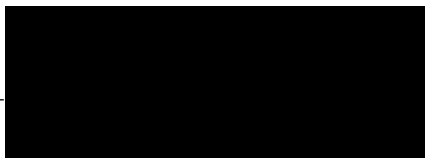


## Declaration of Authorship

I, Amy P. Jones, declare that this thesis titled, ‘Macroevolutionary dynamics and diversity of coccolithophores across long-term cooling periods of the Cenozoic.’ and the work presented in it are my own. I confirm that:

- This work was done wholly or mainly while in candidature for a research degree at this University.
- Where any part of this thesis has previously been submitted for a degree or any other qualification at this University or any other institution, this has been clearly stated.
- Where I have quoted from the work of others, the source is always given. With the exception of such quotations, this thesis is entirely my own work.
- I have acknowledged all main sources of help.
- Where the thesis is based on work done by myself jointly with others, I have made clear exactly what was done by others and what I have contributed myself.

Signed:

A black rectangular box redacting the signature of the author.

Date: 29/10/2021

# Abstract

This thesis addresses the macroevolution of coccolithophores during two significant cooling periods of the Cenozoic: the Eocene-Oligocene Transition (EOT) and the Neogene to Recent. New onshore low-latitude site NKK1, from the Indo-Pacific Warm Pool (IPWP) in the Indian Ocean, documents high-resolution calcareous nannofossil assemblage responses during the EOT. Data from NKK1 consists of detailed high-resolution species relative abundance records documenting the late middle Eocene to early Oligocene, with well-preserved nannofossils. Research on tropical calcareous nannofossil assemblages through the EOT where sediments yield good recovery and well-preserved coccoliths, is uncommon and so NKK1 presents valuable new palaeoceanographic, palaeoecological, palaeoclimatic and biostratigraphic data from calcareous nannofossils across the EOT. Through this time interval species diversity declined coincident with the extinction of rosette-shaped discoasters ( $\sim 34.44$  Ma) termed the *Discoaster* extinction event (DEE). This interval, during the early EOT, represents the decline of oligotrophic taxa due to increased nutrient supply from the Southern Ocean; additionally, an abundance decrease is observed in small ( $< 3.5$   $\mu\text{m}$ ) *Reticulofenestra* morphotype cell sizes through the DEE interval – signifying coccolith size was apparently not limited by atmospheric  $\text{CO}_2$ .

Additionally, a combination of two datasets offers a global perspective to assess the macroevolutionary drivers influencing coccolithophore lineages during declining atmospheric  $\text{CO}_2$  through the late Neogene. The first is a compilation of  $\sim 2.5$  Ma time-slice data from ocean sediments recovered at 9 sites across the Atlantic, Indian, Pacific and Southern Ocean basins that spans the last 15 Ma. The second is a high-resolution (200 ka) dataset from Integrated Ocean Drilling Program Expedition 363, Site U1482, where a continuous sedimentary sequence encompassing the crucial late Miocene to early Pleistocene (7.7-1.7 Ma) interval yields a well-preserved, sub-tropical high diversity calcareous nannofossil assemblage. These two records provide supporting evidence that declining  $p\text{CO}_2$  had a significant impact on evo-

---

lution within the Noelaerhabdaceae family with a correlation between atmospheric CO<sub>2</sub> and a decrease in *Reticulofenestra* coccolith size observed since the late Miocene. Through the Plio-Pleistocene however, the rise of small *Gephyrocapsa* spp., an upper euphotic zone species, is correlated with the rise in deep-photic zone dweller, *Florisphaera profunda*, and a modelled deepening of global nutricline depths. On this basis, we suggest that it is not solely  $p\text{CO}_2$  that drives major macroevolutionary turnover in dominance, but that a deepened nutricline exerted as much of a selective pressure as  $p\text{CO}_2$  with potential impacts across multiple lineages including the extinction of *Discoaster* spp., demise in *Reticulofenestra* groups and the modern dominance of *Florisphaera profunda* - *Gephyrocapsa* assemblages.

## An Ode To Fearless Women

*Defined by no man, you are your own story,  
blazing through the world, turning history into herstory.  
And when they dare to tell you about all the things you cannot be,  
you smile and tell them,*

*“I am both war and woman and you cannot stop me”.*

**Nikita Gill**

# Acknowledgements

I owe my deepest thanks to many people for their help and support throughout my PhD journey. Firstly, I am sincerely thankful to my supervisor Tom Dunkley Jones for the opportunity to work on this project and enabling me to continue my passion in nannopalaeontology. I am also grateful for the many insightful conversations, guidance, support, and opportunities Tom has gifted me.

I would like to thank my co-supervisor Richard Butler for his support, invaluable discussions and assistance throughout the project, as well as sparking “bigger-picture” ideas. To external supervisor and CASE Partner, Liam Gallagher, for always keeping me on my toes - challenging me to think outside the box - through insightful discussions.

I would like to acknowledge Jeremy Young, for his expertise and help with nannoplankton taxonomy. Paul Pearson and Flavia Boscolo-Galazzo for my participation in their exciting modern deep-dwelling plankton project and allowing me to use the materials to form a chapter in this thesis. Thank you to Mariem Saavedra-Pellitero for sharing your infectious enthusiasm for coccolithophores!

To my friends – Ciara, for being there from day one of the PhD and the memories ever since, Mimi, my ray of sunshine on the gloomiest of days, your support, advice, and supply of hugs, Dean for the stomach-hurting laughs, Murray for the adventures, Nicolette for always making me laugh and smile .

To my family – the support and love from my sister, Amanda, to my dogs, Rocky (roo-bear), Leo and Zeus – your antics always brighten my day. To Jamie for seeing in me what I sometimes couldn’t, your endless patience and encouragement. To my mum, Angela, your encouragement and inspiration to chase what I love most from a young age, while always helping, supporting and being there for me. Finally, to my Nan, Pearl – I dedicate this thesis to you - I know you were always proud of me.

This research was funded by CENTA as part of the Natural Environment Research Council

---

(NERC). Samples were provided by the Java Drilling Team and Integrated Ocean Drilling Program (IODP).

# Contents

<b>Declaration of Authorship</b>	<b>i</b>
<b>Abstract</b>	<b>ii</b>
<b>Acknowledgements</b>	<b>v</b>
<b>List of Figures</b>	<b>xii</b>
<b>List of Tables</b>	<b>xiii</b>
<b>List of Plates</b>	<b>xiv</b>
<b>Abbreviations</b>	<b>xv</b>
<b>Publications</b>	<b>xviii</b>
<b>1 INTRODUCTION</b>	<b>1</b>
1.1 OVERVIEW . . . . .	1
1.2 LONG-TERM COOLING PERIODS OF THE CENOZOIC . . . . .	2
1.2.1 THE EOCENE-OLIGOCENE TRANSITION (EOT) . . . . .	2
1.2.2 EARLY-MID NEOGENE TO QUATERNARY CLIMATE . . . . .	5
1.3 CALCAREOUS NANNOPLANKTON . . . . .	9
1.4 THESIS OUTLINE . . . . .	12
1.4.1 THESIS OBJECTIVES . . . . .	12
1.4.2 THESIS STRUCTURE . . . . .	13
<b>2 LOW-LATITUDE CALCAREOUS NANNOFOSSIL RESPONSE IN THE     INDO-PACIFIC WARM POOL ACROSS THE EOCENE-OLIGOCENE     TRANSITION OF JAVA, INDONESIA</b>	<b>15</b>

---

2.1	INTRODUCTION . . . . .	16
2.2	MATERIALS AND METHODS . . . . .	18
2.2.1	LITHOSTRATIGRAPHY AND BIOSTRATIGRAPHY . . . . .	19
2.2.2	SAMPLE PREPARATION . . . . .	21
2.3	RESULTS . . . . .	22
2.3.1	RELATIVE ABUNDANCE . . . . .	22
2.3.2	PRINCIPAL COMPONENT ANALYSIS AND DIVERSITY . . . . .	25
2.3.3	NANNOFOSSIL COCCOLITH SIZE . . . . .	28
2.4	DISCUSSION . . . . .	29
2.4.1	TROPICAL PHYTOPLANKTON EVOLUTION THROUGH THE MID- DLE TO LATE EOCENE . . . . .	31
2.4.2	LATE EOCENE IMPACT EVENTS AND PHYTOPLANKTON DI- VERSITY . . . . .	33
2.4.3	EXTINCTION AND COMMUNITY RESTRUCTURING AT THE START OF THE EOT . . . . .	35
2.4.4	CO <sub>2</sub> CONTROL ON PHYTOPLANKTON SIZE ACROSS THE EOT . . . . .	37
2.5	CONCLUSION . . . . .	38
<b>3</b>	<b>MIDDLE EOCENE TO EARLY OLIGOCENE CALCAREOUS NAN- NOFOSSILS FROM THE NANGGULAN FORMATION, JAVA, INDONESIA</b> . . . . .	<b>40</b>
3.1	INTRODUCTION . . . . .	41
3.2	GEOLOGICAL SETTING . . . . .	43
3.2.1	LITHOSTRATIGRAPHY AND PRESERVATION . . . . .	43
3.3	SAMPLING AND METHODS . . . . .	45
3.4	BIOSTRATIGRAPHY . . . . .	46
3.5	TAXONOMIC DISCUSSION . . . . .	48
3.6	SYSTEMATIC PALAEONTOLOGY . . . . .	54
3.6.1	PLACOLITH COCCOLITHS . . . . .	54
3.6.2	MUROLITH COCCOLITHS . . . . .	65
3.6.3	HOLOCOCOLITHS . . . . .	70
3.6.4	EXTANT NANNOLITHS . . . . .	70



---

3.6.5	EXTINCT NANNOLITHS . . . . .	70
<b>4</b>	<b>DRIVERS OF NEOGENE COCCOLITHOPHORE MACROEVOLUTION</b>	<b>81</b>
4.1	INTRODUCTION . . . . .	81
4.2	METHODS . . . . .	83
4.2.1	COUNTS . . . . .	83
4.2.2	TAXONOMY . . . . .	84
4.2.3	SPECIES RICHNESS . . . . .	84
4.2.4	DIVERSITY . . . . .	85
4.2.5	PRESERVATION . . . . .	86
4.2.6	TIME SLICES AND AGE MODEL . . . . .	88
4.3	RESULTS . . . . .	88
4.3.1	DIVERSITY . . . . .	88
4.3.2	RELATIVE ABUNDANCE . . . . .	90
4.3.3	CALCAREOUS NANNOPLANKTON ECOGROUPS . . . . .	94
4.4	DISCUSSION . . . . .	96
4.4.1	SPECIES RICHNESS . . . . .	96
4.4.2	LITH SIZE vs $p\text{CO}_2$ . . . . .	97
4.4.3	NUTRICLINE . . . . .	98
4.5	CONCLUSION . . . . .	101
<b>5</b>	<b>CONCLUSIONS</b>	<b>107</b>
5.1	SUMMARY . . . . .	107
5.1.1	THE EOCENE-OLIGOCENE TRANSITION . . . . .	108
5.1.2	DRIVERS OF MACROEVOLUTION IN NANNOPLANKTON DURING THE LATE NEOGENE . . . . .	109
5.2	FUTURE WORK . . . . .	110
	<b>APPENDIX</b>	<b>112</b>
<b>A</b>	<b>GLOBAL CALCAREOUS NANNOFOSSIL COUNT DATA (LOW RESOLUTION SAMPLING)</b>	<b>112</b>

A.1	SITE U1482 . . . . .	113
A.2	SITE U1489 . . . . .	114
A.3	SITE U1490 . . . . .	115
A.4	SITE 1138 . . . . .	116
A.5	SITE 242 . . . . .	117
A.6	SITE 1338 . . . . .	118
A.7	SITE 925 . . . . .	119
A.8	SITE 871/872 . . . . .	120
A.9	SITE 516 . . . . .	121
A.10	DIVERSITY METRICS . . . . .	122
	A.10.1 H' DIVERSITY, SPECIES RICHNESS AND RTD . . . . .	122
	A.10.2 ABSOLUTE AND RELATIVE ABUNDANCE . . . . .	124
	A.10.3 ECOGROUP ABUNDANCE . . . . .	127
<b>B</b>	<b>U1482 DATA (HIGH RESOLUTION SAMPLING)</b>	<b>128</b>
B.1	COUNT DATA . . . . .	128
	B.1.1 RANGE THROUGH DIVERSITY AND SPECIES RICHNESS . . . .	132
	B.1.2 RELATIVE ABUNDANCE . . . . .	134
B.2	U1482 AGE MODEL DATA TABLES	
	(FROM IODP EXP. 363 SHIPBOARD DATA) . . . . .	135
	B.2.1 CALCAREOUS NANNOFOSSILS . . . . .	135
	B.2.2 FORAMINIFERA . . . . .	139
	<b>REFERENCES</b>	<b>143</b>

# List of Figures

1.1	NKK1 foraminiferal stable isotopes, micropaleontological proxies and stratigraphic interpretations. . . . .	4
1.2	Miocene to Pleistocene benthic foraminiferal $\delta^{18}\text{O}$ and $\delta^{13}\text{C}$ records from ODP Site 1146 after Holbourn et al. (2018). . . . .	7
1.3	Climate and atmospheric $\text{CO}_2$ over the past 40 Ma with microplankton species diversity and nannofossil species origination and extinction from the Eocene to Recent . . . . .	10
2.1	Late Eocene palaeoreconstruction of the Sunda region . . . . .	18
2.2	Biostratigraphic age model of NKK1 . . . . .	21
2.3	Relative abundance of ecologically important taxa . . . . .	23
2.4	Relative abundance of ecologically important nannofossil groups . . . . .	24
2.5	Principal Component (PC) 1 and 2 scatter plot and line graphs presenting individual ecologically important species loading scores . . . . .	26
2.6	Principal Component scores against nannofossil Groups 1A-B and 2A-B relative abundance . . . . .	28
2.7	Principal Component Analysis (PCA) of NKK1 samples . . . . .	29
2.8	Reticulofenestrid lith size heatmap, species diversity, PC score and SHE analysis plot . . . . .	30
3.1	Map to show the present day location of NKK1 and the IPWP . . . . .	42
3.2	Age/depth plot for NKK1 . . . . .	46
3.3	Stratigraphic ranges for <i>Reticulofenestra reticulata</i> and <i>R. isabellae</i> from northern low-mid latitudes to southern high latitudes . . . . .	53
4.1	World map displaying the locations of all studied localities in Chapter 4 . . . .	83
4.2	IODP Expedition 363 Shipboard Age Model for Site U1482, Holes A-D . . . .	89

4.3	Calcareous nannoplankton diversity records through the Neogene from this study and after Lowery et al. 2020. . . . .	90
4.4	Boxplots of H' diversity and Compiled Species Abundance from the Miocene to Recent . . . . .	92
4.5	Relative abundance boxplots of Miocene-Recent calcareous nannofossils. Plotted with CENOGRID (Westerhold et al. 2020) and coccolith $\delta^{13}\text{C}$ after Bolton et al. (2013). . . . .	93
4.6	List of calcareous nannofossil species depth habitat preferences . . . . .	94
4.7	Global compiled calcareous nannofossil ecogroup abundance and number of species plotted with atmospheric $\text{CO}_2$ over the last 15 Ma . . . . .	95
A.1	Site 1482 low resolution count data . . . . .	113
A.2	Site 1489 count data . . . . .	114
A.3	Site 1490 count data . . . . .	115
A.4	Site 1138 count data . . . . .	116
A.5	Site 242 count data . . . . .	117
A.6	Site 1338 count data . . . . .	118
A.7	Site 925 count data . . . . .	119
A.8	Site 871/872 count data . . . . .	120
A.9	Site 516 count data . . . . .	121
A.10	H' diversity, species richness and RTD values from all global sites . . . . .	122
A.11	Compiled species richness and RTD . . . . .	123
A.12	Global species absolute abundance values . . . . .	124
A.13	Global species relative abundance values used in Chapter 4 . . . . .	125
A.14	Compiled main species absolute and relative abundances . . . . .	126
A.15	Compiled calcareous nannofossil ecogroup absolute abundance values . . . . .	127
A.16	Compiled calcareous nannofossil ecogroup relative abundance values . . . . .	127
B.1	Site U1482 high resolution count data . . . . .	131
B.2	Site U1482 relative abundance data . . . . .	134
B.3	Site U1482 planktic foraminifera biozonation scheme from IODP Exp. 363 . . . . .	142

# List of Tables

3.1	Lithostratigraphic summary for NKK1 . . . . .	44
3.2	Comparative biostratigraphy of NKK1, using the Agnini et al. (2014) and Martini (1971) biozonation schemes. . . . .	49
3.3	Measurements of <i>R. nanggulanensis</i> and <i>S. conicus</i> in NKK1 . . . . .	51
4.1	List of samples, their ages and preservation recorded across low resolution dataset localities used in Chapter 4 . . . . .	87
B.1	Site U1482 RTD and species richness data . . . . .	133

# List of Plates

1	Plate 2.1 A selection of calcareous nannofossils from NKK1 . . . . .	34
2	Plate 3.1 LM images from NKK1 of <i>Reticulofenestra</i> . . . . .	75
3	Plate 3.2 LM images from NKK1 of <i>Coccolithus</i> , <i>Bramletteius</i> , <i>Cruciplacolithus</i> , <i>Campylosphaera</i> , <i>Coronocyclus</i> , <i>Chiasmolithus</i> . . . . .	76
4	Plate 3.3 LM images from NKK1 of <i>Clausicoccus</i> , <i>Calcidiscus</i> , <i>Umbilicosphaera</i> , <i>Pedinocyclus</i> , <i>Helicosphaera</i> , <i>Pontosphaera</i> . . . . .	77
5	Plate 3.4 LM images from NKK1 of <i>Pontosphaera</i> , <i>Scyphosphaera</i> , <i>Blackites</i> , <i>Cal-</i> <i>ciosolenia</i> , <i>Syracosphaera</i> . . . . .	78
6	Plate 3.5 LM images from NKK1 of <i>Lanternithus</i> , <i>Holodiscolithus</i> , <i>Orthozygus</i> , <i>Clathrolithus</i> , <i>Zygrhablithus</i> , <i>Braarudosphaera</i> , <i>Micrantholithus</i> , <i>Pemma</i> , <i>Discoaster</i>	79
7	Plate 3.6 LM images from NKK1 of <i>Discoaster</i> , <i>Sphenolithus</i> , <i>Triquetrorhabdulus</i> .	80
8	Plate 4.1 LM images from U1482 of <i>Calcidiscus</i> , <i>Coccolithus</i> , <i>Gephyrocapsa</i> , <i>Retic-</i> <i>ulofenestra</i> , <i>Helicosphaera</i> , <i>Pontosphaera</i> , <i>Syracosphaera</i> , <i>Rhabdosphaera</i> , <i>Calciosole-</i> <i>nia</i> , <i>Holodiscolithus</i> , <i>Scyphosphaera</i> , <i>Orthorhabdus</i> , <i>Nicklithus</i> , <i>Amaurolithus</i> and <i>Cer-</i> <i>atolithus</i> . . . . .	102
9	Plate 4.2 LM images from U1482 of <i>Sphenolithus</i> , <i>Scyphosphaera</i> and <i>Discoaster</i> .	103
10	Plate 4.3 SEM images from U1482 and 516Z of <i>Calcidiscus</i> , <i>Coccolithus</i> , <i>Gephy-</i> <i>rocapsa</i> , <i>Pseudoemiliana</i> , <i>Reticulofenestra</i> , <i>Helicosphaera</i> , <i>Pontosphaera</i> and <i>Syra-</i> <i>cosphaera</i> . . . . .	104
11	Plate 4.4 SEM images from U1482 and 516Z of <i>Florisphaera</i> , <i>Calciosolenia</i> , <i>Gladi-</i> <i>olithus</i> (?), <i>Holodiscolithus</i> , <i>Sphenolithus</i> , <i>Ceratolithus</i> , <i>Scyphosphaera</i> and <i>Discoaster</i>	105
12	Plate 4.5 SEM images from U1482 and 516Z of <i>Discoaster</i> and <i>Reticulofenestra</i> coccospheres . . . . .	106

# Abbreviations

A = Abundant

C = Common

CCD = Calcite Compensation Depth

CNE = Calcareous Nannofossil Eocene biozones (after Agnini et al. 2014)

CNO = Calcareous Nannofossil Oligocene biozones (after Agnini et al. 2014)

DE = *Discoaster* Extinction

DEE = *Discoaster* Extinction Event

DIC = Dissolved Inorganic Carbon

DSDP = Deep Sea Drilling Project

DWAF = Deep Water Agglutinated benthic Foraminifera

EAIS = East Antarctic Ice Sheet

EOGM = Early Oligocene Glacial Maximum

EOIS = Early Oligocene Isotope Shift

E-O = Eocene-Oligocene

EOB or E/O = Eocene-Oligocene Boundary

EOT = Eocene-Oligocene Transition

F = Few

FCO = First Common Occurrence

---

FO = First Occurrence

FOV = Field of View

G = Excellent/Good

GTS = Geologic TimeScale

H = Shannon diveristy

IAA = Indo-Australian Archipelago

ka = thousand years

LEZ = Lower Euphotic Zone

LCO = Last Common Occurrence

LO = Last Occurrence

LM = Light Microscope

LMCIS = Late Miocene Carbon Isotope Shift

$\ln(S)$  = log of species richness

IPWP = Indo-Pacific Warm Pool

M = Moderate

Ma = million years

mbgl = meters below ground level

MCO = Miocene Climatic Optimum

MECO = Middle Eocene Climatic Optimum

Mi-1 = early Miocene glacial event

MMCT = Middle Miocene Climate Transition

MPT = Middle Pliocene Transition

mPWP = Mid Pliocene Warm Period



---

NH = Northern Hemisphere

NP = NannoPlankton zones (After Martini 1971)

ODP = Ocean Drilling Program

P = Poor

PC = Principle Component

PCA = Principal Component Analysis

$p\text{CO}_2$  = atmospheric carbon dioxide

PETM = Paleocene-Eocene Thermal Maximum

POC = Particulate Organic Matter

RA = Relative Abundance

SEM = Scanning Electron Microscope

SEZ = Sub Euphotic Zone

SH = Southern Hemisphere

SHE = Species richness, Diversity (H) and Evenness analysis

T = Top of stratigraphic range (bioevent)

TCO = Top Common Occurrence

TDP = Tanzania Drilling Project

UEZ = Upper Euphotic Zone

WAIS = West Antarctic Ice Sheet

XPL = Crossed Polarised Light

$95\%_{tile}$  = 95th percentile

# Publications

## Published papers used in this Doctoral Research

This thesis incorporates the following published papers corresponding to the Chapters 2 and 3 respectively:

**Jones, A.P.**, Dunkley Jones, T., Coxall, H., Pearson, P.N., Nala, D., and Hoggett, M. 2019. Low-Latitude Calcareous Nannofossil Response in the Indo-Pacific Warm Pool Across the Eocene-Oligocene Transition of Java, Indonesia. *Paleoceanography and Paleoclimatology*, **34**, pp 1-15. doi.org/10.1029/2019PA003597

**Jones, A.P.**, and Dunkley Jones, T. 2020. Middle Eocene to Early Oligocene calcareous nannofossils from the Nanggulan Formation, Java, Indonesia. *Journal of Nannoplankton Research*, **38(1)**, pp. 57–79. International Nannoplankton Association, ISSN 1210-8049. The Sheridan Press, USA

## Paper intended for publication

The following paper is intended for publication and corresponds to Chapter 4 in this thesis:

**Jones, A.P.**, Dunkley Jones, T., Boscolo-Galazzo, F., and Pearson, P.N. Neogene Drivers of Coccolithophore Macroevolution (*in review*).

---

## Related publications to this doctoral research

Boscolo-Galazzo, F., **Jones, A.P.**, Dunkley-Jones T, Pearson, P.N. Evolution and diversification of modern deep dwelling plankton. (*in prep*).

Coxall, H. K., Dunkley Jones, T., **Jones, A.P.**, Lunt P., MacMillan, I., Marliyani, G.I., Nicholas, C.J., O'Halloran, A., Piga, E., Sanyoto, P., Rahardjo, W., Pearson, P.N. Eocene to Oligocene sediment cores from the Nanggulan Region of central Java: lithostratigraphy, biostratigraphy and foraminifera stable isotopes. *Journal of the Geological Society* doi.org/10.1144/jgs2021-006



# 1 | INTRODUCTION

## 1.1 OVERVIEW

Coccolithophores (also known as calcareous nannoplankton) are calcifying phytoplankton that have played a significant role in marine ecosystems and global biogeochemical cycles throughout Earth history. Their greatest diversity is typically found at low latitudes and are well adapted to a range of environments with differing species being well adapted to oligotrophic, eutrophic and mesotrophic environments (Hannisdal et al. 2012). Yet, calcareous nannoplankton are sensitive to environmental changes (temperature and nutrients are key controls; Aubry 1992*a*) making them excellent in reconstructing palaeoceanography and palaeoecology, as their assemblages respond to oceanographic and climatic changes.

Understanding the drivers of coccolithophore diversity, evolutionary and ecological change during cooling periods of the Cenozoic is a main focus of this thesis. Assessing the timing of climate cooling and the associated impact on calcareous nannoplankton assemblages can aid the understanding of macroevolutionary drivers, diversity and ecological changes influencing communities. Additionally, by evaluating climatic and oceanic changes over long-term periods including significant cooling periods, specifically the Eocene-Oligocene Transition (EOT) and the mid-Miocene to Recent, can provide insight into how modern coccolithophore communities were established. Furthermore, understanding the environmental drivers forcing coccolithophore macroevolution can inform the mapping of future directions of ocean change.

The aim of this thesis is to record calcareous nannoplankton response, diversity and macroevolutionary during cooling periods of the Cenozoic using successions recovered by Deep Sea Drilling Project (DSDP), Ocean Drilling Program (ODP) and Integrated Ocean Drilling Program (IODP) expeditions. These records focus mostly on new low latitude, tropical sites where continuous records through cooling periods are scarce and includes the reassessment

of calcareous nannofossil macroevolutionary drivers over the past 15 Ma. In particular, these localities are selected to record biotic responses across the middle Eocene to early Oligocene (39.33-31.23 Ma) and the middle Miocene to Recent (15-0 Ma) relating to times of declining atmospheric CO<sub>2</sub>.

This chapter outlines the background state of knowledge on calcareous nannoplankton assemblage responses through these specific cooling intervals of the Cenozoic. Firstly, the Eocene-Oligocene Transition (EOT) climatic restructuring and suspected drivers of climatic change are reviewed, while noting microplankton ecological trends associated with the transition. The currently available EOT nannoplankton records are considered as well as a summary of the new EOT core used in Chapters 2 and 3 in this thesis. The long-term climatic changes from the mid-Miocene to Recent are discussed, along with published nannoplankton evolutionary trends and the locations and sites used for Chapter 4. Following this, the fossil record of coccolithophores is evaluated for the purposes of the study of evolution, ecology, biodiversity and community change, along with the intimate link between these parameters and global climate change. The calcareous nannoplankton records during the chosen climate intervals, the EOT and mid-Miocene to Recent are also discussed. This chapter ends with the objectives and structure of this thesis; the key objectives of the thesis are listed and the structure outlines the thesis giving detail on each individual chapter.

## **1.2 LONG-TERM COOLING PERIODS OF THE CENOZOIC**

### **1.2.1 THE EOCENE-OLIGOCENE TRANSITION (EOT)**

The Eocene-Oligocene Transition (EOT), one of the most significant climate events of the Cenozoic, was characterised by an abrupt shift from the long-term Cretaceous – early Paleogene “greenhouse” world to the modern “icehouse” conditions (Coxall and Pearson 2006, Coxall et al. 2021, Hutchinson et al. 2021, Westerhold et al. 2020, Zachos et al. 2001). This transition was associated with major community overturning occurring in marine and terrestrial realms (Coxall and Pearson 2007, Dunkley Jones et al. 2008, Sahy et al. 2015). In marine sediment records, the transition, from ~34.5-33.5 Ma (Coxall and Pearson 2007) is characterised by a large, ~1.0 to 1.5%, positive shift in deep-ocean benthic foraminiferal  $\delta^{18}\text{O}$  isotope values. In high-resolution EOT records this positive  $\delta^{18}\text{O}$  shift occurs in two distinct “steps” (termed

step 1 and step 2; Figure 1.1 after Coxall et al. 2021) separated by a  $\sim 200$  ka plateau (Bohaty et al. 2012, Coxall and Wilson 2011, Coxall et al. 2005, 2021, Katz et al. 2008, Lear et al. 2008). Overall, this positive  $\delta^{18}\text{O}$  shift signifies global cooling and increased continental ice volume, mostly of the East Antarctic Ice Sheet (EAIS), with the most positive  $\delta^{18}\text{O}$  values at the end of the second step representing the end of the EOT and the initiation of the of the Early Oligocene Glacial Maximum (EOGM) (Coxall and Pearson 2007, Lear et al. 2008, Miller et al. 2009). Antarctic ice sheet growth is thought to have initiated as a result of the drawdown of atmospheric  $\text{CO}_2$  (1100 – 760 ppm; Pearson et al. 2009) causing global cooling into the range of Antarctic ice sheet stability (DeConto and Pollard 2003, Goldner et al. 2014, Pagani et al. 2011, Pearson et al. 2009). Moreover, marine sedimentary records recovering the EOT reveal a rapid  $>1$  km calcite-compensation depth (CCD) deepening (Coxall et al. 2005, Pälike et al. 2012), most likely driven by a repartitioning of shelf to open ocean carbonate factory in response to a eustatic sea level fall of  $\sim 60 - 80\text{m}$  (Miller et al. 2009).

The EOT expansion of Antarctic ice sheets (Bohaty et al. 2012, Coxall et al. 2005, Lear et al. 2008, Scher et al. 2011) is closely associated with global cooling (Liu et al. 2009), a reorganisation of ocean circulation (Coxall et al. 2018, Egan et al. 2013, Elsworth et al. 2017, Goldner et al. 2014, Hutchinson et al. 2018, McKinley et al. 2019), and an altered biogeochemical cycle (whereby interactions between marine biota, the surface ocean and atmosphere were directly affected due to declining  $\text{CO}_2$  across the EOT)(Egan et al. 2013, Lyle and Lyle 2006). High-latitude drivers, including the Southern Ocean’s increased role in global ocean overturning circulation and biogeochemistry (diatom radiatiton through the late Eocene)(Egan et al. 2013, Goldner et al. 2014), likely caused far-field environmental changes through the EOT interval. In turn, the forcing of this glacial expansion was likely a combination of long-term decline in atmospheric  $p\text{CO}_2$ , potentially linked to the opening of Southern Ocean gateways (Sijp et al. 2014) and shorter-term orbital configurations favouring Antarctic ice growth (DeConto and Pollard 2003).

In long-term compilations of Cenozoic marine microplankton diversity the EOT is identified as the interval of maximum change (Bown et al. 2004, Lowery et al. 2020, Rabosky and Sorhannus 2009) including the restructuring of important ecological groups (Ezard et al. 2011) and an extensive dominance switch across multiple clades (Bown et al. 2004, Egan et al. 2013, Falkowski and Oliver 2007) whereby specific genera across multiple plankton groups under-

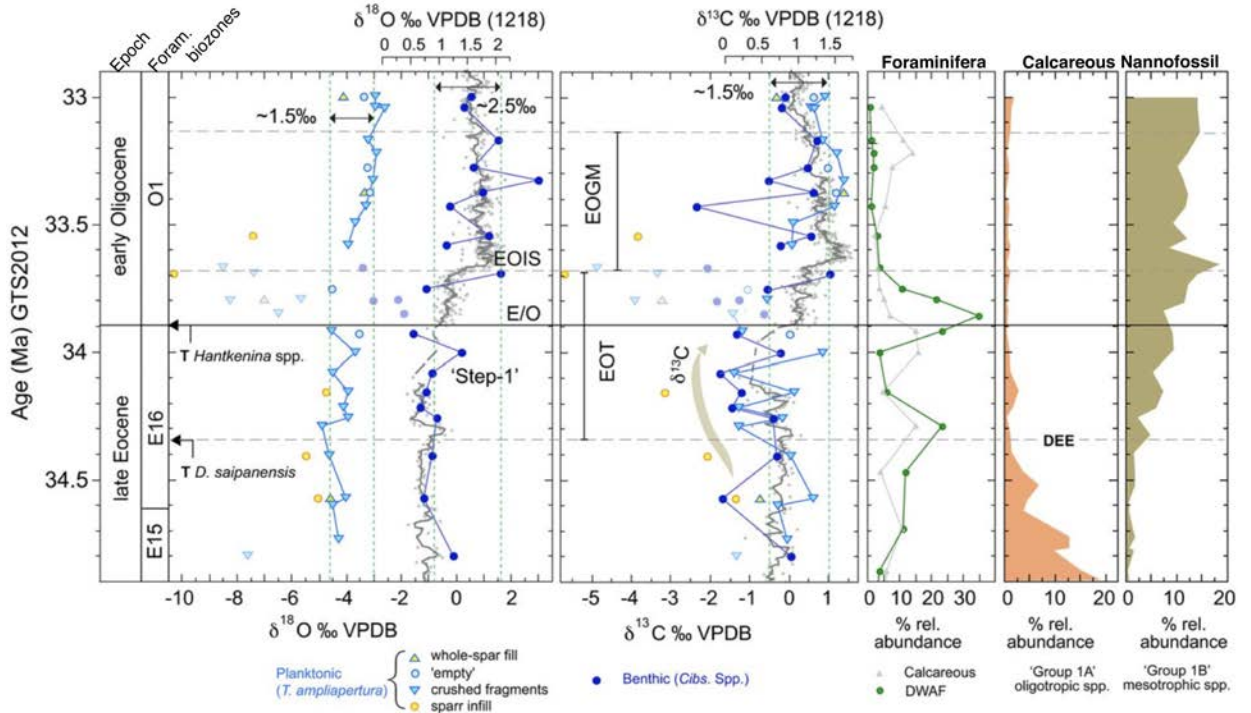


Figure 1.1: NKK1 foraminiferal stable isotopes, micropaleontological proxies and stratigraphic interpretations. From left to right: planktonic (light blue) and benthic (dark blue) foraminifera  $\delta^{18}\text{O}$  and  $\delta^{13}\text{C}$ . NKK1 isotope data after Coxall et al. (2021) with ODP Site 1218 (dark grey) from Coxall et al. (2005) and Coxall and Wilson (2011) overlain; calcareous (light grey) and deep water agglutinated (DWAf; green) benthic foraminifera relative abundance counts; calcareous nannofossil relative abundance of mesotrophic and oligotrophic species through the NKK1 interval. "T" = Top of stratigraphic range (bioevent), Eocene Oligocene Transition (EOT), the Eocene-Oligocene boundary (E/O), the Early Oligocene Isotope Shift (EOIS), the Early Oligocene Glacial Maximum (EOGM) and Discoaster Extinction Event (DEE). Modified after Coxall et al. (2021).

went restructuring due to a series of abiotic and biotic factors and climatic changes associated with the EOT. However, understanding how the observed and well-documented climate dynamics of this interval are linked – both temporally and mechanistically – with biotic change remains uncertain (Ezard et al. 2011), in large part because detailed biotic records, of similar resolution to climate proxy data, across this transition are relatively rare.

From records that are available, calcareous microplankton diversity loss and turnover through the EOT and into the early Oligocene is pronounced (Berggren et al. 1995, Bown et al. 2004, Coxall and Pearson 2007, Coxall et al. 2021, Dunkley Jones et al. 2008, Martini 1971). The timing of species extinctions amongst plankton groups, however, is not co-ordinated. For example, in calcareous nannofossils, the extinction of the rosette-shaped (multi-rayed) discoasters, which is considered one of the most important extinctions of the Cenozoic (Martini



1971), precedes the main extinction phases within the planktic foraminifera *Turoborotalia cerroazulensis* and the family Hantkeninidae, the latter denoting the Eocene-Oligocene boundary (EOB)(Figure 1.1)(Coxall et al. 2021, Wade and Pearson 2008). It is clear that community restructuring across zoo- and phytoplankton groups, recorded via biological turnover and/or diversity loss, can be related to the global climatic and oceanic perturbations prior and leading up to the EOB, but only an improved spatial coverage, across all main ocean basins, of high-resolution biotic records will be able to determine the degree of coordinated change across latitudes, and so start to untangle the high-latitude drivers of this major evolutionary transition.

Tropical nannoplankton assemblage records during the EOT do already exist, specifically in the western- (Bown et al. 2008, Dunkley Jones et al. 2008) and central Indian Ocean (Fioroni et al. 2015), however, this data remains limited from other low-latitude sites due to either poor preservation, poor nannofossil recovery or an incomplete EOT record (Backman 1987, Coccioni et al. 1988, Monechi 1986, Wei and Wise 1990, Wei et al. 1992). Analysis of calcareous nannofossil assemblages from a new onshore core – NKK1, of the Nanggulan Formation, Java, Indonesia – reveals a continuous sedimentary record across the EOT, with good recovery and good to excellent preservation of nannofossils. NKK1 yields a ~60m succession of marine clay and claystones and its palaeolocation was close to the region of modelled peak-sea surface temperatures of the Indo-Pacific Warm Pool (IPWP) during the Eocene (Huber and Caballero 2011, Lunt et al. 2012). This new record is a valuable archive of phytoplankton ecology, biostratigraphy, and reconstruction ocean-climate interactions, including the evolution and extinctions of plankton in the IPWP (Coxall et al. 2021).

### 1.2.2 EARLY-MID NEOGENE TO QUATERNARY CLIMATE

The Oligocene to Miocene hosts an overall further decline in  $p\text{CO}_2$  with the abrupt Mi-1 glacial event which represents the start of the Miocene (Zhang et al. 2013). This thesis, however, focuses on the mid-Miocene to Recent, therefore, the climatic events of these Epochs are not further discussed. A long-term atmospheric  $\text{CO}_2$  decline through the mid-to-late Neogene, saw the gradual development of icehouse conditions into the bi-hemispheric glacial climates of the Pleistocene (Mejía et al. 2017, Zhang et al. 2013).

The Miocene Climatic Optimum (MCO; ~15–17 Ma), was the warmest interval of the

Neogene and is associated with an interval of long-term positive carbon isotope excursion (or “Monterey Excursion”) ending approximately 400 ka after the expansion of the Antarctic icesheet that terminated the MCO (Diester-Haass et al. 2009, Holbourn et al. 2007, 2013, Zachos et al. 2008)(Figure 1.2). The interval from the MCO to the mid-Pliocene, M2 glacial (3.3 Ma), is characterised by increasing  $\delta^{18}\text{O}$  and cooling (Holbourn et al. 2013, 2018, Westerhold et al. 2020). The positive shift in benthic  $\delta^{18}\text{O}$  that terminates the MCO – known as the Middle Miocene Climate Transition (MMCT; 14.7–13.8 Ma) - and closely follows obliquity cycles from ~14.6-14.1 Ma indicating the progressive cooling and glaciation in high-latitudes. The MMCT represents the major regrowth of the East Antarctic Ice Sheet (EAIS; ~13.9 Ma)(Holbourn et al. 2013, 2018)(Figure 1.2) and is defined by a ~60 - 125 ppmv decline in atmospheric  $\text{CO}_2$  (Badger et al. 2013, Super et al. 2018).

The late Miocene (~11.6 – 5.3 Ma) marks profound environmental changes across both terrestrial and marine ecosystems (Herbert et al. 2016, Holbourn et al. 2018). Moreover, the late Miocene carbon isotope shift (LMCIS; Figure 1.2) - a permanent  $-1\text{‰}$  shift in oceanic  $\delta^{13}\text{C}_{DIC}$  - represents the last significant carbon cycle shift recorded across all ocean basins (Drury et al. 2017). This negative shift in  $\delta^{13}\text{C}_{DIC}$  occurred during a period of increased marine biological productivity (also known as the “late Miocene biogenic bloom”) and is associated with increased delivery of organic carbon to the oceans from continental reservoirs, the shift from C3 to C4 vegetation and increased seasonality and aridity (Diester-Haass et al. 2006, Holbourn et al. 2018). Following this, at approximately 6.7 Ma, inter-oceanic  $\delta^{13}\text{C}$  gradients were established with near-modern values (Herbert et al. 2016, Hodell and Venz Curtis 2006), indicating the advance of strong equator to pole sea-surface temperature (SST) gradients presenting enhanced cooling at high-latitudes but only slight changes at low-latitudes (Drury et al. 2017, Herbert et al. 2016). Further, planktonic foraminifera  $\delta^{18}\text{O}$  records of IODP Site U1338 in the eastern equatorial Pacific indicates a  $2^\circ\text{C}$  cooling between 7.2 and 6.1 Ma (Drury et al. 2018). At the same time, the expansion of C4 grasslands occurred during the late Miocene resulting in a decline of previously C3-dominated ecosystems across the tropics and subtropics (Herbert et al. 2016, Strömberg 2011). Despite evidence for cooling and expansion of C4 grasslands, there is no significant change in proxy estimates of atmospheric  $\text{CO}_2$  during the late Miocene (Beerling and Royer 2011, Herbert et al. 2016).

Global cooling and the development of near-modern meridional thermal gradients devel-

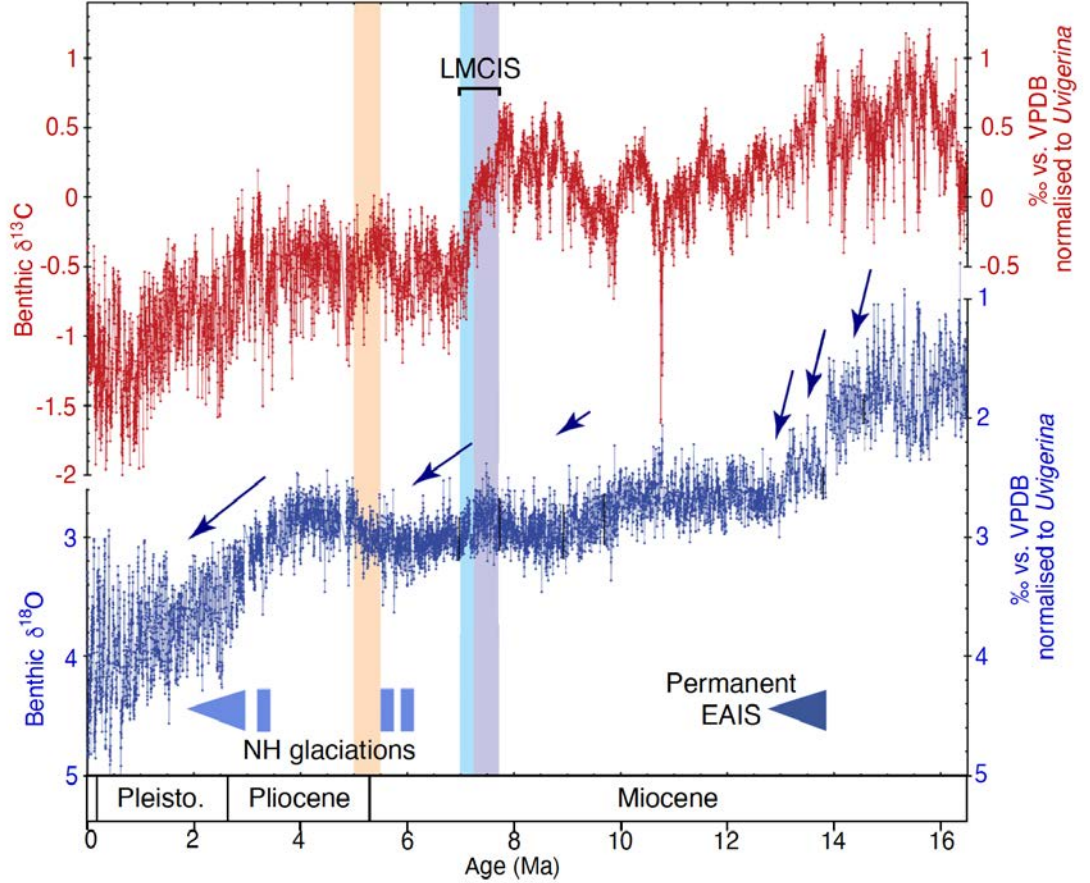


Figure 1.2: Miocene to Pleistocene benthic  $\delta^{18}\text{O}$  and  $\delta^{13}\text{C}$  records from ODP Site 1146, compiled from Holbourn et al. (2005, 2007, 2013, 2018). Blue arrows indicate main phases of glacial expansion/deep water cooling. Lilac vertical shading indicates global  $\delta^{13}\text{C}$  decline coincident with planktic  $\delta^{18}\text{O}$  increase. Blue vertical shading signifies final stage of global  $\delta^{13}\text{C}$  decline. Light orange shading is climate warming after 5.5 Ma. Figure modified after Holbourn et al. (2018). LMCIS = Late Miocene Carbon Isotope Shift; NH = Northern Hemisphere; EAIS = East Antarctic Ice Sheet.

oped synchronously across the northern and southern hemispheres during the late Miocene-early Pliocene (7-5.4 Ma; Herbert et al. 2016, Drury et al. 2018). Following this, the long-term cooling trend stalled in the early Pliocene ( $\sim 3$  Ma), with global mean temperatures  $2\text{-}3^\circ\text{C}$  warmer than pre-industrial during the mid Pliocene Warm Period (mPWP), a time when reconstructed atmospheric concentrations are equivalent to modern values ( $\sim 400$  ppm; Seki et al. 2010, Pagani et al. 2010). This warm period instigated significant retreat of the West Antarctic ice sheet (WAIS) (Pollard and DeConto 2009) and Greenland's ice sheet mass declined by 50-70 % (Hill et al. 2007, Koenig et al. 2015, Naish et al. 2009), therefore, the mPWP is considered an analogue for near-future climate (Burke et al. 2018, Pontes et al. 2020).

Intensification of the Plio-Pleistocene icehouse conditions are linked to the further decline of atmospheric CO<sub>2</sub> (Rae et al. 2021). The Pleistocene is the culmination of enhanced cooling which includes variable northern hemisphere ice sheets during lower CO<sub>2</sub> conditions of the glacials and more widespread retreat during interglacials (Chalk et al. 2017, Rae et al. 2021). The early Pleistocene glacial-interglacial cycles correlated to obliquity cycles of ~40 kyr, by the mid Pleistocene transition (MPT) the glacial-interglacial cycles intensified over multiple obliquity cycles of 80-120 kyr periodicity (Chalk et al. 2017, Clark et al. 2006, Huybers 2011), resulting in the rise of extended and colder ice ages with lower eustatic sea level and greater continental ice sheets into the late Pleistocene (Elderfield et al. 2012, Rohling et al. 2014).

Since the middle Miocene selection of smaller coccolithophore morphotypes is recognised across multiple groups, *Calcidiscus* (Knappertsbusch 2000), *Helicosphaera* (Šupraha and Henderiks 2020) and *Reticulofenestra* (Bendif et al. 2019) signifying that common macroevolutionary driver(s), favour smaller cell size and therefore, smaller coccoliths (Šupraha and Henderiks 2020). The late Neogene is a time of decreased diversity and community restructuring amongst calcareous nannoplankton (Bown et al. 2004, Henderiks et al. 2020), therefore, understanding the short- and long-term adaptations of coccolithophores and their ancestral lineages is important for modelling in the biogeochemical role of the group and the perturbations recorded in the global carbon cycle (Šupraha and Henderiks 2020).

To document the impact of long-term cooling and carbon limitation on nannoplankton assemblages through the Neogene, two datasets were analysed. First, new ocean drilling material from low latitude Integrated Ocean Drilling Program (IODP) Expedition 363, Site U1482, situated on the edge of the IPWP, with 200 ka sample resolution. The sedimentary section of U1482 (Rosenthal et al. 2018), comprising mostly of clay-rich nannofossil oozes, spans the late Miocene to early Pleistocene (7.7-1.7 Ma) and allows for detailed quantification of species diversity and assemblage composition due to very-well preserved nannoplankton. The second dataset utilised was a compilation of nine global sites from ocean drilling projects (Deep Sea Drilling Project, Ocean Drilling Program and IODP) at lower sample resolution (~2.5 Ma) but spanning the last 15 Ma. The comparison between U1482 and these 9 global sites allows for the evaluation of macroevolutionary driving mechanisms of nannoplankton communities on a global scale. Additionally, U1482 should serve as a representative tropical succession to detail and compare nannoplankton global community responses during the Miocene-Holocene

interval.

### 1.3 CALCAREOUS NANNOPLANKTON

Coccolithophores, calcifying haptophyte algae, are an important constituent of the biogeochemical carbon cycle and have been abundant in marine realms since the late Triassic ( $\sim 200$  Ma)(Bown and Young 1998*a*, Bown et al. 2004). Calcareous nannofossil long-term diversity records reveal that nannoplankton assemblages were an important component of surface water microplankton communities during the early Cenozoic (Bown et al. 2004). Their high abundance, common occurrence, and long-ranging continuous fossil record make nannoplankton ideal for palaeoceanographic and palaeoecological reconstructions (Beaufort et al. 2011, Dunkley Jones et al. 2008, Gibbs et al. 2018, Henderiks and Pagani 2007, Villa et al. 2008, 2013) and the coupling between nannoplankton community changes and global climate is intimately linked due to their sensitivity to environmental changes (Aubry 1992*a*, Roth 1994, Winter et al. 1994). Nutrients, temperature, light, and latitude (Aubry 1992*a*, Baumann et al. 1999, Liu et al. 2018, Winter et al. 1994), are some of the controlling factors in species abundance changes and ecological diversity in the modern (Beaufort et al. 2011, Rickaby et al. 2010, Rost and Riebesell 2004) and palaeoecological studies (Dunkley Jones et al. 2008, Gibbs et al. 2013, Stoll et al. 2007, Villa et al. 2008, 2013). The tolerance of individual species to varying environmental conditions and how this relates to palaeoclimatic and palaeoenvironmental changes can help to identify palaeoceanographic events. Typically, nannoplankton are eurytopic however, some taxa have specific ecological tolerances and preferences for conditions such as cold-water eutrophic or warm-water oligotrophic, therefore, changes in environment can have a profound impact on the population dynamics of nannoplankton. It is plausible that nannofossils and their living relatives today, share broadly similar ecological tolerances; mostly they are photic-zone dwellers, have a widespread global distribution and have greater diversity in tropical latitudes (Bown and Young 1998*a*, Lowery et al. 2020).

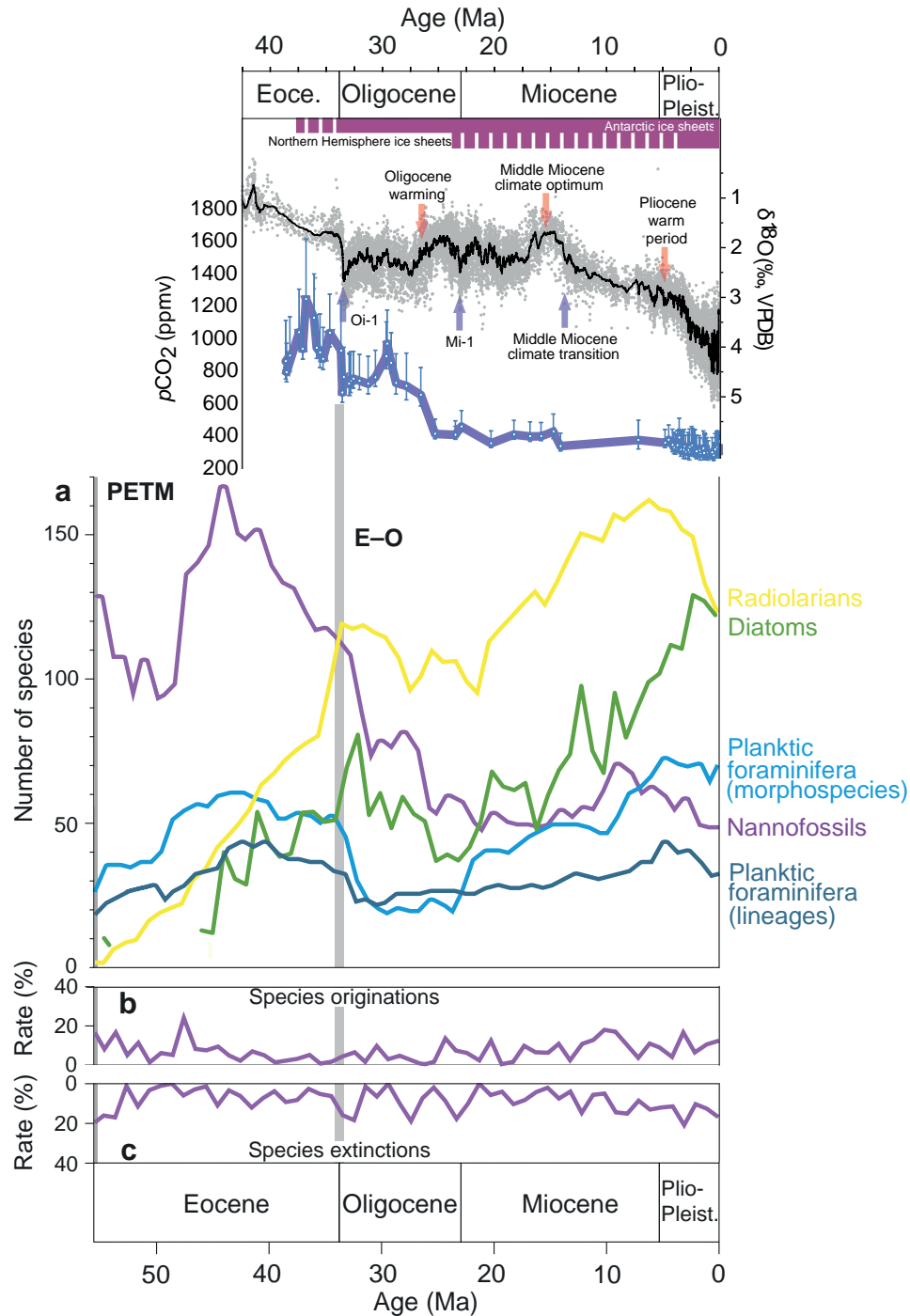


Figure 1.3: Climate (black and grey plots) and atmospheric CO<sub>2</sub> (lilac) over the past 40 Ma, major warming (orange arrows) and cooling (blue arrows) events indicated (modified after Zhang et al. (2013)); microplankton species diversity and nannofossil species origination and extinction from the Eocene to Recent. **(a)** Calcareous nannoplankton (purple), planktic foraminifera (blues), diatom (green) and radiolarian (yellow) species diversity from the Eocene to the Recent. **(b)** Calcareous nannofossil rates of origination and **(c)** rates of extinction. PETM = Palaeocene-Eocene Thermal Maximum and E-O = Eocene-Oligocene. Modified after Lowery et al. (2020).

Since a Cenozoic peak in the middle Eocene, calcareous nannofossil species diversity has

decreased, despite a small recovery during the late Miocene (Figure 4.3) (Bown et al. 2004, Lowery et al. 2020). Diversity decline observed in the nannoplankton typically correlates with global climate cooling and decreasing atmospheric CO<sub>2</sub> via changes in water column structure (and therefore nutrient availability) and ocean circulation, ultimately creating selective pressures on nannoplankton through the geological record, prompting diversity decline (Bown et al. 2004, Lowery et al. 2020, Šupraha and Henderiks 2020). Rates of diversity decline are not linear through time and rate of species loss appears to be coupled with palaeoceanographic changes across the mid Paleogene to Quaternary (Lowery et al. 2020, Šupraha and Henderiks 2020).

Studies on EOT nannoplankton assemblage records across high- to low latitudes within multiple ocean basins signify assemblage shifts corresponding with distinct climatic perturbations during this interval (Dunkley Jones et al. 2008, Fioroni et al. 2015, Persico and Villa 2004, Shamrock and Watkins 2012, Villa et al. 2008, 2013, Wei and Wise 1990). However, there is limited low-latitude nannofossil assemblage datasets that exhibit good-preservation and a continuous EOT sedimentary record. Such studies include the Tanzania Drilling Project in the western Indian Ocean (TDP; cores 12 and 17) (Bown et al. 2008, 2009, Dunkley Jones et al. 2008, 2009) and ODP Site 711 in the central Indian Ocean (Fioroni et al. 2015, Wei and Wise 1992). Data from the new NKK1 core from the IPWP exhibits all these necessary characteristics and therefore, adds to the limited low-latitude nannofossil data over the EOT.

Similarly, selective pressures on ancestral coccolithophore lineages associated with factors of long-term global cooling and carbon limitation during the Neogene, results in diversity and overall coccolith size reduction (Bolton et al. 2016, Finkel et al. 2007, Hannisdal et al. 2012, Šupraha and Henderiks 2020). Coccolithophores are used to signify a relationship between Cenozoic global climate changes and their diversity, cell size and community restructuring (Bolton et al. 2013, 2016, Šupraha and Henderiks 2020, Henderiks et al. 2020). Between 7-5 Ma carbon limitation effects on coccolith carbon isotope vital effects imply a physiological response including the active re-allocation of carbon to photosynthesis, supported by the degree of calcification within the coccolith (Bolton et al. 2013). Coccolithophore cell and coccolith sizes, specifically in the Noelaerhabdaceae lineage and *Helicosphaera*, shift towards the production of smaller, thinner coccoliths over the past 15 Ma (Bolton et al. 2016, McClelland et al. 2016, Rae et al. 2021, Šupraha and Henderiks 2020). These trends are associated with

declining atmospheric CO<sub>2</sub>, ocean alkalinity and dissolved inorganic carbon (DIC) concentrations in the surface ocean (Bendif et al. 2019, Knappertsbusch 2000, Šupraha and Henderiks 2020).

Recent research has proposed that the enhanced efficiency of the biological carbon pump is an additional driver of Neogene microplankton macroevolution (Boscolo-Galazzo et al. 2018, 2021). Records and biogeochemical modelling of planktonic foraminifera isotopes reveal a decrease in surface water remineralisation of particulate organic carbon (POC), driven by ocean and climate cooling across the last 15 Ma. This provides an opportunity to review the role of nutricline depth as a further macroevolutionary driver – associated with climatic changes - on coccolithophore evolution.

## 1.4 THESIS OUTLINE

### 1.4.1 THESIS OBJECTIVES

This thesis focuses on the response of calcareous nannoplankton during two of the most significant cooling periods of the Cenozoic, the EOT and the long-term cooling of the Neogene. Calcareous nannofossil ecological response, diversity and macroevolutionary drivers are all key factors during such prolific global climatic changes. Mainly, this research addresses low-latitude sites; there are limited studies on nannoplankton at low-latitude sites over the last 40 million years - even more restricted is the availability of a continuous record during the EOT at tropical sites. Two new low-latitude sites enable us to improve on such deficient areas in research. NKK1, an onshore core drilled in the south-central region of Java and IODP Exp. 363, Site U1482 on the north-west Australian Margin, together with a global compilation of 9 DSDP, ODP and IODP Sites for the last 15 million years, addresses the questions behind diversity loss, ecological response and macroevolutionary drivers in coccolithophores in tropical locations. This research is focused within two themes: the response of calcareous nannofossils to the dramatic climate shift during the EOT and the macroevolutionary drivers of coccolithophores during the late Neogene (Miocene-Recent).

The key objectives of this thesis are to:

1. Investigate calcareous nannoplankton diversity, ecological response and to determine if



there is a relationship between coccolith size and declining CO<sub>2</sub> across the EOT.

2. Provide a detailed record of the late Middle Eocene to Early Oligocene calcareous nanofossil assemblages of NKK1 in the Indo-Pacific Warm Pool.
3. Analyse the effects of long-term global cooling during the Neogene and to investigate the driving mechanisms of macroevolutionary changes in coccolithophore communities with respect to diversity and coccolith size.

## 1.4.2 THESIS STRUCTURE

This thesis documents calcareous nanoplankton response across long-term cooling periods of the Cenozoic, detailing coccolithophore ecological response, diversity change and driving mechanisms of macroevolution. High-resolution records of middle Eocene to early Oligocene calcareous nanofossil assemblages are presented for NKK1 of the Nanggulan Formation, Java, Indonesia, providing a continuous sedimentary sequence of good to excellent preserved nanofossils across the EOT at a new low-latitude location. Furthermore, high sample resolution records from IODP Exp. 363 (Site U1482) in the IPWP yield middle Miocene to early Pleistocene sediments and low sample resolution records of a global compilation of nine sites, together aids the investigation of coccolithophore response to climatic changes of the past 15 Ma. Chapters 2 to 4 are the scientific results of this work, and chapters 2 and 3 have been slightly modified from their print version to best fit the formatting guidelines required for this thesis.

Chapter 2 presents a palaeoceanographic investigation of NKK1 and the calcareous nanofossil assemblage response of the middle Eocene to early Oligocene, with particular interest across the EOT interval (~34.5-33.5 Ma). Statistical analyses are performed to evaluate nanoplankton trends in diversity (species and ecological diversity) and the relative abundances of species aim to determine the dominant temporal trends within the assemblage by grouping species of similar response to environmental forcing, before, during and after the EOT interval. Moreover, the mean lith size of reticulofenestrids are assessed from the middle Eocene to early Oligocene to ascertain if a relationship exists between declining CO<sub>2</sub> and coccolith size.

Chapter 3 is a detailed record of the middle Eocene to early Oligocene (40.40–32.02 Ma) calcareous nanofossil communities from NKK1 situated in the IPWP. Biostratigraphic events

and zonal boundaries are determined for NKK1 employing standard zonation schemes after Martini's (1971) NP zones and Agnini et al.'s (2014) CNE/O zones. The chapter addresses this site as a potential key location for coccolithophore speciation and a source of increased diversity during the EOT interval, with younger occurrences and diachroneity noted within specific nanoplankton species. A comprehensive systematic taxonomic list of all species recorded within the assemblage is provided with two new species described.

Chapter 4 documents the impact of climatic factors associated with long-term global cooling and carbon limitation on calcareous nannofossil diversity and coccolith size. Two datasets are analysed; Site U1482 at high resolution (200 ka) recording the late Miocene to early Pleistocene (7.7-1.7 Ma) interval and a global compilation of 9 Sites at low-resolution ( $\sim 2.5$  Ma) spanning the last 15 Ma. By combining these two datasets we aim to determine macroevolutionary driving mechanisms of calcareous nanoplankton communities in a deep-time perspective, while high-resolution results from U1482 serve as a representative tropical, high diversity succession with a continuous record, to detail the global response of the nanoplankton during this key climatic interval.



## 2 | LOW-LATITUDE CALCAREOUS NANNOFOS- SIL RESPONSE IN THE INDO-PACIFIC WARM POOL ACROSS THE EOCENE-OLIGOCENE TRANSITION OF JAVA, INDONESIA

This chapter is slightly altered from the following publication as is presented in *Paleoceanography and Paleoclimatology*:

**Jones, A.P.**,<sup>1</sup> Dunkley Jones, T.,<sup>1</sup> Coxall, H.,<sup>2</sup> Pearson, P.N.,<sup>3</sup> Nala, D.,<sup>1</sup> and Hoggett, M.<sup>1</sup>(2019) Low-Latitude Calcareous Nannofossil Response in the Indo-Pacific Warm Pool Across the Eocene-Oligocene Transition of Java, Indonesia. *Paleoceanography and Paleoclimatology*, 34, pp 1-15.

<sup>1</sup> School of Geography, Earth and Environmental Sciences, University of Birmingham, Birmingham, UK

<sup>2</sup> Department of Geological Sciences, Stockholm University, Stockholm, Sweden

<sup>3</sup> School of Earth and Ocean Sciences, Cardiff University, Cardiff, UK

Modifications from the print version of this chapter include, altered formatting; modified text in section 2.2.1 and other small text changes throughout chapter; The Age Depth Model (now Figure 2.2) and Plate 2.1 have been updated and both have been moved in text. The Age Depth Model is now positioned in Section 2.2 and Plate 2.1 is now in Section 2.4.

This publications full text and supplementary files can be retrieved at: <https://doi.org/10.1029/2019PA003597>

*The research presented in this chapter, including: data collection of nannofossil assemblages, data analysis, sample preparation, interpretation of results and writing the manuscript was conducted by myself. Co-author Tom Dunkley Jones (Calcareous nannofossil and palaeoceanography expert) co-designed the methodology and Tom, Helen Coxall (Planktonic foraminifera evolution and Eocene palaeoceanography expert) and Paul Pearson (Foraminifera, palaeoclimate and climate proxy expert) co-designed the research. Dominika Nala (Palaeontology and Geology BSc graduate) collected the coccolith size measurement data and from this I analysed and interpreted the data. Murray Hoggett (Geophysics and coding expert) wrote the R script code to the heatmap (Figure 2.8) used in this chapter, all other coding was completed by myself. All co-authors provided feedback on the interpretation of the results, and gave useful comments on early versions of the manuscript. The editorial "we" used herein reflects these contributions.*

## 2.1 INTRODUCTION

The geologically rapid step change in the global climate system across the Eocene-Oligocene Transition (EOT;  $\sim 34.5$ – $33.5$  Ma) (Coxall and Pearson 2007) is the most significant of the Cenozoic (Zachos et al. 2008). It is closely associated with the major expansion of continental Antarctic ice sheets (Bohaty et al., 2012; Coxall et al., 2005; Lear et al., 2008; Scher et al., 2011), global cooling (Liu et al. 2009), a reorganization of ocean circulation (Coxall et al. 2018, Egan et al. 2013, Elsworth et al. 2017, Goldner et al. 2014, Hutchinson et al. 2018, McKinley et al. 2019), and an altered biogeochemical cycle (the interaction between different plankton groups, the surface ocean and atmosphere were perturbed during the EOT due to declining  $\text{CO}_2$ ) (Egan et al. 2013, Lyle and Lyle 2006). Due to the fundamental changes in climate and biogeochemistry across the EOT, it is an important target for determining how large magnitude global environmental change can restructure key ecosystems, niche construction, and the evolutionary adaptive landscapes. Environmental changes across these intervals are primarily attributed to high-latitude drivers, specifically, the continental-scale glaciation of Antarctica (Bohaty et al. 2012, Coxall et al. 2005, Lear et al. 2008, Scher et al. 2011) and an increased role for the Southern Ocean in global circulation in global ocean overturning systems and

biogeochemistry (Egan et al. 2013, Goldner et al. 2014). Compilations of Cenozoic marine microplankton diversity shows the EOT is consistently identified as the interval of maximum change (Bown et al. 2004, Rabosky and Sorhannus 2009), often with important restructuring of ecological groups (Ezard et al. 2011), and a large shift in dominance between clades, through which multiple microplankton groups underwent community reorganisations due to environmental, oceanic and climatic changes during the EOT, therefore, previously dominant groups become outcompeted (Bown et al. 2004, Egan et al. 2013, Falkowski and Oliver 2007). Understanding the detailed climate drivers of this change remains largely unresolved (Ezard et al. 2011).

Coccoliths are the biocalcified plates produced by the phytoplanktonic coccolithophore algae, which post-mortem are often preserved in great abundances within marine sediments (Bown et al. 2004). The fossil record of the coccolithophores, and other associated calcareous nannofossils, is one of the most complete of any Cenozoic clade (Bown et al. 2004), exceeded only by the planktonic foraminifera (Ezard et al. 2011). Coccolithophore algae are a key component of modern pelagic ecosystems, especially in the tropical and mid-latitude oceans, estimated to be responsible for up to ~10% of total phytoplankton primary production (Poulton et al. 2006, 2007, 2017) and similar proportions of particulate inorganic carbon flux from the surface to the deep ocean (Schiebel 2002). Long-term diversity records indicate that nannofossils were an even more significant component of pelagic microplankton communities in the warm climates of the early Cenozoic (Bown et al. 2004). Strong evidence from the modern oceans (Beaufort et al. 2011, Rickaby et al. 2010, Rost and Riebesell 2004), and paleoecological studies (Dunkley Jones et al. 2008, Gibbs et al. 2013, Stoll et al. 2007, Villa et al. 2008, 2013) show that nannoplankton assemblages are controlled by environmental conditions, including nutrient availability and euphotic zone depth (Baumann et al. 1999, Liu et al. 2018). The exceptional calcareous nannofossil record, their importance to marine ecosystems, and their sensitivity to environmental change make them ideal for the reconstruction of the coupling between oceanic microplankton ecosystems and global climate change.

Here, we seek to determine the nature and drivers of tropical calcareous phytoplankton restructuring through the global cooling of the EOT. Our study section, the NKK1 borehole, is located in the center of the Indo-Pacific Warm Pool (IPWP) within late Eocene paleogeographic reconstructions and so provides the only continuous EOT sedimentary record from

the central IPWP known to date. NKK1 is one of few sites globally containing very well-preserved late Eocene and early Oligocene nannofossils, and we use this to analyse trends in coccolith size of the dominant placolith-forming reticulofenestrid coccolithophores, which is closely coupled to cell size (Henderiks and Pagani 2008). The Neogene reduction in coccolith size and calcification has been linked to declining surface ocean dissolved inorganic carbon (DIC) concentrations with falling atmospheric carbon dioxide levels ( $\text{CO}_2$ ) (Bolton et al. 2012, 2016, Bolton and Stoll 2013). The timing of the onset of this coupling is unclear with isotopic evidence indicating carbon limitation from the late Miocene (Bolton et al. 2016, Bolton and Stoll 2013), while others infer a  $\text{CO}_2$  control on lith size across the EOT (Bordiga et al. 2015). The tropical oligotrophic surface waters of the IPWP have the lowest DIC in the modern oceans (Krumhardt et al. 2017). If a carbon uptake limitation exists across the EOT, this should be most clearly seen in IPWP coccolith size records.

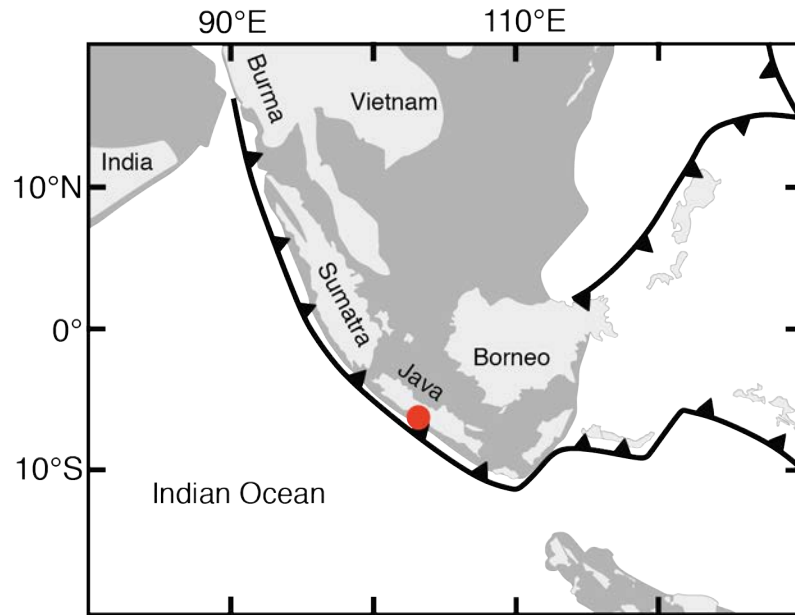


Figure 2.1: Paleoreconstruction of the Sunda region, southeast Asia during the late Eocene. Shades of grey represent Eurasian crust and red dot indicates the location of NKK1. Redrawn from Hall (2012).

## 2.2 MATERIALS AND METHODS

We present new records of calcareous nannoplankton species assemblages and diversity from the EOT deriving from a sequence of hemipelagic, continental slope and clay-rich sediments from the Nanggulan Formation of Java situated within the IPWP (Plate 2.1). Today

the IPWP, where surface water temperatures exceed 28°C throughout the year (De Deckker 2016), stretches across the western Pacific Ocean, through the Indonesian archipelago and into the eastern Indian Ocean, with climate models indicating it was much more extensive in the Eocene (Huber and Sloan 2001, Lunt et al. 2012, 2016). This study focuses on the middle Eocene to lower Oligocene succession of the Nanggulan Formation, recovered from a single borehole, NKK1, drilled in 2006 in the province of Nanggulan, south central Java (-7.788555°S, 110.20578°E, Figure 2.1).

### 2.2.1 LITHOSTRATIGRAPHY AND BIOSTRATIGRAPHY

Recovered strata consists of the middle Eocene upper Jetis Beds (88.02–99.98 meters below ground level (mbgl), totalling 11.98 m) and the upper Eocene to lower Oligocene Tegalsari Marls (86.85–41.04 mbgl, 45.81 m in total). Sixty-five core samples were analysed for calcareous nannofossil content, between samples NKK1-30 to NKK1-82 and are interpreted as belonging to calcareous nannofossil Zones CNE15 and CNE19–CNO3 of Agnini et al. (2014), equivalent to Zones NP17 and NP19/20–NP23 of Martini (1971). Three lithological units are recognised for this section of NKK1; Units VA, VB and VI (Figure 2.2). Unit VA is a greenish grey silty clay and mudstone and is documented above the top of the studied core interval at 40.7 mbgl to 70.5 mbgl and 75.5–89.0 mbgl. This unit is interrupted between 70.5–75.5 mbgl by Unit VB, a reddish-brown interval during the late Eocene, comprised of silty clays and mudstones (Figure 2.2). At 53 mbgl (core sample NKK1-38, 146 cm) an abrupt colour change occurs, from greenish grey to a lighter greenish grey and micropalaeontological evidence (the LO of planktic foraminifera *Hantkenina alabamensis*) suggests this is the Eocene-Oligocene Boundary (EOB) horizon. Nannofossil preservation and recovery was overall good from 55.71–74.95 mbgl of the VA and VB units and noted as good/excellent at 60 mbgl (late Eocene; CNE20 / NP19/20). Deduced to have originated from a hardground surface, numerous chips of brown cemented carbonate indicates a short-lived interruption of sedimentation seen at 76.14 mbgl (core NKK1-57, 38–39 cm). Hardening is noted at the base of Unit VA which terminates at 89 mbgl. An unconformity is recorded between 88.02 and 86.85 mbgl at the contact between the upper Jetis Beds and lower Tegalsari Marls (Figure 2.2). The Jetis Beds are Bartonian in age corresponding to CNE15 (NP16–NP17) and incorporates a small portion of the lower-most Unit VA and Unit VI. Unit VI consisted of thinly-bedded green-



ish grey sandy mudstones and are interbedded with alternating dark greenish grey volcanic sandstones. The nannofossil preservation varied from moderate in samples with a higher sand content to good in silty clay samples.

The Nanggulan Formation was most likely deposited in an outer shelf environment in proximity to a northward directed subduction zone, on the northern side of a relatively wide Indo-Pacific “gateway” (Hall 2012). In this scenario, the paleolatitude of the site during the late Eocene would have been similar to today at  $\sim 6.5^{\circ}\text{S}$  (Figure 2.1, redrawn after Hall 2012).

All data presented is on an integrated calcareous nannofossil and planktonic foraminiferal biostratigraphy, based on the biostratigraphic schemes and calibrations of Wade et al. (2011) for planktonic foraminifera and Agnini et al. (2014) for calcareous nannofossils, providing a coherent age model for NKK1 (Figure 2.2). All calibrated ages use the 2012 Geological Timescale (Gradstein et al. 2012), with the age-depth plot shown in Figure 2.2. Our study section spans  $\sim 8$  Ma of time, from the late Bartonian (39.33 Ma) to the early Rupelian (31.23 Ma) and includes a stratigraphically continuous succession through the EOT (CNE19-CNO3; Agnini et al. (2014), NP19/20-NP23; Martini (1971)).

A clear unconformity is present between the Jetis Beds and Tegalsari Marls between  $\sim 86.85$  to  $88.02$  mbgl with has an estimated time gap spanning  $\sim 38.59$  to  $36.05$  Ma and indicates the lithological boundary between Units VA and VI, nonetheless, dating the late middle Eocene was therefore problematic. We assume the LO of *Sphenolithus obtusus* to be true and use the First Occurrence (FO) of *Reticulofenestra bisecta* in NKK1 to establish an assumed model line. Above the unconformity, the Last Occurrence (LO) of *Globigerinatheka semiinvoluta* and the First Common Occurrence (FCO) of *Reticulofenestra isabellae* indicate Priabonian (late Eocene) aged sediments, representing a loss of  $\sim 2.5$  Ma. The FCO of *Reticulofenestra isabellae* and Last Common Occurrence (LCO) of *Reticulofenestra reticulata* are offset from the trend line. Both species are known to be diachronous and occur younger in NKK1 than other mid and high latitude localities (Berggren et al. 1995), therefore, we use the LO of the rosette-shaped Discoaster’s *D. saipanensis* and *D. barbadiensis* to mark the end of CNE20 (NP19/20).

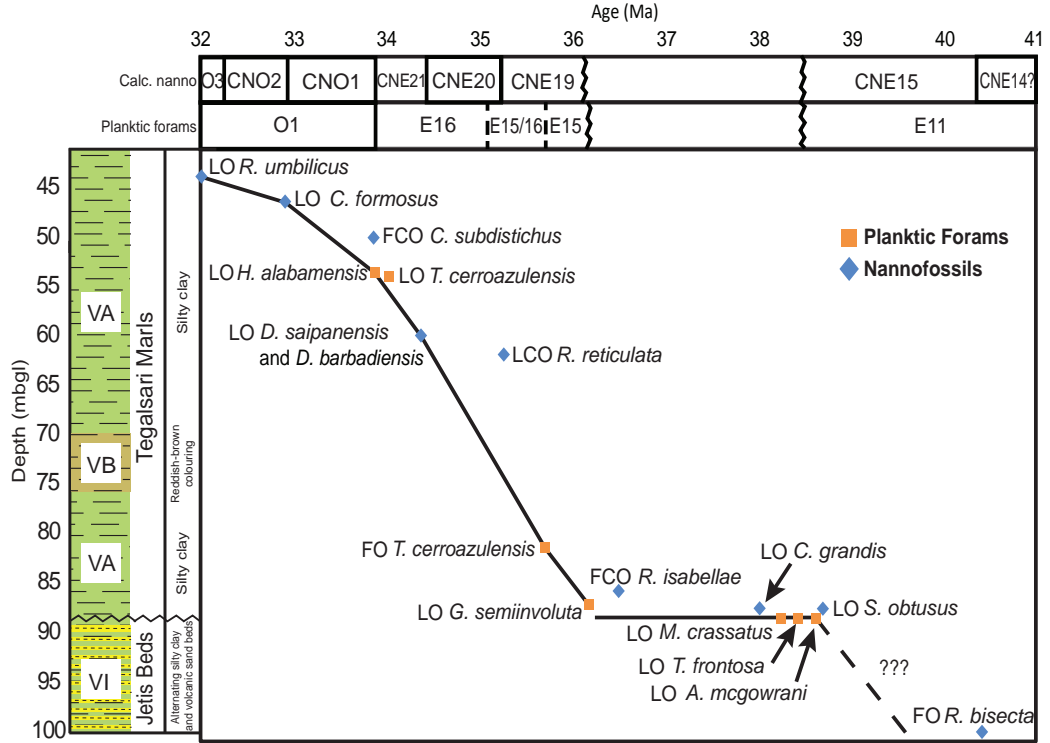


Figure 2.2: Age model for NKK1, displaying nannofossil and planktic foraminifera biostratigraphic datums with accompanying lithostratigraphic log. Bioevents after Agnini et al. (2014); datums and timescale recalibrated to GTS2012 (Gradstein et al., 2012).

Additionally, the FCO of *Clausicoccus subdistichus* is a subjective datum (assigned based on the opinion of the researcher) and therefore, was not used in the age depth model and instead, the LO of *Hantkenina alabamensis* depicted the Eocene-Oligocene Boundary (EOB) more accurately. The Top *Reticulofenestra umbilicus* event held uncertainty due to rare occurrences in the early Oligocene of NKK1. We surmised the position of *Reticulofenestra umbilicus* to be true (at 41.04 mbgl) and discounted the species rare occurrence. Well documented examples of mid-to-high latitude preferences for *R. umbilicus* exist, accounting for this species rarity in the early Oligocene (Villa et al. 2008).

## 2.2.2 SAMPLE PREPARATION

Samples were prepared using the “simple smear slide technique” after Bown and Young (1998b). Examination of smear slides was completed using a transmitted-light microscope (Zeiss AxioScope at X1,000 magnification) under cross-polarized light and plane-polarized light. Digital imaging was undertaken with a QImaging camera and the QCapture Pro 7

imaging software. Nannofossil assemblages were recorded quantitatively using a similar technique to the extended count technique (Bown and Young 1998b). This technique was modified by counting a total of 400 specimens and incorporated an additional scan of two complete slide transects to record the presence of further rare species not observed during the extended count, which are included in total species diversity analyses. Morphometric data for reticulofenestrid coccoliths were recorded from 31 samples at roughly equal spacing (approximately every other sample) through the succession. For each sample the maximum and minimum axes of more than 310 specimens of reticulofenestrid coccoliths were measured using the automated line measurement tool within the QCapture software. Due to the limitations of accurately identifying very small coccoliths with Light Microscope (LM) imaging, measurements were limited to specimens  $>2\text{ }\mu\text{m}$ .

## 2.3 RESULTS

### 2.3.1 RELATIVE ABUNDANCE

Calcareous nannofossils are abundant or common within sediments from the NKK1 cores, with preservation that is typically good in middle Eocene sediments and varies between good to excellent within the upper Eocene to lower Oligocene sediments (Unit VA). In the rare instances where samples have been taken from thin more sand-rich intervals, of the Jetis Beds, nannofossil preservation is moderate. (Figure 2.2). Percent relative abundances for key taxa are shown in Figures 2.3 and 2.4 with key trends noted below. A short succession of upper middle Eocene (Bartonian; Unit VI) sediments are recovered from NKK1, below the middle to upper Eocene unconformity commencing at 88.02 mbgl at the contact between the uppermost Jetis Beds (Unit VI) and lowermost Tegalsari Marls (Unit VA). Species within the *Reticulofenestra bisecta* group (*R. bisecta*  $<10\text{ }\mu\text{m}$ ; *Reticulofenestra stavensis*  $>10\text{ }\mu\text{m}$ ) dominate below the unconformity (Unit VI), but both decrease in abundance immediately above it (Figure 2.4). The *R. bisecta* group shows the most significant fall in abundance, decreasing to  $<1\%$  throughout the early late Eocene, in the Tegalsari Marls (Unit VA), before recovering during the first stages of the EOT ( $\sim 34.3\text{ Ma}$ ). The *Reticulofenestra reticulata* group (*Reticulofenestra isabellae*, *R. reticulata*, and *Reticulofenestra* sp. A) show differences in their abundance through the late middle Eocene to early late Eocene, above and below

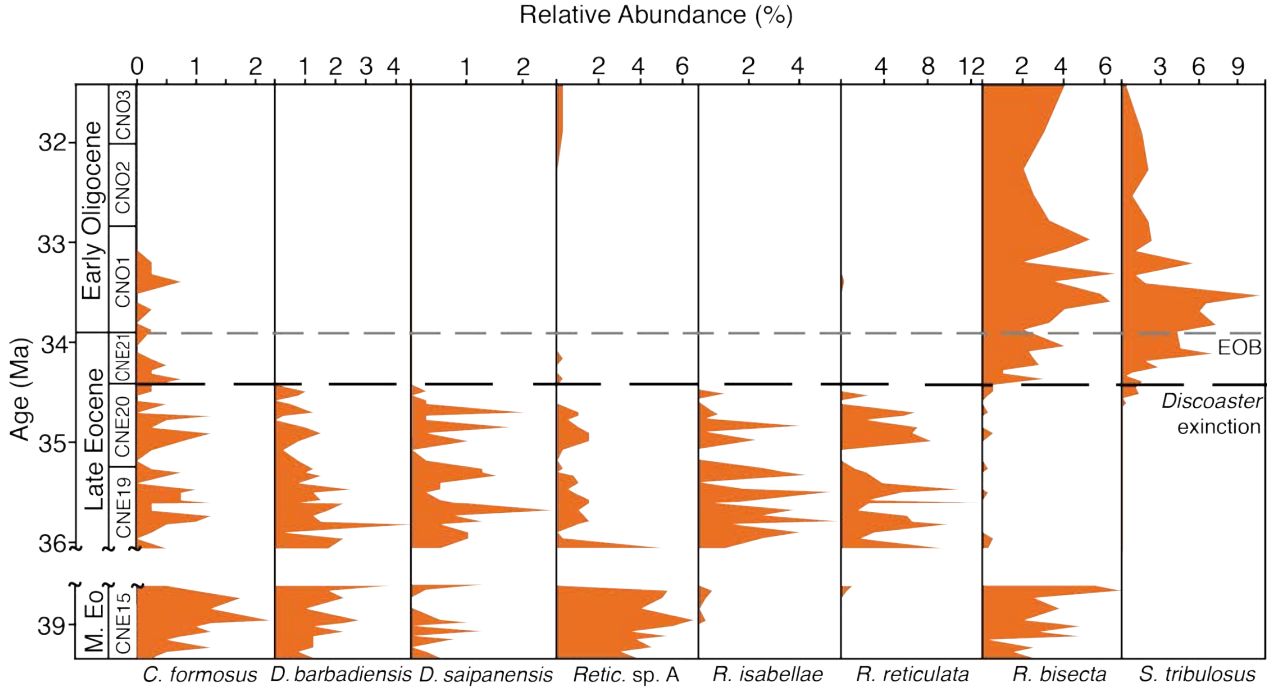


Figure 2.3: Relative abundance (%) of ecologically important nannofossil species against age, throughout the NKK1 core. Black long dashed line indicates Discoaster extinction, and light grey dashed line signifies the Eocene-Oligocene boundary(EOB). Unconformity ranges from 38.59–36.05 Ma.

the unconformity (Units VI and VA). *Reticulofenestra* sp. A is described as having a wide gridded central area similar to that of *R. reticulata* but is slightly smaller (medium to large placoliths) and lacks the distinct inner tube cycle present in *R. reticulata* and *R. isabellae*. *Reticulofenestra* sp. A is highest in abundance within the Jetis Beds, during the middle Eocene, and in this succession, is the first of the circular, gridded reticulofenestrids to appear, preceding both *R. reticulata* and *R. isabellae*. *Reticulofenestra reticulata* and *R. isabellae* are at their highest abundance within the late Eocene Tegalsari Marls (lower Unit VA) with *R. reticulata* being more abundant than *R. isabellae*. Immediately at the *Discoaster* extinction event (DEE), however, the group declines in abundance, and all but *Reticulofenestra* sp. A disappear, which has sporadic, potentially reworked, occurrences within the upper Tegalsari Marls lower Oligocene sediments (upper Unit VA).

*Discoaster barbadiensis* and *Discoaster saipanensis* show similar patterns of relative abundance (Figure 2.4) but with *D. barbadiensis* typically more common. In this record, both of these rosette *Discoaster* species disappear together, although given the sample resolution

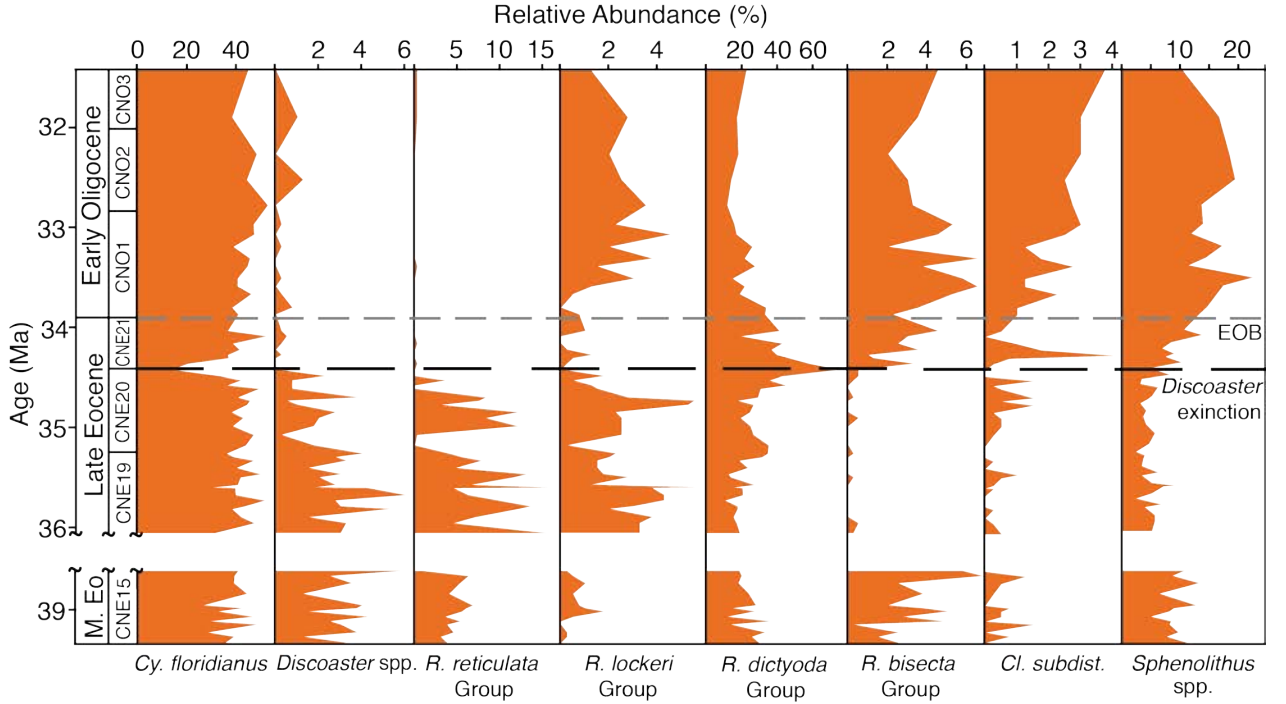


Figure 2.4: Relative abundance (%) of ecologically significant nannofossil groups and species against age. Black long dashed line indicates point of *Discoaster* extinction, and light grey dashed line signifies the Eocene-Oligocene boundary (EOB).

there is the potential for some small offset between these extinctions—up to 6 ka, based on the age model. We assign this biohorizon to the calibrated age for the *D. saipanensis* extinction of  $\sim 34.44$  Ma and use the extinctions of both species as a marker for the initiation of nannoplankton diversity decline in NKK1 before the Eocene-Oligocene Boundary (EOB) which we term the DEE. Following Pearson et al. (2008), this characteristic extinction of the rosette-shaped discoasters (end of biozone CNE20; Agnini et al. 2014) are used to mark the start of the EOT interval and associated biotic perturbations. This DEE coincides with a decline in the abundance of several significant species, including *Reticulofenestra isabellae* and *R. reticulata* (Figure 2.3). These declines are matched by abundance increases in *R. bisecta* group, *Sphenolithus* spp., and *Sphenolithus tribulosus* through the same interval, with the *R. bisecta* group increasing back to abundances similar to those in the middle Eocene succession ( $\sim 3$ –6%). *Cyclicargolithus florianus* consistently dominates assemblages from both middle and upper Eocene sediments, with relative abundances typically greater than 40%. At the DEE, however, there is a sharp and sudden but transient drop in *C. florianus* abundance, down to less than 15%. This fall in abundance appears to be compensated within the reticulofenestrids by a significant increase in the abundance of the *Reticulofenestra dic-*

*tyoda* group (*R. dictyoda*, *Reticulofenestra minuta*, *Reticulofenestra moorei*, *Reticulofenestra umbilicus*, and *Reticulofenestra wadeae*), which reaches its highest values for the entire succession (Figure 2.4). At the DEE there is also a fall in abundance of the *Reticulofenestra lockeri* group (including *Reticulofenestra daviesii*, *Reticulofenestra filewiczii*, *R. lockeri*, and *Reticulofenestra macmillani*), with abundances that remain low until the later stages of the EOT (~33.8 Ma).

Through the EOT, key abundance trends that started at the DEE tend to continue, with further increases in *Sphenolithus* spp. and *R. bisecta* group abundances, while the *R. lockeri* group displays a full recovery during the latter part of the EOT. *Clausicoccus subdistichus* was present throughout the middle to late Eocene but increased significantly immediately after the start of the DEE. After this large spike, abundance dipped slightly before recovering and continuing to rise in the latter part of the EOT and its FCO is assigned to sample NKK1-35b, 109-110 cm.

### 2.3.2 PRINCIPAL COMPONENT ANALYSIS AND DIVERSITY

To determine the dominant temporal trends in overall assemblage compositions, including groupings of species with similar responses to environmental forcing, a principal component analysis (PCA) was undertaken using the R software. Species of low abundance were excluded from the PCA, identified as those with a standard deviation of relative abundance across all samples of less than 0.5% (Dunkley Jones et al. 2008). Species relative abundances were then resummmed to 100% and zero values replaced with nonnegative values (0.01%) prior to an additive log ratio transformation of the relative abundance data. Only the first two principal components, PC1 and PC2, are taken into consideration, representing the majority of the assemblage variability (eigenvalues of 39.8% and 19.2%, respectively, for PC1 and PC2). Taxa are ranked with respect to their PC1 and PC2 loadings in Figure 2.5. We identify subgroups of taxa with the greatest positive and negative loadings for PC1 and PC2: Groups 1A and 1B and Groups 2A and 2B (Figures 2.5 and 2.6). For each of these groups, we plot the summed total relative abundances of all the species within each group and show their variation through time in Figure 2.6, alongside PC1 and PC2 score for each sample. A cross-plot of PC1 and PC2 scores demonstrates a clear three-way separation of samples: middle Eocene (Bartonian) assemblages with strongly positive PC2 scores and slightly negative PC1

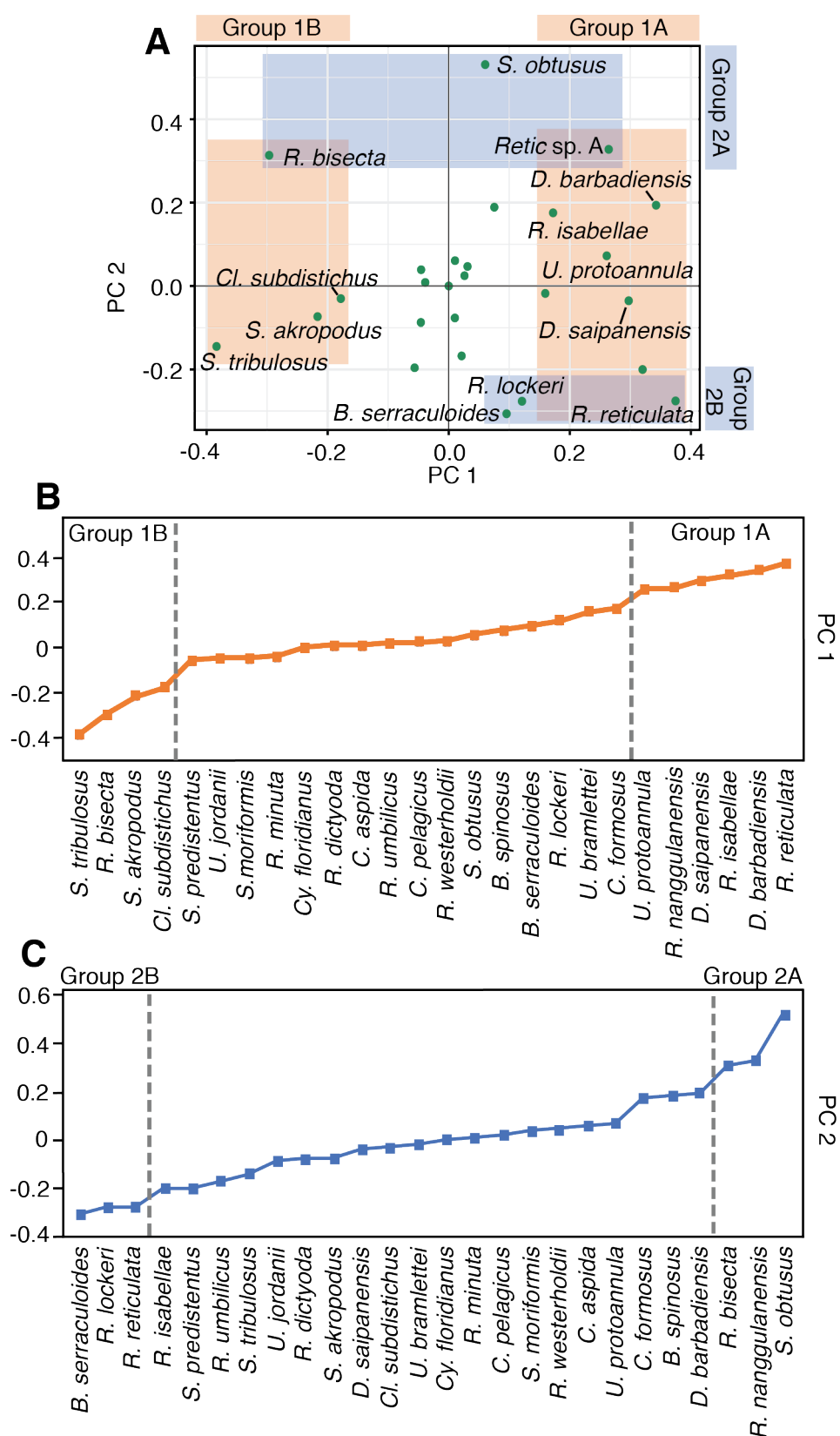


Figure 2.5: (a) Scatter plot to show species loading scores of the ecologically important nannofossil groups for PC1 and PC2. Groups 1A and 1B are indicated vertically by orange boxes, and Groups 2A and 2B are horizontal and in blue. (b) Line graph to show the loading scores of individual species in PC1 for Group 1. Vertical grey dashed lines separate the taxa defining Group 1. (c) Line graph to show the loading scores of individual species seen in PC2; vertical grey dashed lines indicate taxa comprising Group 2.

scores; late Eocene (Priabonian) assemblages with negative PC1 and PC2 scores; and early Oligocene assemblages with strongly positive PC1 scores and slightly negative PC2 scores (Figure 2.7). This analysis provides clear evidence for two major shifts in the calcareous nannofossil assemblages—one across the middle to upper Eocene unconformity and one at the DEE event, when PC1 scores shift from negative to positive values.

Strongly positive PC2 scores of middle Eocene assemblages reflect the presence of *Sphenolithus obtusus*, which is only present in the middle Eocene, and high abundances of *R. bisecta* and *Reticulofenestra* sp. A (Figures 2.5 and 2.6). Together these species make up Group 2A, which forms ~20% of assemblages within these late middle Eocene assemblages (Figure 2.6). Late Eocene assemblages are dominated (15%) by the strongly positive PC1 scoring taxa (Group 1A) *Discoaster barbadiensis*, *D. saipanensis*, *R. isabellae*, *Umbilicosphaera protoannula*, and *Reticulofenestra reticulata* (Figures 2.5 and 2.6). Through the DEE, Group 1B taxa—*Reticulofenestra bisecta*, *Cl. subdistichus*, *S. akropodus*, and *Sphenolithus tribulosus*—increase in abundance (Figure 2.6). These assemblage shifts demonstrate a clear response within the entire calcareous phytoplankton community structure to the DEE event. In contrast to the shifts in assemblages coupled to the DEE, calcareous phytoplankton assemblages are relatively stable through the later, main phases of the EOT climate shift.

A total of 120 calcareous nannofossil species were observed within sediments recovered from the NKK1 borehole. To explore trends in species diversity through the recovered succession, we plot the Shannon diversity (H) and the natural log of species richness ( $\ln(S)$ ) in Figure 2.8. The difference between these two indexes is the natural log of evenness, such that when H diversity approaches  $\ln(S)$  assemblages are more even, and when these two metrics diverge assemblages are more dominated by fewer taxa. The middle Eocene has the highest recorded species diversity, with relatively stable and high values of both H and  $\ln(S)$ . Through the late Eocene there is a steady decline in both H and  $\ln(S)$  diversity, but with particular species diversity lows centered on ~35.6 and 35.3 Ma. Species and ecological diversity continue to fall following the DEE, with both metrics reaching their lowest values between the DEE and the EOB. Both metrics of diversity then recover slightly into the early Oligocene.



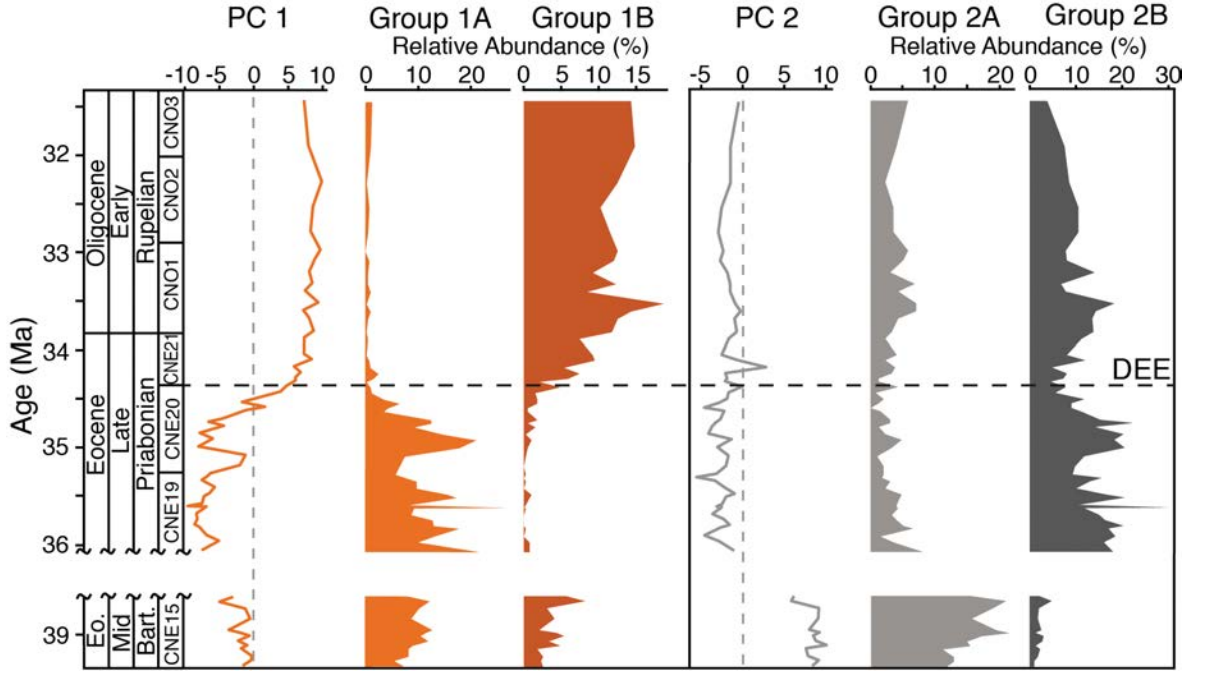


Figure 2.6: Principal Component score with respect to their corresponding nannofossil groups (the summed total relative abundances of all the species within a group) against age, demonstrating the ecological effects on each group moving through time. PC1 and PC2 have differing group results; the different species composing each group react according to ecological changes. Biozonation scheme after Agnini et al. (2014).

### 2.3.3 NANNOFOSSIL COCCOLITH SIZE

An interpolated heat map of the frequency distribution of reticulofenestrid coccolith size is shown in Figure 2.8, along with the mean and the 95th percentile ( $95\%_{tile}$ ) coccolith size—a metric which is less biased by outliers than maximum size (Chapelle and Peck, 1999). Middle Eocene assemblages have an average lith size around  $\sim 4 \mu\text{m}$ , with minimal variation, and include a high proportion (40–63%) of smaller reticulofenestrids ( $< 3.5 \mu\text{m}$ ) (Figure 2.8). There is a marked change in coccolith size across the middle to late Eocene unconformity, with an increase in mean coccolith size from  $\sim 4$  to  $\sim 5 \mu\text{m}$ . This is mostly driven by a reduction in the abundance of very small coccoliths ( $< 3.5 \mu\text{m}$ ) in the late Eocene, from an average of 52% to  $< 22\%$ , although there is also an increase in the frequency of coccoliths larger than  $8 \mu\text{m}$ , which is clearly visible in the heat map during intervals when the  $95\%_{tile}$  exceeds  $10 \mu\text{m}$ . This trend away from small coccolith size continued from the late Eocene to the early Oligocene. The  $< 3.5 \mu\text{m}$  coccoliths immediately preceding the DEE dominate with a percentage of  $> 40\%$ , but this falls to  $< 5\%$  after this event. The loss of this small size fraction will influence mean and  $95\%_{tile}$  coccolith size, but the re-emergence of taxa such as

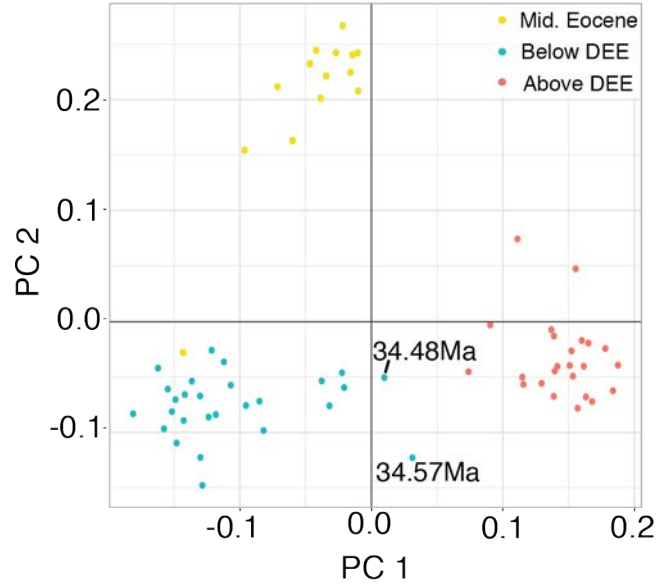


Figure 2.7: Principal Component Analysis (PCA) scatter plot to depict the relationship between middle Eocene samples and samples occurring above and below the *Discoaster* extinction (DEE). Yellow dots indicate Middle Eocene samples; blue dots and pink dots represent above and below the DEE, respectively.

*Reticulofenestra bisecta* group, with relative abundances going from <1% before the DEE to 3% after the DEE and then >6% (Figure 2.4) in the early Oligocene, indicates a genuine re-emergence of larger reticulofenestrid morphotypes.

## 2.4 DISCUSSION

The succession recovered from the NKK1 borehole allows for the reconstruction of tropical calcareous phytoplankton dynamics through the critical EOT interval. It is one of few tropical sites with continuous and good calcareous nannoplankton preservation through this time period, enabling examination of environmental drivers associated with long-term tropical phytoplankton ecosystems. The NKK1 record provides information on three key components of middle to late Eocene biotic and oceanographic change: first, a distinguishable transition between late middle and early late Eocene tropical phytoplankton communities that can be associated with similar changes in the Southern Ocean; second, the presence of a major community restructuring and extinction event at the very start of the EOT; and finally, determining if there is any evidence for coccolithophore cell size limitation in response to declining global CO<sub>2</sub> across the EOT.

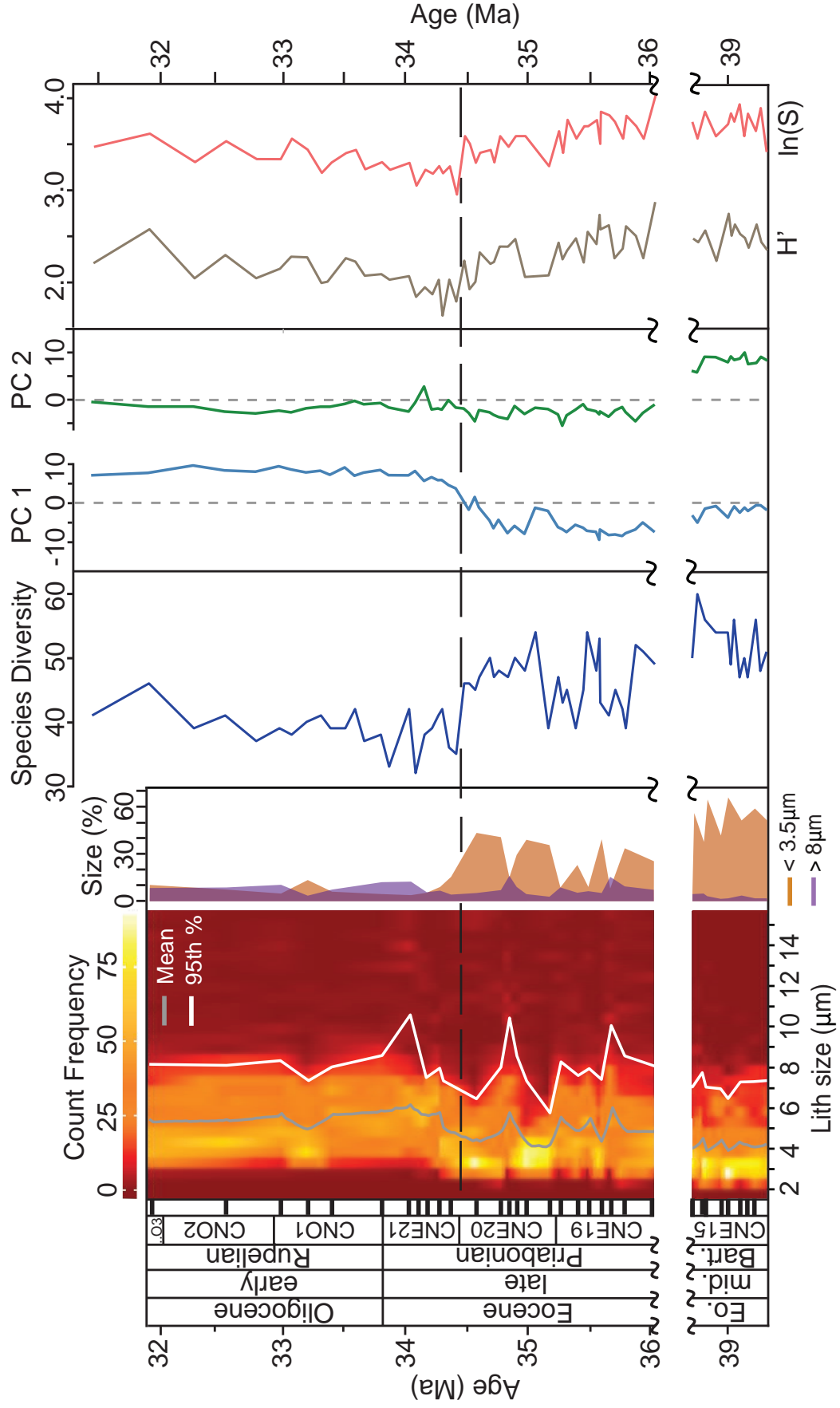


Figure 2.8: Heatmap, nannofossil size (%), species diversity, PC score, and SHE analysis (Species richness, diversity (H) and Evenness) diversity plotted against age. Grey dashed line represents the *Discoaster* extinction. Age calibration after Agnini et al. (2014).

### 2.4.1 TROPICAL PHYTOPLANKTON EVOLUTION THROUGH THE MIDDLE TO LATE EOCENE

The upper middle Eocene succession of NKK1 ( $\sim 39.3$  Ma to 38.5 Ma) recovers sediments deposited after the Middle Eocene Climatic Optimum (MECO) but before the Middle Late Eocene Turnover (Newsam et al. 2017). Therefore, assemblage changes between the middle and upper Eocene of NKK1 should be independent of perturbations associated with the MECO, but rather, record longer term shifts associated with global cooling across the middle to late Eocene boundary (Cramwinckel et al. 2018). Across the middle to upper Eocene unconformity, which represents a time gap of  $\sim 2.5$  Ma ( $\sim 38.59$  to 36.05 Ma), there is a marked change in assemblages including 10 species extinctions and seven inceptions. Although it is impossible to assess the rates and timing of assemblage change during the unconformity, this interval includes the marked transition from oligotrophic to eutrophic-favoring calcareous phytoplankton assemblages in the Southern Ocean at  $\sim 36.2$  Ma (Villa et al. 2013). In NKK1, there is also a clear decline in the abundance of distinct warm-water/oligotrophic taxa, such as *Coccolithus formosus*, *Discoaster* spp., and *Sphenolithus obtusus* and an increase in known colder-water eutrophs within the *R. lockeri* group (Newsam et al. 2017, Villa et al. 2008) across the unconformity (Figures 2.3 and 2.4). This change in assemblage composition is also clearly shown in the shift from strongly positive to negative values in PC2 (Figure 2.6). The late Eocene increase in *R. reticulata* group abundance (Figure 2.6), interpreted as warm to temperate eurytopic and mesotrophic taxa (Newsam et al. 2017), also supports this shift from strongly oligotrophic conditions in the late middle Eocene to more mesotrophic conditions within the late Eocene.

This shift from warm-water and oligotrophic conditions to mesotrophic in the late Eocene seen in NKK1 nanoplankton assemblages reflects long-term changes in Southern Ocean ecosystems across the late middle to late Eocene, including an increased dominance of the siliceous microplankton (Baldauf 1992, Diester-Haass 1995, Diester-Haass and Zachos 2003, Diester-Haass and Zahn 2001). Southern Ocean cooling and enhanced circulation driven by the progressive opening of the Drake Passage and Tasman Gateway in the middle to late Eocene (Goldner et al. 2014) might be the ultimate cause of these ecosystem changes, but such changes in primary production can drive strong biogeochemical feedbacks that drawdown atmospheric CO<sub>2</sub> and accelerate global cooling (Egan et al. 2013, Goldner et al. 2014, Za-

chos and Kump 2005). These changes are consistent with increased nutrient leakage from the Southern Ocean to lower latitudes (Egan et al. 2013), driven by a combination of enhanced deep-water mixing and nutrient supply to the surface Southern Ocean and then enhanced intermediate water advection of these waters toward the tropical ocean. This observed restructuring of far-field tropical phytoplankton communities in the IPWP, during the middle to late Eocene, seems to largely be driven by this process, which dominates nutrient supply to the modern tropical oceans (Sarmiento et al. 2004).

One of the most notable signals within the NKK1 record is the near-complete loss of *R. bisecta* (abundances <1%; Figure 2.3) within the late Eocene, when this species is abundant in both the upper middle Eocene and recovers to high abundances in lower Oligocene sediments. Such a pattern of partial abundance decline is not easily related to the dominant trend of global cooling from the late middle Eocene to early Oligocene. A reduction in *R. bisecta* abundance is recorded from mid-latitude sites in the western (DSDP [Deep Sea Drilling Project] Site 516) and eastern (DSDP Site 360) South Atlantic through the middle to late Eocene transition (Wei and Wise 1990), but at these locations abundances remain low into the early Oligocene. Although without a complete record through the late Eocene, *R. bisecta* relative abundances reach over 30% in the earliest Oligocene of DSDP Site 366 in the western tropical Atlantic and first appear and then peak in abundance during the early Oligocene at equatorial Indian Ocean ODP (Ocean Drilling Program) Site 711 (Fioroni et al. 2015). The pattern of long-term declining *R. bisecta* abundance in middle to high latitudes through the late middle to late Eocene, followed by increased abundances in the tropics in the earliest Oligocene, is consistent with a “temperate-warm water” affinity (Wei and Wise 1990, Persico and Villa 2004), a niche which gradually shifts toward tropical locations through the middle Eocene to early Oligocene cooling. The anomaly in this pattern is the relatively high abundances of *R. bisecta* morphotypes in the late middle Eocene of the NKK1 core. This pattern could either represent a transient post-MECO response of *R. bisecta* (Fioroni et al. 2015, Wei and Wise 1990) or imply the presence of two ecotypes—a tropical middle Eocene form and a more temperate late middle Eocene to Oligocene form with different ecological and biogeographic ranges.

### 2.4.2 LATE EOCENE IMPACT EVENTS AND PHYTOPLANKTON DIVERSITY

Calcareous nannofossil species diversity is variable within the late Eocene with two particular lows at 35.8 and 35.4 Ma (Figure 2.8). These changes in species diversity are broadly contemporaneous with the onset of the late Eocene “climate instability” in the Southern Ocean between 35.8 and 34.1 Ma (Passchier et al., 2017; Scher et al., 2014). The late Eocene also witnessed two of the Cenozoic’s largest impact events, the Popigai impact situated in the Anabar Shield of central Siberia, which generated a widely distributed microspherule strewn fields at  $\sim 35.7 \pm 0.2$  Ma (Bottomley et al., 1997; Rampino and Calderia 2017), and the Chesapeake Bay impact at  $\sim 35.3 \pm 0.1$  Ma that produced a tektite/microtektite strewn field across south eastern North America (Liu et al., 2009; Rampino and Caldeira, 2017). The far-field effects of the Popigai impact are recorded in the Southern Ocean ODP Sites 689 and 1090, with a clinopyroxene spherule layer and an iridium spike at circa 35.8 Ma coinciding with a decrease in benthic and bulk carbonate  $\delta^{13}\text{C}$  ( $\sim 0.5\text{‰}$ ) (Passchier et al., 2017), which is interpreted as an enhanced phase of cooling and increased productivity. In the northern midlatitudes, there is evidence for persistent postimpact environmental change within dinoflagellate and calcareous nannofossil assemblages (Coccioni et al., 2000; Vonhof et al., 2000), consistent with enhanced productivity and/or transient cooling. Although a tight correlation between the notable late Eocene minima in species diversity and these impact events is not yet possible, they are closely associated in time based on the current age model (Figure 2.2).

Plate 2.1

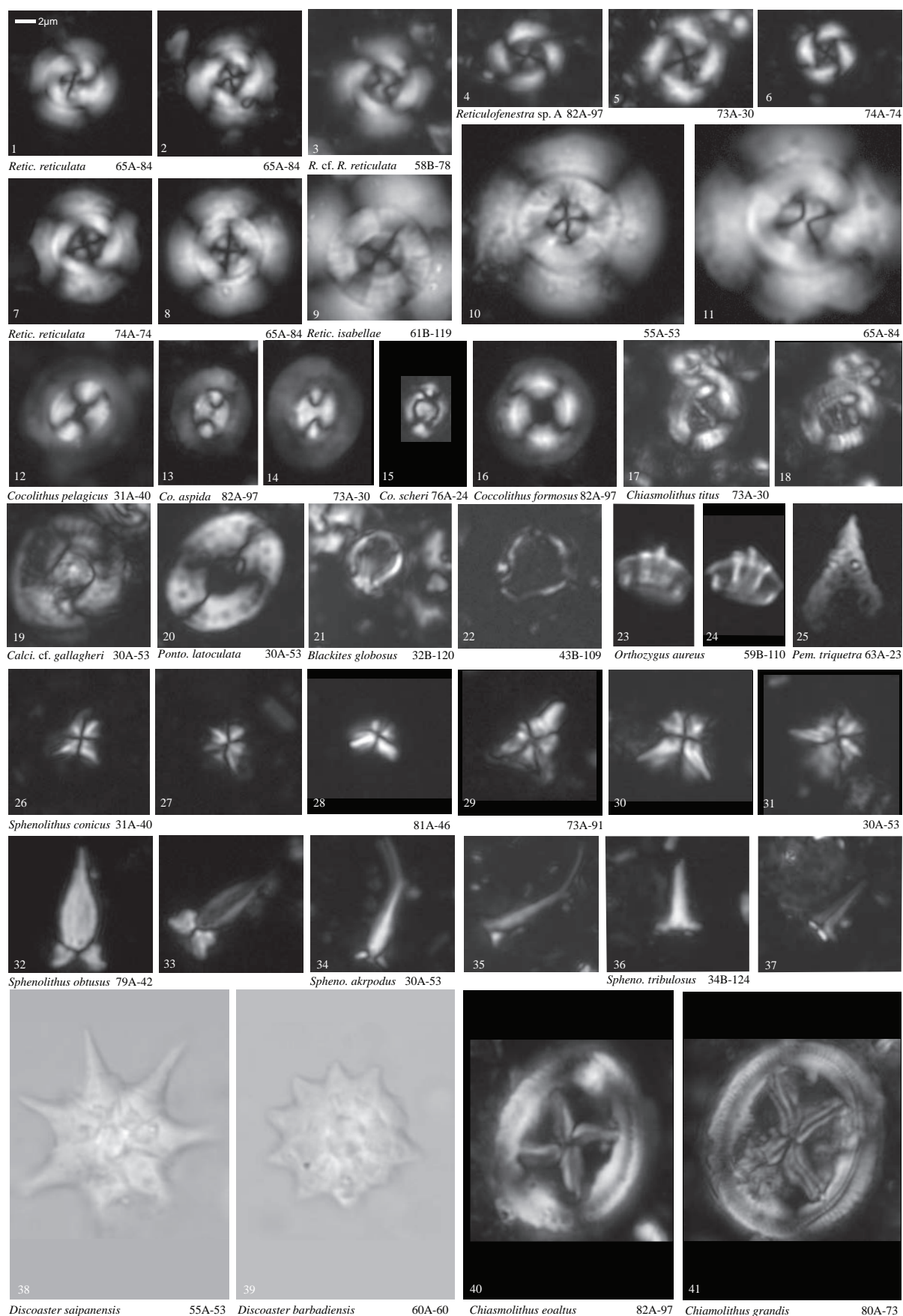


Plate 2.1: A selection of calcareous nannofossils from NKK1. Scale bar in top left corner is representative for all images. **1-2.** *Reticulofenestra reticulata*, **3.** *Reticulofenestra* cf. *reticulata*, **4-6.** *Reticulofenestra* sp. A, **7-8.** *Reticulofenestra reticulata*, **9-11.** *Reticulofenestra isabellae*, **12.** *Coccolithus pelagicus*, **13-14.** *Coccolithus aspida*, **15.** *Coccolithus scheri*, **16.** *Coccolithus formosus*, **17-18.** *Chiasmolithus titus*, **19.** *Calcidiscus* cf. *gallagheri*, **20.** *Pontosphaera latoculata*, **21-22.** *Blackites globosus*, **23-24.** *Orthozygus aureus*, **25.** *Pemma triquetra*, **26-31.** *Sphenolithus conicus*, **32-33.** *Sphenolithus obtusus*, **34-35.** *Sphenolithus akropodus*, **36-37.** *Sphenolithus tribulosus*, **38.** *Discoaster saipanensis*, **39.** *Discoaster barbadiensis*, **40.** *Chiasmolithus eoaltus*, **41.** *Chiasmolithus grandis*.

### 2.4.3 EXTINCTION AND COMMUNITY RESTRUCTURING AT THE START OF THE EOT

The most prominent ecological transition seen in NKK1 tropical calcareous phytoplankton assemblages is directly associated with the extinction of the rosette-shaped discoasters at ~34.4 Ma (Agnini et al. 2014, Fioroni et al. 2015). At the DEE level in the NKK1 core, extinctions of several species are coupled with a systematic shift in species dominance. Documenting this change is important because it occurs at the onset of the EOT, preceding the proposed onset of Antarctic glaciation at the first  $\delta^{18}\text{O}$  step by ~300 kyr (Westerhold et al. 2014) and clearly indicates a major perturbation in the global surface ocean. The extinction of the rosette discoasters has long been known as one of the most important of the Cenozoic (Martini 1971) and led the characteristic EOB extinctions of the hantkeninid planktonic foraminifera (Berggren et al. 1995) but have only recently been correlated in detail with the climate evolution of the EOT (Pearson et al. 2008). Our PCA clearly demonstrates the distinction between phytoplankton communities above and below the DEE (Figure 2.6), with a decrease in Group 1A (*Reticulofenestra reticulata*, *R. isabellae*, *Reticulofenestra* sp. A, *D. saipanensis*, *D. barbadiensis*, and *U. protoannula*) and increase in Group 1B (*R. bisecta*, *S. akropodus*, and *S. tribulosus*) taxa across this event (Figures 2.3 and 2.4). Given the ecological associations of these taxa, we argue that this change in PC1 is primarily driven by a shift from oligotrophic to more mesotrophic conditions. The most rapid fall in species richness in NKK1 is directly associated with the DEE, including the loss of taxa with specific ecological tolerances, e.g. *Reticulofenestra* spp. (Figure 2.8) (*D. barbadiensis*, *D. saipanensis*, *Reticulofenestra* sp. A, *R. reticulata*, *R. isabellae*, and *R. reticulata*). Almost all of these abundance shifts are remarkably similar, in timing and nature, to those recorded at ODP Site 711 in the equatorial Indian Ocean (Fioroni et al. 2015), indicating a regional, basin-wide re-



sponse. This is supported by the timing of the major assemblage shifts in the western tropical Indian Ocean, which are also focused on the DEE and substantially lead the “first step” of the EOT climate transition (Dunkley Jones et al. 2008). The nature of these assemblage shifts and the DEE event points toward a global-scale increase in nutrient supply to the tropical and subtropical surface ocean at the onset of the EOT.

The of *R. reticulata* in NKK1 occurs just before the DEE at  $\sim 34.5$  Ma, in a similar position to that recorded in equatorial Indian Ocean ODP Site 711 (Fioroni et al. 2015). This event is known to be diachronous across latitudes (Berggren et al. 1995), with calibrated ages of 35.29 Ma in the subtropics (Agnini et al. 2014) updated to GTS 2012, Gradstein et al. 2012) and between 36.5 and 36.3 Ma in the high latitudes (Persico et al. 2012, Villa et al. 2008). The last occurrence of *R. isabellae* (or *Cribrocentrum isabellae*), is coincident with the last occurrence of *R. reticulata* in NKK1, and both forms show parallel fluctuations in abundance through the late Eocene. Both species are absent across a short interval just below the DEE, between 64.55 and 61.75 mbgl, with their final occurrence recorded at 61.57 mbgl, or  $\sim 10$  kyr before the DEE (biozone CNE20; Agnini et al. 2014). These trends strongly suggest that, in the NKK1 assemblages at least, *R. isabellae* are simply large morphotypes of *R. reticulata*. These findings are similar to the abundance variations of these two taxa, including a coincident last occurrence, found by Fornaciari et al. (2010). There are two potential interpretations of the proximity of top *R. reticulata* to top *D. saipanensis* in NKK1; either there is a substantial slowdown or cessation of sedimentation at this level or the known latitudinal diachroneity of the top *R. reticulata* between the high and mid latitudes continues to the low latitude oceans, where this species persists the longest. This event is calibrated to occur at 36.3 and 36.5 Ma at Southern Ocean ODP Holes 784B (Villa et al. 2008) and 689D (Persico et al. 2012), respectively. At middle and low latitudes (IODP Sites: 1218, 1051, 1052, and 1262; DSDP Site 522 and Cicogna and Possagno sections) (Agnini et al. 2014), calibrate the bioevent at 35.29 Ma, making it clearly diachronous across latitudes. Given the coherency of the independently derived planktonic foraminiferal and calcareous nannofossil biostratigraphies (Figure 2.2), most consistent with continuous sedimentation through upper Eocene successions of NKK1, we suggest the most likely resolution of the clear offset of the top *R. reticulata* biohorizon is latitudinal diachroneity in this bioevent.

The peak in the abundance of the *R. dictyoda* group at the DEE, to over 60% of the assem-

blage, with a simultaneous decrease in the otherwise abundant *Cyclicargolithus floridianus*, indicates a transient change in communities associated with this event. *Reticulofenestra minuta*, a major component of this *R. dictyoda* group excursion, is suggested to be a cooler-water eutroph and an opportunist (Newsam et al. 2017, Wade and Bown 2006) unlike *C. floridianus* which dominates in late Eocene and Oligocene low- and middle-latitude assemblages (Dunkley Jones et al. 2008, Wei and Wise 1990). The switch in dominance between these two taxa is consistent with a significant but transient eutrophication of tropical surface waters, accounting for the final demise of the Paleogene rosette-shaped discoasters. We argue for a nutrient rather than temperature control on these assemblage changes because there is no evidence for global or regional surface water cooling at this time. For example, planktonic foraminiferal Mg/Ca records from the western Indian Ocean show no sea surface cooling associated with the nannofossil species turnover of the DEE at 34.44 Ma, with any cooling linked to the first step of the EOT at  $\sim 34$  Ma (Lear et al. 2008). The cause of increased nutrient supply to the tropical oceans at  $\sim 34.4$  Ma is uncertain, but new data from the continental margin of East Antarctica indicate the development of ephemeral mountain glaciers from 35.9 Ma with a major ice sheet advance at 34.44 Ma (Passchier et al. 2017). Silicon isotopes also show increased nutrient leakage out of the Southern Ocean during the late Eocene (Egan et al. 2013), a process which may have increased with the cooling of Southern Ocean waters once the East Antarctic Ice Sheet (EAIS) reached the continental margin (Passchier et al. 2017).

#### **2.4.4 CO<sub>2</sub> CONTROL ON PHYTOPLANKTON SIZE ACROSS THE EOT**

There is increasing evidence that the long-term decline in atmospheric CO<sub>2</sub> concentrations through the Cenozoic is a significant driver of calcareous nannoplankton macroevolution and cell physiology (Bolton and Stoll 2013, Bolton et al. 2012, 2016). Within the Neogene, declining atmospheric  $p\text{CO}_2$  reduced aqueous[CO<sub>2</sub>] within the surface ocean (Bolton and Stoll 2013) and caused a reallocation of bicarbonate ions (HCO<sub>3</sub><sup>3-</sup>) from coccolithophore calcification to photosynthesis (Bolton and Stoll 2013). Two robust lines of evidence exist: first, the onset of large size-dependent coccolith  $\delta^{13}\text{C}$  vital effects (Bolton and Stoll 2013) and second, a systematic reduction in coccolith size and mass (Bolton et al. 2016, Suchéras-Marx and Hendriks 2014). Both strongly support this change in cellular carbon allocation from the late Miocene onward. On longer timescales, the presence of very large coccolith taxa during the

high  $p\text{CO}_2$  and warm climates of the early to middle Eocene (Henderiks and Pagani 2008), together with the clear patterns of Eocene to Oligocene cooling (Cramer et al. 2011, Lear et al. 2004, Liu et al. 2009, Zachos et al. 2001, 2008) and declining  $p\text{CO}_2$ , poses the question of whether Paleogene nannofossil macroevolution was also strongly controlled by  $p\text{CO}_2$ . Some studies of coccolith size do indicate a loss of large coccoliths across the EOT and infer this to be driven by cell size limitation with declining  $p\text{CO}_2$  (Bordiga et al. 2015)(Plate 2.1).

The new reticulofenestrid size records presented here show no increased dominance of smaller coccoliths with declining  $p\text{CO}_2$  across the EOT (Pagani et al. 2011, Pearson et al. 2009). These records come from the tropical IPWP, a region with the lowest DIC concentrations in the modern system and where algal communities experience the strongest carbon uptake limitation. In the NKK1 record we observe an increase in both the mean and 95%<sub>tile</sub> reticulofenestrid coccolith size across the EOT with a shift toward the dominance of larger species such as *Reticulofenestra umbilicus*, *R. bisecta*, and *R. stavensis* and a notable loss of small reticulofenestrids ( $<3.5\mu\text{m}$ ; Figure 2.8). These coccolith size records provide no evidence for a significant  $p\text{CO}_2$  limitation on cell size across the immediate EOT. This is not to say that there is no longer-term  $p\text{CO}_2$  control on coccolithophore cell size through the Paleogene, as by the late Eocene the very large early to middle Eocene taxa are mostly absent. In other words, the cell size distribution present during the late Eocene appears to have been insensitive to  $p\text{CO}_2$ , but this cell size distribution might have already been strongly selected by earlier cooling and  $p\text{CO}_2$  declines between the middle and late Eocene (Gibbs et al. 2018, Henderiks and Pagani 2008).

## 2.5 CONCLUSION

Our data provides the first recorded response of IPWP calcareous phytoplankton communities to global cooling from the late middle Eocene to early Oligocene. We interpret assemblage changes and the progressive loss of species through this interval to be a direct response to enhanced nutrient supply to tropical surface waters from Southern Ocean-sourced subthermocline waters. Community restructuring and extinctions were most intense across the extinction of the rosette-shaped discoasters, *D. barbadiensis*, and *D. saipanensis* at  $\sim 34.4$  Ma. The nature and timing of these assemblage changes are shown to have consistent features between globally distributed locations, including the extinction of warm-water oligotrophs and

the increased dominance of eutrophic and/or those with temperate- and cool-water affinities. The DEE event is also the earliest biotic response to the large-scale environmental changes of the EOT, occurring substantially before the planktonic and benthic foraminiferal extinctions at the EOB. In contrast, there is relatively little change in calcareous phytoplankton communities across the EOB. Overall, our results indicate a substantial increase in nutrient supply to the tropical oceans at the very start of the EOT, potentially associated with either increased continental weathering or nutrient leakage from the Southern Ocean. Whether these perturbations at the start of the EOT are a result of the early stages of Antarctic ice sheet expansion or a potential biogeochemical trigger for CO<sub>2</sub> drawdown and ice sheet growth is yet to be determined. We show that coccolith size (mean and 95%<sub>tile</sub>) increases through the EOT interval, with the pronounced loss of smaller reticulofenestrid morphotypes. Over the DEE the switch in dominance of smaller to larger cell size is rapid. As a result, we interpret that there is no obvious or significant  $p\text{CO}_2$  limitation on cell size in NKK1 through the EOT but perhaps instead a longer-term  $p\text{CO}_2$  control on coccolithophore cell size exists through the Paleogene.



### 3 | MIDDLE EOCENE TO EARLY OLIGOCENE CALCAREOUS NANNOFOSSILS FROM THE NANGGULAN FORMATION, JAVA, INDONESIA

This chapter is slightly altered from the following publication as is presented in print at the Journal of Nannoplankton Research:

**Jones, A.P.**, and Dunkley Jones, T. 2020. Middle Eocene to Early Oligocene calcareous nannofossils from the Nanggulan Formation, Java, Indonesia. *Journal of Nannoplankton Research*, **38(1)**, pp. 57–79

Modifications from the print version of this chapter include, altered formatting; modified text in section 3.2 and other small changes throughout chapter; the addition of Table 3.1, updates to Figure 3.2 and Plates 3.1 and 3.2.

Supplementary files can be retrieved at:

<https://doi.org/10.6084/m9.figshare.12488783.v1>.

*My contribution to this research was completing all parts of the research, collecting and analysing the data, light microscope imaging and writing the manuscript. Co-author Tom Dunkley Jones co-designed the methodology and research and provided important feedback on the taxonomy, biostratigraphy, age model and the manuscript during initial drafts. As in Chapter 2 the editorial "we" is used here to reflect their contribution to this research.*

### 3.1 INTRODUCTION

Calcareous nannofossils were examined from sediment cores that were recovered in 2006 from the Middle Eocene to Lower Oligocene portion of the Nanggulan Formation of Java. The cores were taken from drill-site NKK1, near the village of Nanggulan, in the Special Region of Yogyakarta (7.788555°S, 110.20578°E; Figure 3.1). A full description of the drilling operations, sedimentology and integrated biostratigraphy can be found in Coxall et al. (2021). Sediments from these cores contain abundant and well-preserved calcareous nannofossils. The sedimentary sequences in NKK1 span the upper Middle Eocene to Lower Oligocene, including a continuous record of the Eocene–Oligocene Transition (EOT), and can be used to generate new records of tropical nannoplankton ecology and biostratigraphy through this critical interval of Earth history. Today, Java is located within the Indo-Pacific Warm Pool (IPWP), which extends from the western waters of the equatorial Pacific Ocean, through the Indo-Australian Archipelago (IAA) and into the eastern Indian Ocean. The extent of the IPWP is defined by ocean surface-waters with year-round temperatures exceeding 28°C. In the modern climate system, these are the warmest surface ocean-waters in the world (De Deckker 2016). In the Eocene, climate models have suggested that the IPWP was both warmer and covered a larger region of the Indo-Pacific Ocean than today (Huber and Caballero 2011, Lunt et al. 2012). Palaeogeographic reconstructions (Hall 2009, 2012, 2013) have placed NKK1 at the centre of this palaeo-IPWP during the Late Eocene. Today, the IAA is the tropical centre of maximum diversity in marine benthic communities (Renema et al. 2008).

Fossil and molecular evidence indicate that these diversity hotspots have moved over the past ~50 Myr, in conjunction with major tectonic events (Renema et al. 2008). During the Eocene, neither Java nor the IAA were areas of maximum invertebrate biodiversity (Renema et al. 2008). However, the Eocene equatorial Indian Ocean region, including the East African margin, has recorded higher species diversities than other, contemporary fossil communities at similar tropical latitudes (Renema et al. 2008). For the plankton, and especially the calcareous phytoplankton, exceptionally-preserved Middle Eocene fossil assemblages from the tropical East African margin record peak species diversities (Bown et al. 2008). It is not clear whether these high diversities are a product of exceptional preservation or reflect a primary biogeographic diversity hotspot for calcareous phytoplankton in the tropical Indo-

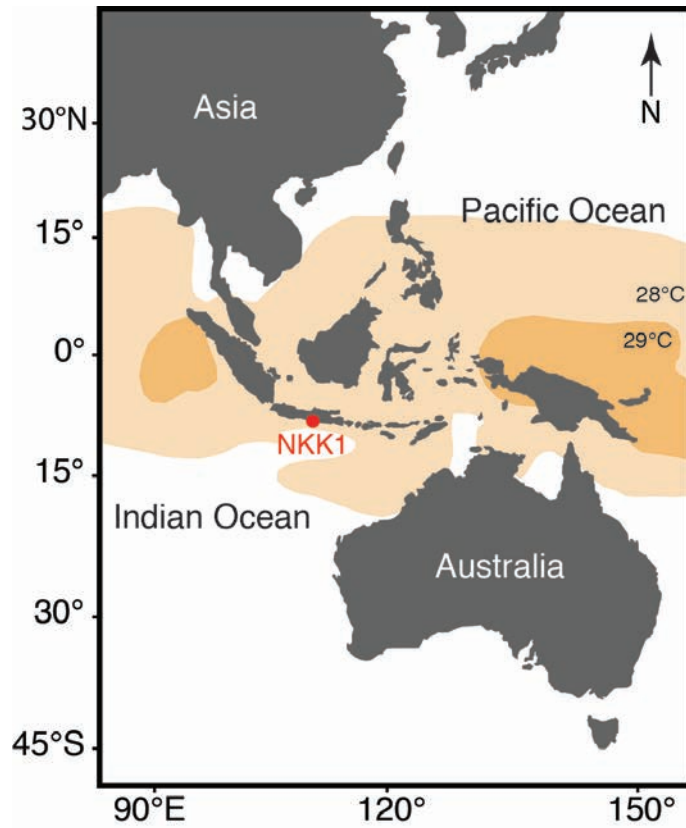


Figure 3.1: Present day map of Eastern Asia, Indonesia and Australia, depicting the modern IPWP temperature gradients (orange) and the location of core NKK1 in the southern region of Java

Pacific Ocean. The taxonomic assessment of calcareous nannofossil assemblages from Java, close to the centre of the palaeo-IPWP, help to address these questions of latitudinal and spatial diversity gradients of microplankton in the Middle and Late Eocene.

During the Late Eocene to Early Oligocene, and especially across the EOT, there was a long-term decline in the diversity of calcareous phytoplankton species (Bown et al. 2004). High-resolution studies of this transition have shown a gradual, progressive loss of species in the central (Fioroni et al. 2015) and eastern (Dunkley Jones et al. 2008) Indian Ocean. The current study, from the central IPWP, has enabled the development of detailed assemblage and biostratigraphic records that test the nature of species loss and extinction diachroneity across the tropical Indo-Pacific. Here, we test the recently-proposed biostratigraphic zonation schemes developed for the mid-latitudes (Agnini et al. 2014) in a tropical low-latitude region close to conditions of peak ocean warmth. The zonation of Agnini et al. (2014) included events based on the evolution and extinction of species in the *Reticulofenestra reticulata* group, in which there are subtle taxonomic discriminations across a group of morphologically similar



or intergrading species. We sought to test these species concepts in Late Eocene ‘tropical endmember’ assemblages as a way of assessing the recently-proposed bioevents, given the known extinction diachroneity in this group (Berggren et al. 1995, Villa et al. 2008, Persico et al. 2012).

## 3.2 GEOLOGICAL SETTING

During the Middle Eocene, Australia and Antarctica began to separate as Australia migrated northwards. This placed the Java region in a convergent tectonic regime that reinitiated Cretaceous subduction zones around the Sunda Arc, an active margin on the southerly side of Sundaland (Hall 2009, 2012). Extensive islands and shallow seas were created (Hall 2012, 2013) by subduction of the Australian and Pacific Plates below the continental part of Southeast Asia (Hall 2012). Southeast Asia increased in size through the addition of continental fragments that rifted away from Australia and were subsequently added to the margins of Sundaland (Hall 2009). Palaeogeographic reconstructions of Sundaland (the Malay Peninsula, Sumatra, Java, Borneo and surrounding small islands) during the Palaeogene are subject to some uncertainty (Hall 2013), but they indicate an Eocene palaeolatitude for NKK1 of  $\sim -6.5^{\circ}\text{S}$ , which is not dissimilar to the position of Java today (Hall 2012; Figure 3.1).

### 3.2.1 LITHOSTRATIGRAPHY AND PRESERVATION

NKK1 was positioned to maximise the recovery of the Middle Eocene to Oligocene sediments of the Nanggulan Formation that crops out northwest of the village of Kenteng, on the eastern flank of the Menoreh Hills. NKK1 penetrated a total depth of 100 m, and core recovery was  $>90\%$  for most of the Tegalsari Marls and Jetis Beds of the Nanggulan Formation. Barren horizons or poorly preserved nannofossil assemblages occurred in sediments both immediately below and for an interval of  $\sim 3$  m above a basalt unit at  $\sim 40$  m in the core. Nannofossil preservation and recovery was more variable in the Lower to Middle Oligocene upper Tegalsari Marls that occur above the basalt horizon, and none of this material was included in the current study. We focused on core samples between 41.04 and 99.98 m below ground level (mbgl), including samples NKK1-30 to NKK1-82, interpreted as belonging to calcareous nannofossil Zones CNE15 and CNE19–CNO3 of Agnini et al. (2014), equivalent to Zones NP17 and NP19/20–NP23 of Martini (1971).

Unit	Lithostratigraphy	Lithology	Thickness (m)	Sedimentary structures	Core depth (mbs)	Age	Cores	Comment
VA	Tegalsari Marls	Greenish grey silty clay and mudstone	30 and 13.5	Bioturbation	40.7-70.5 and 75.5-89.0	early Eocene to early Oligocene	NKK1-30 to NKK1-52 and NKK1-57 to NKK1-67	
VB	Tegalsari Marls	Reddish brown silty clay and mudstone with greenish grey spots	5	Bioturbation	70.5-75.5	late Eocene	NKK1-53 to NKK1-56	Harder at base
VI	Jetis beds	Alternating greenish grey sandy mudstone and dark greenish grey volcanic sandstone and radiolaria	11	Bioturbation. Bedded volcanic sands	89.0-100.0	middle Eocene	NKK1-66 to NKK1-82	

Table 3.1: Lithostratigraphic summary for NKK1. mbs = meter below surface. Modified after Coxall et al. (2021)

The Tegalsari Marls represented the majority of the material examined (Units VA and VB; Figure 3.2), ranging from 86.85–41.04 mbgl (totalling 45.81 m), and dated as CNE19 (NP19/20, Priabonian) at the base to CNO3 (NP23, early Oligocene) to the top of the studied interval. All samples comprised silty clays and mudstones, varying from dark to light olive-greens and greys. Between 70.5 and 75.5 mbgl, there was a reddish-brown interval (Unit VB) but had no lithology change, remaining a silty clay and mudstone as seen in Unit VA. Between 55.71–74.95 mbgl (Units VA and VB) hosted the core's best-preserved nannofossil specimens, with good/excellent preservation at 60 mbgl (late Eocene; CNE20 / NP19/20). Greenish-grey spots are recorded throughout the recovered clays and are bioturbation. In core 57 (76.14 mbgl) a short-lived interruption of sedimentation is evidenced by numerous chips of brown cemented carbonate, deduced to have originated from a hardground surface. An unconformity is recorded between 88.02 and 86.85 mbgl at the contact between the upper Jetis Beds and lower Tegalsari Marls and Unit VA terminates abruptly at 89 mbgl (Figure 3.2). The Jetis Beds (100–88.02 mbgl, totalling 11.98 m) are Bartonian in age, spanning CNE15 (NP16–NP17), and consist of thinly-bedded, silty claystones, interbedded with alternating tuffaceous, andesitic sandstones. The nannofossil preservation varied from moderate in samples with a higher sand content to good in silty clay samples.

### 3.3 SAMPLING AND METHODS

Sixty-five sediment samples were collected from NKK1 for calcareous nannofossil analysis. They were prepared using the simple smear-slide technique of Bown and Young (1998*b*). Specimens were observed using a Zeiss AxioScope in cross-polarised light (XPL) at x1000 magnification. Images were captured using QImaging and QCapture Pro 7 software. Calcareous nannofossil preservation and abundances were determined for all samples using a standard semi-quantitative scale, where abundance was A – abundant (>10–100 specimens per field of view [FOV]), C – common (>1–10 specimens per FOV), F – few (1 specimen per 1–10 FOV), and preservation was G – excellent/ good (little/no dissolution and/or recrystallisation, primary morphological characteristics slightly altered, specimens identifiable to species level), M – moderate (minimal etching and/or recrystallisation, primary morphological characteristics somewhat altered, most specimens identifiable to species level), P – poor (badly etched/overgrown, primary morphological characteristics mostly destroyed, with fragmenta-

tion and specimens not identifiable to species/genus level). Nannofossil assemblage composition data for NKK1 from the Middle Eocene to Lower Oligocene can be found on figshare (<https://doi.org/10.6084/m9.figshare.12488783.v1>) in the form of a range-chart for all samples studied. At least 400 specimens were counted from each sample, followed by an additional scan of at least two transects of each slide, in order to maximise the identification of rare species. Any species noted outside of the count are represented by an asterisk (\*) in the chart.

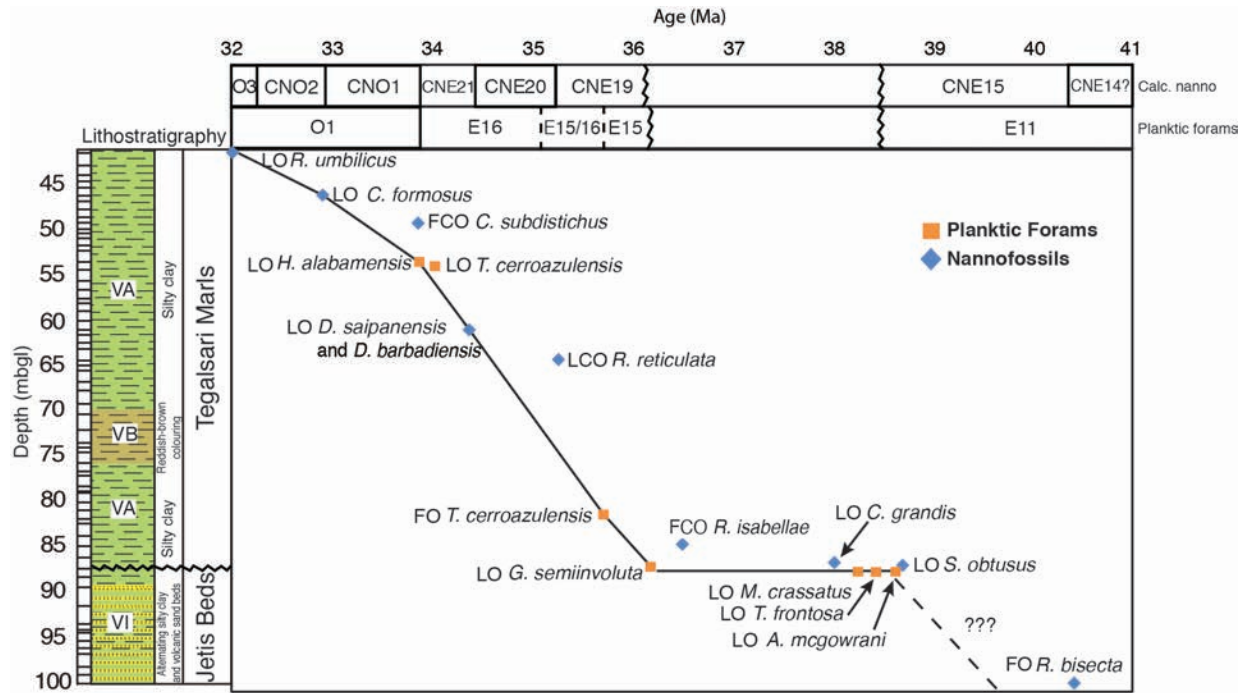


Figure 3.2: Age/depth plot for NKK1, showing the nannofossil bioevents from Table 2 modified after Jones et al. (2019). Scale and biozones after Agnini et al. (2014). Ages adjusted to the GTS2012 (Gradstein et al. 2012).

### 3.4 BIOSTRATIGRAPHY

The biostratigraphic interpretation of the NKK1 samples (Figure 3.2) employed the calibrated bioevents of Agnini et al. (2014); both the Agnini et al. (2014) and Martini (1971) biozonation schemes are shown for reference in Table 3.2. All ages were adjusted to the Geologic Timescale 2012 (Gradstein et al. 2012). Establishing robust bioevents for biozonation schemes for the Late Eocene has been difficult. Of those bioevents proposed by Martini (1971), the bases of *Sphenolithus pseudoradians* and *Isthmolithus recurvus* are diachronous across latitudes, and *I. recurvus* is entirely absent from tropical environments (Wei and Wise

1990, Dunkley Jones et al. 2008, 2009, Fioroni et al. 2015). Agnini et al. (2014) sought to remedy this lack of reliable bioevents with the addition of a series of events based on the *Reticulofenestra* (*Cribrrocentrum*) *reticulata* lineage. The successive appearances and extinctions of these typically tropical to subtropical species through the Late Eocene has the potential to significantly improve low- to mid-latitude nannofossil biozonations. However, one possible complicating factor involves the morphotypes in the *R. reticulata* lineage. Fornaciari et al. (2010) defined two new species - *Cribrrocentrum* (*Reticulofenestra*) *isabellae* for large (>12  $\mu\text{m}$ ) forms with narrow central-areas and *C. erbae* with a broad tube and distinctly closed central-area. Agnini et al. (2014) used both species as biohorizon marker taxa, but it is not clear how their revised taxonomy relates to previous biostratigraphic studies that did not make any distinction between the morphotypes of *R. reticulata*. Here, we carefully examined the variability in the *R. reticulata* lineage, with the purpose of refining the existing taxonomy of its morphotypes and documenting the range of these morphotypes through the late Middle to Late Eocene in a tropical location.

The calibrated ages of calcareous nannofossils and planktic foraminifera bioevents provided a coherent age model for NKK1 (Figure 3.2). The unconformity seen in NKK1 (89 mbgl) lies below the Last Occurrence (LO) of *Globigerinatheka semiinvoluta* and indicates the lithological boundary between Units VA and VI. This unconformity made dating the late middle Eocene problematic, yet, we assume the LO of *Sphenolithus obtusus* to be true and use First Occurrence (FO) of *Reticulofenestra bisecta* to establish a hypothesised model line. The First Common Occurrence (FCO) of *Reticulofenestra isabellae* and Last Common Occurrence (LCO) of *Reticulofenestra reticulata* are offset from the general age-model trend, however, these species occur younger in the NKK1 section than other mid and high latitude localities and both are known to be diachronous (Berggren et al. 1995)(further discussed below; Figure 3.3). A strong extinction occurs with the LO of the rosette-shaped Discoaster's *D. saipanensis* and *D. barbadiensis* which mark the end of CNE20 (NP19/20). The FCO of *Clausicoccus subdistichus* was not incorporated into the age-depth model line as it is a subjective datum and, in this study, the LO of *Hantkenina alabamensis* depicts the Eocene-Oligocene Boundary (EOB) more accurately. Another uncertainty was found with the Top *Reticulofenestra umbilicus* event due to rare occurrences in the early Oligocene. In this study, we surmise the position of *Reticulofenestra umbilicus* to be true (at 41.04 mbgl) while discounting the species

rare occurrence. Assuming the *Reticulofenestra umbilicus* to be “correct” suggests a decrease in sedimentation rate between 45-55 mbgl. Additionally, there exists well documented preferences in mid-to-high latitudes for *R. umbilicus* rarity during the early Oligocene (Villa et al. 2008). Overall, our age-model depends more heavily on the planktic foraminifera datums for reliable age control during the late Eocene, despite this, the combined calcareous nannofossil and planktic foraminifera bioevents established a reliable age model for NKK1.

### 3.5 TAXONOMIC DISCUSSION

Two species (*Sphenolithus conicus* and *Triquetrorhabdulus carinatus*), which typically appear in the mid- to Late Oligocene (de Kaenel and Villa 1996, Blaj et al. 2009, Bergen et al. 2017), were identified in the Middle to Upper Eocene sediments of NKK1. This does not appear to be a function of preservation, as both of these species are absent from other Upper Eocene assemblages that have excellent preservation, such as the Tanzanian successions and IODP Expedition 342 in the the North Atlantic Ocean (Bown 2005*b*, Dunkley Jones et al. 2008, 2009, Bown and Newsam 2017).

*Sphenolithus conicus* is a common mid- to Upper Oligocene species in many pelagic successions (Blaj et al. 2009, Dunkley Jones et al. 2009, Bergen et al. 2017). In NKK1, however, *S. conicus* morphotypes appeared in the latest Eocene (Sample NKK1-54a, CNE19, ~35.1 Ma), typically with low abundances that increased into the Lower Oligocene. The *S. conicus* morphotype observed in NKK1 is smaller than the specimens originally described by Bukry (1971), although (Bown and Dunkley Jones 2012) also documented a small morphotype in sediments from CNE21 (NP21) from IODP Expedition 320 in the equatorial Pacific. In NKK1, these small *S. conicus* morphotypes are consistently present in assemblages interpreted as CNE19 (NP19/20) (72.44 mbgl, ~35.18 Ma). These specimens are the smallest at the base of their observed range (latest Eocene), increasing in size into the Oligocene (Table 3.3). *Sphenolithus conicus* first appeared in the IPWP, only later appearing in the East Pacific, suggesting that, in the Early Oligocene, this species was limited to the tropical Pacific.

Bioevent	Top/ Base	Species	Biozone (Martini, 1971)	Biozone (Agnini et al., 2014)	Age (Ma) (Agnini et al., 2014)	Age (Ma) GTS2012 (Grad- stein et al., 2012)	Sample ID Bottom	Sample ID Top	Bottom Sample Core Depth (m)	Top Sample Core Depth (m)	Mid- point (m)	Depth error $\pm$ m
1	Top	<i>Reticulofenestra umbilicus</i>	NP23	CNO3	32.02	32.02	NKK-1/33a, 43-44	NKK-1/30a, 53-54	45.44	41.04	43.24	2.2
2	Top	<i>Coccolithus formosus</i>	NP22	CNO2	32.92	32.92	NKK-1/33b, 120-121	NKK-1/33, 43-44	46.21	45.44	45.83	0.39
3	FCO	<i>Clausiococcus subdistichus</i>	–	CNO1	33.88	33.86	NKK-1/36a, 43-44	NKK-1/35b, 109-110	49.94	49.1	49.52	0.42
4	Top	<i>Discoaster saipanensis</i>	NP21	CNE21	34.44	34.47	NKK-1/46a, 55-56	NKK-1/45, 48-49	61.06	59.99	60.53	0.54
5	Top	<i>R. reticulata</i>	–	CNE20	35.24	35.26	NKK-148a, 54-55/	NKK-1/47b, 111-112	64.55	63.12	63.84	0.72
6	Base	<i>R. isabellae</i>	NP19/20	CNE19	36.13	36.49	NKK-1/65, 84-85	NKK-1/64, 23-24	86.85	84.25	85.55	1.3
7	Top	<i>Sphenolithus obtusius</i>	NP17	CNE16	38.47	38.68	NKK-1/66, 51-52	NKK-1/65, 51-52	88.02	86.85	87.44	0.59
8	Base	<i>R. bisecta</i>	NP16/17	CNE15	40.34	40.4	NKK- 1/>82, 97-98	–	>99.98	–	99.98	–

Table 3.2: Comparative biostratigraphy of NKK1, using the Agnini et al. (2014) and Martini (1971) biozonation schemes. FCO = First Common Occurrence.

*Triquetrorhabdulus carinatus*, a nannolith with uncertain taxonomic affinities, was also present, albeit rarely and sporadically, in CNE19 to CNO3 (NP19/20–NP23,  $\sim 35.9 - \sim 31.2$  Ma) in the Tegalsari Marls, although it occurred frequently in Sample NKK1-48a (64.55 mbgl,  $\sim 34.7$  Ma). Young et al. (1998) and Agnini et al. (2014) stated that the base of *T. carinatus* is in CNO5 (NP25). In our section, it was first observed in CNE19 (NP19/20), approximately 7–8 Myr earlier. Lower Middle Eocene occurrences of *T. carinatus* have been reported from ODP Sites 1209, 1210 and 1211, Shatsky Rise, NW Pacific Ocean (Bralower 2005). Its reported abundances varied from rare to abundant, but there are no figures to accompany this data, and its identification may have been uncertain. There are multiple occurrences of this morphotype in NKK1, in several samples, suggesting that early forms of *T. carinatus* first appeared in the Late Eocene in tropical locations.

Circular reticulofenestrid coccoliths, with distinct central-area nets, are key Middle to Late Eocene taxa with *R. isabellae* and *R. reticulata* being stratigraphically important (Agnini et al. 2014). They are also palaeoenvironmental markers of relatively warm-water conditions (Bukry 1973, Aubry 1992a,b, Newsam et al. 2017). Some authors have placed these forms in the genus *Cribrocentrum* (Fornaciari et al. 2010, Shamrock and Watkins 2012, Agnini et al. 2014, Self-Trail et al. 2019), but we have retained their placement in the genus *Reticulofenestra*, whilst recognising the same species-level distinctions that are in use. *Reticulofenestra isabellae* was described by Fornaciari et al. (2010) as having large ( $>12\ \mu\text{m}$ ), circular placoliths with a central-area net. These morphotypes are effectively a large variant of *Reticulofenestra reticulata*, which includes medium to large (6–12  $\mu\text{m}$ ) coccoliths with a small central-area and distinctive extinction pattern of two crossed ‘dumbbells’ in the light microscope (LM) (Perch-Nielsen 1985). *Reticulofenestra erbae* is similar to *R. reticulata*, but has a broad tube and closed central-area (Fornaciari et al. 2010). This morphotype was not seen in NKK1, as its stratigraphic range falls within the unconformity between the Jetis Beds and Tegalsari Marls.

The top of *R. reticulata* is known to be diachronous across latitudes (Berggren et al. 1995), occurring at  $\sim 35.32$  Ma in the northern mid-latitudes (Agnini et al. 2014), between 36.30 and 36.69 Ma in the southern high latitudes (Villa et al. 2008, Persico et al. 2012) and with a top common occurrence (TCO) at  $\sim 34.99$  Ma at equatorial Indian Ocean ODP Site 711 (Fioroni et al. 2015). According to Fornaciari et al. (2010), the top of *R. isabellae*



<i>Reticulofenestra nanggulanensis</i>	Sample ID	Length ( $\mu\text{m}$ )	Central Area width ( $\mu\text{m}$ )	Rim width ( $\mu\text{m}$ )	Ratio (Central- area:Rim)	<i>Sphenolithus conicus</i>	Sample ID	Height ( $\mu\text{m}$ )	Proximal Rim Width ( $\mu\text{m}$ )
1	NKK-1/73A, 30-32	6.82	3	1.91	1.57	1	NKK-1/81A, 46-47	4.12	3.53
2	NKK-1/73A, 30-32	6.79	3.22	1.78	1.8	2	NKK-1/81A, 46-47	5.26	4.87
3	NKK-1/73A, 30-32	6.47	2.82	1.82	1.54	3	NKK-1/73A, 30-32	6.53	6.04
4	NKK-1/75, 21-22	5.68	2.77	1.45	1.9	4	NKK-1/73A, 30-32	4.55	4.85
5	NKK-1/75, 21-22	6.44	3.04	1.7	1.78	5	NKK-1/49, 25-26	4.23	3.88
6	NKK-1/80, 73-75	6	2.88	1.56	1.84	6	NKK-1/31A, 40-41	7.81	7.34
7	NKK-1/80, 73-75	5.44	2.49	1.47	1.68	7	NKK-1/31A, 40-41	4.4	4.21
8	NKK-1/80, 73-75	5.61	2.71	1.45	1.86	8	NKK-1/30A, 52-54	6.2	4.12
9	NKK-1/81A, 46-47	5.03	2.61	1.21	2.15	9	NKK-1/30A, 52-54	6.34	6.03
10	NKK-1/81A, 46-47	5.02	2.8	1.11	2.52	10	NKK-1/30A, 52-54	6.2	6.9

Table 3.3: Measurements of *R. nanggulanensis* and *S. conicus* in NKK1

is coincident with the top of *R. reticulata* at 35.21 Ma in the Massignano, Zermagnone and Bottaccione sections. This finding is supported by the NKK1 biostratigraphy, where the top of *R. isabellae* coincides with the top of *R. reticulata* at 61.57 mbgl. However, based on the age model for NKK1 (Figure 3.2), we estimate the synchronous extinctions of *R. reticulata* and *R. isabellae* to be at ~34.5 Ma (CNE20; Figure 3.3), which is ~0.7 - 0.8 Myr younger than reported for the northern low to mid-latitudes (Fornaciari et al. 2010, Agnini et al. 2014). Several other Late Eocene tropical nannoplankton have also shown a pattern of continued existence in tropical environments, while being absent from more northerly and southerly regions (Berggren et al. 1995, Dunkley Jones et al. 2008, Fioroni et al. 2015). The co-extinction of these two morphotypes in NKK1 and at other locations (Fornaciari et al. 2010) poses the question whether separating the two species, based on a 12  $\mu\text{m}$  size difference, is an arbitrary division of a population with continuous size variability. However, the limited age range of the large morphotype may still have biostratigraphic utility in the Upper Eocene (Agnini et al. 2014).

*Reticulofenestra nanggulanensis* sp. nov. is distinguished from *R. reticulata* by its characteristically wide central-area, and from *R. lockeri* by its subcircular shape (Plate 1, figs 40–42). *Reticulofenestra nanggulanensis* is medium in size (5–7  $\mu\text{m}$ ), with a single, slim outer cycle, and lacks the inner cycle that is present in *R. reticulata* and *R. isabellae*. This morphotype has been illustrated previously by Bown and Newsam (2017) (Plate 2, figs 7–9) as *R. reticulata* (wide). This new species is not only distinct, but also has a different stratigraphic range from *R. reticulata*. It occurs in stratigraphically older sediments, in CNE15 (NP16/17, 99.98–88.86 mbgl), and with rare abundances above the extinction of *R. reticulata*, up to CNO1 (NP21, 46.21 mbgl) in the Lower Oligocene. Once *R. reticulata* appears in the section (88.86 mbgl), the abundance of *R. nanggulanensis* decreases, although it occurs consistently in all samples up to the end of CNE19 (NP19/20, 64.55 mbgl), and then continues as rare occurrences into the lowest Oligocene.

The recognition of species of *Calcidiscus* throughout the Palaeogene is growing (Bown and Dunkley Jones 2012, Bown et al. 2007, Dunkley Jones et al. 2009, da Gama and Varol 2013). Calcidiscids are present, although not particularly diverse, in NKK1, but two species were recognised—*C. bicircus* and *C. cf. C. gallagheri* (Plate 3, figs 9–11, Plate 3, figs 14–17). It is possible that additional species are present in the oldest section of the core, but the

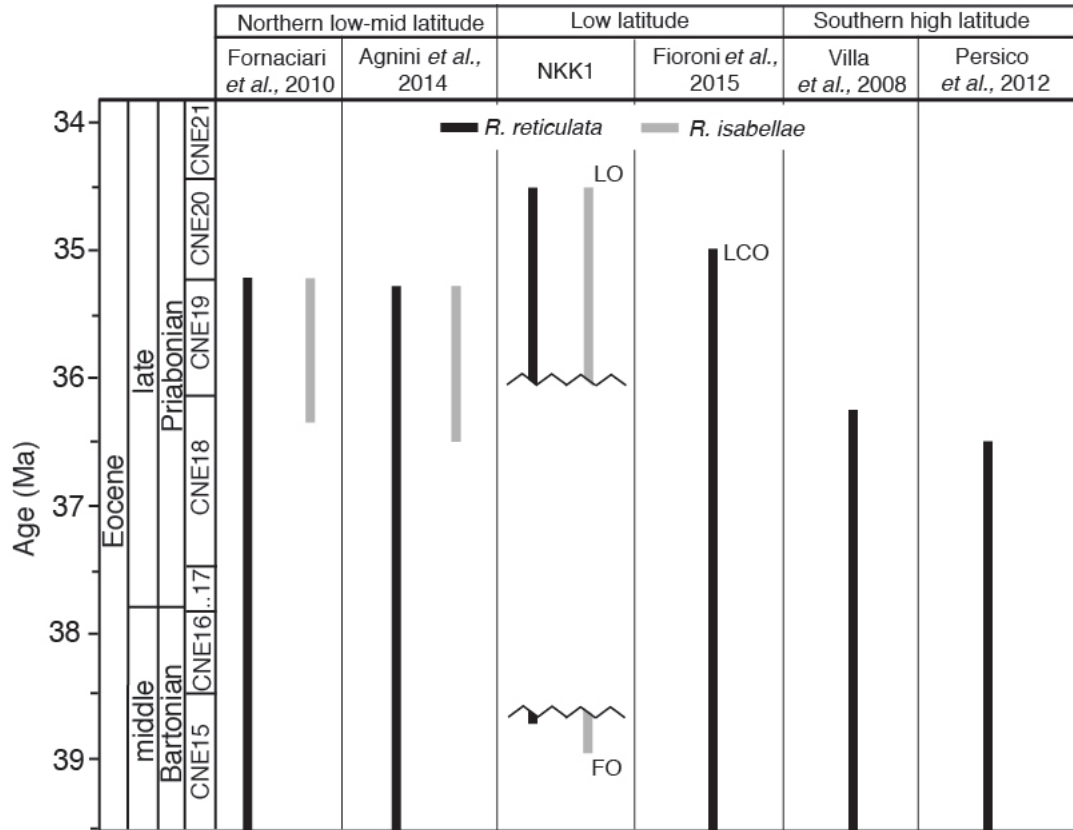


Figure 3.3: Stratigraphic distribution of *R. reticulata* and *R. isabellae*, showing diachroneity in the occurrences of these species across different latitudes. The northern, low- to mid-latitude data are from IODP Site 1218, ODP Sites 1051 and 1052, the Cicogna and Possagno sections and the Mediterranean area (Fornaciari et al. 2010, Agnini et al. 2014). The equatorial low-latitude data are from NKK1 (this study) and ODP Site 711 (Fioroni et al. 2015). DSDP Site 522 and IODP Site 1262 give the southern mid-latitude data (Fornaciari et al. 2010, Agnini et al. 2014). The southern highlatitude data are from ODP Holes 784B (Villa et al. 2008) and 689D (Persico et al. 2012). Ages for the occurrences of *R. reticulata* and *R. isabellae* have been recalibrated against the GTS2012 (Gradstein et al. 2012).

poor preservation of central-area structures in these samples makes this equivocal. From DSDP Leg 25 Site 242 in the western Indian Ocean, along the Davis Ridge, da Gama and Varol (2013) described one new species—*C. gallagheri*—from CNO5 (NP25). We recorded the occurrence of a specimen similar to *C. gallagheri* in the Upper Eocene. The base of *C. cf. C. gallagheri* in the NKK1 core was found in CNE19 (NP19/20), above which, this species became progressively more common into the lowest Oligocene (64.55–41.04 mbgl).

A new species of *Coccolithus*—*C. aspida* (Plate 2, figs 1, 2)—is described from NKK1. The morphological variation in the genus *Coccolithus* in the NKK1 assemblages was high, in terms of both size and central-area structure. Closely-coupled genetic and morphological variation in modern *Coccolithus* species (Narciso et al. 2006) supports a robust differentiation

among species based on subtle morphological differences. *Coccolithus aspada* is clearly distinct from *C. pelagicus* due to its closed central area and broad outer rim, and it is persistently common throughout NKK1. *Coccolithus pelagicus* and its morphotypes all have an open central-area, some spanned by bars and crosses, but this is the first species to be described with a fully-closed central-area.

Overall, application of the Agnini et al. (2014) biozonation scheme to the NKK1 data worked well, whilst using both Agnini et al. (2014) and Martini (1971) improves the stratigraphic subdivision of the Upper Eocene, with more nannofossil biohorizons being identified at low- and low-mid-latitude locations. The calibrated ages of Late Eocene bioevents from Agnini et al. (2014) provided a coherent age model for NKK1, and are highly consistent with the bioevent ages from planktonic foraminifera. The only problematic datum was the top of *R. reticulata*, which was offset from the general age-depth trend defined by the nannofossil and planktonic foraminiferal age constraints (Figure 3.2). Based on the age model for NKK1, we estimate that the top of *R. reticulata* was ~0.7–0.8 Myr younger in NKK1 than was estimated by Agnini et al. (2014), supporting previous indications for latitudinal diachroneity of this event (Berggren et al. 1995). The Middle and Middle–Upper Eocene biostratigraphy of NKK1 was complicated by the unconformity between the upper Jetis Beds and lower Tegalsari Marls (88.02–86.85 mbgl), which spanned CNE17–CNE18 and NP18. As a result, the boundary between the Middle and Upper Eocene was not present in the section, and it was thus not possible to assess the applicability of these zones in this study.

Taxonomic assessment of calcareous nannofossil assemblages at both Java (NKK1, this study) and Tanzania (TDP12 and 17), suggest such peak diversities are the result of a combination of exceptional preservation (Tanzania) and primary biogeographic peak diversity in the palaeo-IPWP and East African margin. Combined, these assemblages imply a potentially powerful tool in reflecting tropical calcareous nannoplankton peak diversity during the Middle Eocene.

## 3.6 SYSTEMATIC PALAEONTOLOGY

### 3.6.1 PLACOLITH COCCOLITHS

Order ISOCHRYSIDALES Paascher, 1910

Family NOELAERHABDACEAE Jerkovic, 1970

emend. Young & Bown, 1997

*Cyclicargolithus floridanus* group

Pl. 1, figs 8–10

**Description:** Small to large, subcircular to broadly elliptical reticulofenestrids displaying a narrow central-area and indiscernible net (which may be missing or non-birefringent).

*Cyclicargolithus floridanus* (Roth & Hay *in* Hay et al., 1967) Bukry, 1971

Pl. 1, figs 9, 10

**Remarks:** All small to large (3–11 µm), subcircular reticulofenestrids possessing a narrow central-area. Specimens with a closed central-area were here placed in *C.* cf. *C. floridanus*.

*Cyclicargolithus* cf. *C. floridanus* (Roth & Hay *in* Hay et al., 1967) Bukry, 1971

Pl. 1, fig. 8

**Remarks:** *C. floridanus* with a closed central-area.

*Reticulofenestra bisecta* group

Pl. 1, figs 20, 21, 31–34

**Description:** *Reticulofenestra* (*Dictyococcites* of some authors) with a central-area that is birefringent, and closed by a distinct plug. Included species: *R. bisecta* (*D. scrippsiae*), *R. filewiczii*, *R. stavensis* (*D. bisectus*).

*Reticulofenestra bisecta* (Hay et al., 1966) Roth, 1970

Pl. 1, figs 31, 32

**Remarks:** Elliptical and medium to large (less than 10  $\mu\text{m}$  long), with a solid plug.

*Reticulofenestra filewiczii* (Wise & Wiegand *in* Wise, 1983) Dunkley Jones et al., 2009

Pl. 1, figs 20, 21

**Remarks:** Differs from the rest of the group in having a small central opening and weakly birefringent net.

*Reticulofenestra stavensis* (Levin & Joerger, 1967) Varol, 1989

Pl. 1, figs 33, 34

**Remarks:** Similar morphology to *R. bisecta*, but distinguished by its larger size ( $>10\ \mu\text{m}$ ).

*Reticulofenestra lockeri* group

Pl. 1, figs 13–19, 22–24

**Description:** Elliptical reticulofenestrids with a visible (birefringent) net, with perforations that are sometimes discernible in the LM. Included species: *R. daviesii*, *R. lockeri*, *R. cf. R. lockeri*, *R. macmillanii*.

*Reticulofenestra daviesii* (Haq, 1968) Haq, 1971

Pl. 1, figs 22–24

**Remarks:** Differentiated from *R. lockeri* by the single row of perforations on each side of the netted central-area. The species became more common above the EOB, but was sporadic throughout the section.

*Reticulofenestra lockeri* Müller, 1970

Pl. 1, figs 13–16

**Remarks:** Elliptical, with a visible central-area net that has no perforations observable in the LM. The central-area is narrow; those with wider central-areas were placed in *R.* cf. *R. lockeri*.

*Reticulofenestra* cf. *R. lockeri* Müller, 1970

Pl. 1, fig. 17

**Remarks:** Similar to *R. lockeri*, but with a wider central area that has a visible (birefringent) net.

*Reticulofenestra macmillanii* Dunkley Jones et al., 2009

Pl. 1, figs 18, 19

**Remarks:** Similar to *R. lockeri*, but smaller, and with a wider central-area.

*Reticulofenestra reticulata* group

Pl. 1, figs 25, 26, 37–47

**Description:** Medium to very large, circular reticulofenestrids with a circular to broadly-elliptical central-area, spanned by a robust and conspicuous (birefringent) net. Included species: *R. isabellae*, *R. nanggulanensis*, *R. reticulata*, *R.* cf. *R. reticulata*, *R. westerholdii*.

*Reticulofenestra isabellae* (Catanzariti et al. in Fornaciari et al., 2010) Bown & Newsam,

2017

Pl. 1, figs 45–47

**Remarks:** Very large reticulofenestrid ( $>12\ \mu\text{m}$ ), with a relatively narrow central-area and broad tube-cycle. **Occurrence:** CNE16–CNE20, NP17–NP19/20.

*Reticulofenestra nanggulanensis* sp. nov.

Pl. 1, figs 40–42

2017 *R. reticulata* (wide) Bown and Newsam in: Journal of Nannoplankton Research, 37(1), p. 47, Pl. 2, figs 7-9

**Derivation of name:** After the Nanggulan Formation in south-central Java, the geological formation from which the NKK1 samples originated. **Diagnosis:** Small to medium, subcircular reticulofenestrid, with a distinct, wide central-area ( $>1.5$  times the rim width). The central-area is spanned by a visible (birefringent) net. **Differentiation:** Similar to *R. reticulata*, but has only one outer shield and a distinctly wider central-area, which varies from broadly elliptical to subcircular. **Remarks:** Most common in CNE15 (NP17), and more common than other members of the *R. reticulata* group in this core. Consistently observed up to the top of CNE19 (NP19/20), and present to the top of CNO1 (NP21). **Dimensions:** Holotype length =  $6.0\ \mu\text{m}$ ; paratype length =  $7.2\ \mu\text{m}$ . **Holotype:** Plate 1, fig. 40. **Paratype:** Plate 1, fig. 41. **Type locality:** NKK1, Nanggulan, Java. **Type level:** Upper Middle Eocene, NKK1-82A-97cm, CNE15, NP17. **Occurrence:** Recorded in upper Middle Eocene to Lower Oligocene sediments, CNE15–CNO1, NP16–NP17. Top recorded in sample NKK1-33b (46.21 mbgl).

*Reticulofenestra reticulata* (Gartner & Smith, 1967) Roth & Thierstein, 1972

Pl. 1, figs 38, 39, 43, 44

**Remarks:** Used broadly for medium to large ( $<12\ \mu\text{m}$ ), circular reticulofenestrids, with a broad tube-cycle and narrow central-area having a visible (birefringent) net.



*Reticulofenestra* cf. *R. reticulata* (Gartner & Smith, 1967) Roth & Thierstein, 1972

Pl. 1, fig. 37

**Remarks:** Similar to *R. reticulata*, but with a larger central-area. This form has two distinct cycles and, therefore, is not *R. nanggulanensis*.

*Reticulofenestra reticulata* (protolith) (Gartner & Smith, 1967) Roth & Thierstein, 1972

Pl. 1, figs 28–30

**Remarks:** Similar to *R. reticulata*, but lacking outer cycle.

*Reticulofenestra westerholdii* Bown & Dunkley Jones, 2012

Pl. 1, figs 25, 26

**Remarks:** Circular, with a central-area net that is not visible in the LM. Morphologically very similar to other members of the *R. reticulata* group.

*Reticulofenestra umbilicus* group

Pl. 1, figs 1–7, 11, 35, 36

**Description:** Elliptical and subcircular reticulofenestrids with an open central-area, spanned by a thin, faint (nonbirefringent or missing) net. Included species: *R. dictyoda*, *R. minuta*, *R. umbilicus* and *R. wadeae*.

*Reticulofenestra dictyoda* (Deflandre *in* Deflandre & Fert, 1954) Stradner *in* Stradner & Edwards, 1968

Pl. 1, figs 3–7

**Remarks:** Used broadly to distinguish medium to large, elliptical reticulofenestrids, with relatively-open central areas.

*Reticulofenestra minuta* Roth, 1970

Pl. 1, figs 1, 2

**Remarks:** Used broadly here for elliptical reticulofenestrids that are very small ( $<3\ \mu\text{m}$ ).

*Reticulofenestra umbilicus* (Levin, 1965) Martini & Ritzkowski, 1968 Pl. 1, figs 35, 36

**Remarks:** Very large ( $>14\ \mu\text{m}$ ), elliptical reticulofenestrid.

*Reticulofenestra wadeae* Bown, 2005

Pl. 1, fig. 11

Order COCCOLITHALES Haeckel, 1894

emend. Young & Bown, 1997

Family COCCOLITHACEAE Poche, 1913

emend. Young & Bown, 1997

*Coccolithus pelagicus* group

Pl. 2, figs 1–5, 11, 17, 21, 22

**Description:** Elliptical to subcircular *Coccolithus*, with a central opening sometimes having a delicate bar or cross.

*Coccolithus aspida* sp. nov.

Pl. 2, figs 1, 2

**Derivation of name:** From the Greek ‘aspída’, meaning ‘shield’, referring to the distinctive Coccolithus-type outer rim. **Diagnosis:** Medium to large, elliptical *Coccolithus*, with

a noticeable V-unit-dominated outer rim that is larger than the tube-cycle and possesses an apparently-closed central-area. **Differentiation:** Distinguished from *C. pelagicus* by its closed central-area. **Remarks:** This species occurred commonly in all the samples from NKK1. Although this species is characterised by a closed central area, its overall morphology and crystallography are very similar to those of *C. pelagicus*, and so we have placed the new species in *Coccolithus*, pending further observations of this morphotype. In the future, the generic description of *Coccolithus* (having an open central-area) may need to be emended. **Dimensions:** Holotype length = 10.8 µm, paratype length = 8.1 µm. **Holotype:** Plate 2, fig. 2. **Paratype:** Plate 2, fig. 1. **Type locality:** NKK1, Nanggulan, Java. **Type level:** Middle Eocene, Sample NKK1-73A-30cm, CNE15, NP17. **Occurrence:** Recorded in Middle Eocene to Lower Oligocene sediments, CNE15-CNO3, NP16–NP23.

*Coccolithus eopelagicus* (Bramlette & Riedel, 1954) Bramlette & Sullivan, 1961 Pl. 2, figs  
11, 17

*Coccolithus pelagicus* (Wallich, 1877) Schiller, 1930  
Pl. 2, figs 3–5

*Coccolithus biparteoperculatus* group  
Pl. 2, figs 9, 10, 12–16, 18–20

**Description:** The central-area, which can be broad or netted, is filled by a bar.

*Coccolithus biparteoperculatus* (Varol, 1991) Bown & Dunkley Jones, 2012  
Pl. 2, figs 15, 16, 18

*Coccolithus* cf. *C. biparteoperculatus*  
Pl. 2, figs 19, 20

**Remarks:** Similar to *C. biparteoperculatus*, but the bipartite, oval bar appears perforated, making it look like a net or grill, which may be the result of over calcification.

*Coccolithus cachaoi* Bown, 2005

Pl. 2, figs 12–14

*Coccolithus scheri* Bown & Dunkley Jones, 2012

Pl. 2, figs 9, 10

Other *Coccolithus* species

*Coccolithus formosus* (Kamptner, 1963) Wise, 1973

Pl. 2, fig. 23

*Coccolithus hulliae?* Bown & Newsam, 2017

Pl. 2, figs 6–8

**Remarks:** Questionable assignment because the central area cross is different from that described by Bown and Newsam (2017). As pictured in Plate 2, *C. hulliae?* has a disjunct axial cross that intersects the inner cycle. However, the rim morphology is similar to that described by Bown and Newsam (2017).

*Chiasmolithus bidens* group

Pl. 2, figs 43–45

*Chiasmolithus eoaltus* Persico & Villa, 2008

Pl. 2, fig. 43

*Chiasmolithus grandis* (Bramlette & Riedel, 1954) Radomski, 1968

Pl. 2, figs 44, 45

**Remarks:** This species was recorded from the base of the core, although its presence was rare. However, an acme of *C. grandis* was observed in one sample (NKK-1/66, 51–52), just below the unconformity between 88.02 and 86.85 mbgl.

*Chiasmolithus consuetus* group

Pl. 2, figs 36–42

*Chiasmolithus nitidus* Perch-Nielsen, 1971

Pl. 2, figs 36–39

*Chiasmolithus titus* Gartner, 1970

Pl. 2, figs 21–22 and 40–42

*Campylosphaera–Cruciplacolithus* group

Pl. 2, figs 24–34 *Bramletteius serraculoides* Gartner, 1969

Pl. 2, figs 24–27

*Campylosphaera dela* (Bramlette & Sullivan, 1961) Hay & Mohler, 1967

Pl. 2, figs 33, 34

*Cruciplacolithus cruciformis* (Hay & Towe, 1962) Roth, 1970

Pl. 2, figs 31, 32

*Cruciplacolithus primus* Perch-Nielsen, 1977

Pl. 2, figs 28, 29

**Description:** Small, elliptical *Cruciplacolithus*, with a disjunct, axial cross in the central-area. Very narrow, bicyclic rim.

*Cruciplacolithus tarquinius* Roth & Hay in Hay et al., 1967

Pl. 2, fig. 30

**Description:** Narrowly elliptical, and small to medium in size. The central-area contains a small, delicate axial cross. The rim is bicyclic, and broader than that of *C. primus*.

*Clausicoccus* group

*Clausicoccus fenestratus* (Deflandre & Fert, 1954) Prins, 1979

Pl. 3, figs 5–8

*Clausicoccus subdistichus* (Roth & Hay in Hay et al., 1967) Prins, 1979

Pl. 3, figs 1–4

*Coronocyclus* group

*Coronocyclus nitescens* (Kamptner, 1963) Bramlette & Wilcoxon, 1967

Pl. 2, fig. 35

Family CALCIDISCACEAE Young & Bown, 1997

*Calcidiscus bicircus* Bown, 2005

Pl. 3, figs 9–11

*Calcidiscus* cf. *C. bicircus* Bown, 2005

Pl. 3, figs 12, 13

**Remarks:** Similar to *C. bicircus*, but with a closed central area and visible (birefringent) net.

*Calcidiscus* cf. *C. gallagheri* da Gama & Varol, 2013

Pl. 3, figs 14–17

**Description:** Broadly elliptical, medium to very large. The central-area is distinctive, with a delicate net (partially missing in both specimens) and small perforations visible in the LM.

**Remarks:** The central-area is more irregular than that described by da Gama and Varol

(2013); this specimen appears to be more heavily calcified, despite being of a similar size and shape.

*Umbilicosphaera bramlettei* (Hay & Towe, 1962) Bown et al., 2007 Pl. 3, figs 23, 24

**Remarks:** A variation in size was documented in the Upper Eocene through Lower Oligocene of NKK1. Larger specimens ( $>8\ \mu\text{m}$ ) occurred in the lower Upper Eocene (CNE19, NP19/20).

*Umbilicosphaera detecta* (de Kaenel & Villa, 1996) Young & Bown, 2014

Pl. 3, fig. 19

*Umbilicosphaera edgariae* (Bown & Dunkley Jones, 2012) Young & Bown, 2014

Pl. 3, fig. 20

*Umbilicosphaera jordanii* Bown, 2005

Pl. 3, fig. 21

*Umbilicosphaera protoannulus* (Gartner, 1971) Young & Bown, 2014

Pl. 3, fig. 22

#### **Placolith coccoliths incertae sedis**

*Pedinocyclus larvalis* (Bukry & Bramlette, 1969) Loeblich & Tappan, 1973

Pl. 3, figs 18, 25

### **3.6.2 MUROLITH COCCOLITHS**

Order ZYGODISCALES Young & Bown, 1997

Family HELICOSPHERACEAE Black, 1971

*Helicosphaera bramlettei* (Müller, 1970) Jafar & Martini, 1975

Pl. 3, fig. 27

*Helicosphaera clarissima* Bown, 2005

Pl. 3, fig. 32

*Helicosphaera compacta* Bramlette & Wilcoxon, 1967

Pl. 3, fig. 31

*Helicosphaera euphratis* Haq, 1966

Pl. 3, fig. 26

*Helicosphaera lophota* (Bramlette & Sullivan, 1961) Locker, 1973

Pl. 3, figs 33, 34

*Helicosphaera reticulata* Bramlette & Wilcoxon, 1967

Pl. 3, figs 29, 30

*Helicosphaera wilcoxonii* (Gartner, 1971) Jafar & Martini, 1975

Pl. 3, fig. 28

Family PONTOSPHAERACEAE Lemmermann, 1908

*Pontosphaera alta* Roth, 1970

Pl. 3, figs 44–49

*Pontosphaera distincta* (Bramlette & Sullivan, 1961) Roth & Thierstein, 1972

Pl. 3, figs 41, 42

*Pontosphaera duocava* (Bramlette & Sullivan, 1961) Romein, 1979

Pl. 4, figs 1–4

*Pontosphaera enormis* (Locker, 1967) Perch-Nielsen, 1984

Pl. 4, fig. 7

*Pontosphaera exilis* (Bramlette & Sullivan, 1961) Romein, 1979

Pl. 3, figs 35–37



*Pontosphaera formosa* (Bukry & Bramlette, 1969) Romein, 1979

Pl. 4, fig. 5

**Remarks:** Our forms were smaller than the originally described size of 14–17  $\mu\text{m}$  (Romein, 1979).

*Pontosphaera latoculata* (Bukry & Percival, 1971) Perch-Nielsen, 1984

Pl. 4, figs 8–11

**Remarks:** This species exhibited a wide variation in rim thickness. It also had a single cycle of perforations around the rim and an open central-area that varied in width.

*Pontosphaera multipora* (Kamptner, 1948 ex Deflandre *in* Deflandre & Fert, 1954) Roth,

1970

Pl. 3, figs 38–40

*Pontosphaera pectinata* (Bramlette & Sullivan, 1961) Sherwood, 1974

Pl. 4, fig. 6

*Pontosphaera plana* (Bramlette & Sullivan, 1961) Haq, 1971

Pl. 4, figs 12–14

*Pontosphaera obliquipons* (Deflandre *in* Deflandre & Fert, 1954) Romein, 1979

Pl. 3, fig. 43

*Scyphosphaera columella* Stradner, 1969

Pl. 4, fig. 15

*Scyphosphaera expansa* Bukry & Percival, 1971

Pl. 4, figs 16, 17

Family ZYGODISCACEAE Hay & Mohler, 1967

*Neochiastozygus tenansa* (Deflandre *in* Deflandre & Fert, 1954) Self-Trail, 2011

Pl. 5, figs 8–12

Family RHABDOSPHAERACEAE Haeckel, 1894

*Blackites amplus* Roth & Hay *in* Hay et al., 1967 Pl. 4, fig. 18

*Blackites* cf. *B. globosus* Bown, 2005 Pl. 4, figs 19, 20

**Remarks:** Small, squat and bulbous *Blackites*, with no observed basal coccolith. These were likely broken specimens, with missing or very short, hollow spines. No ornamentation was seen across the sphere.

*Blackites culter*? Dunkley Jones et al., 2009

Pl. 4, fig. 21

**Remarks:** Only one specimen was recorded, and the species was questionable due to the specimen having a slimmer spine and a missing basal coccolith.

*Blackites gladius*? (Locker, 1967) Varol, 1989

Pl. 4, fig. 25

**Remarks:** A single, broken specimen was recorded, hence the species identification is questionable.

*Blackites inversus* (Bukry & Bramlette, 1969) Bown & Newsam, 2017

Pl. 4, figs 33, 34

*Blackites spiculiformis* Bown & Dunkley Jones, 2006

Pl. 4, figs 22, 23

*Blackites spinosus* (Deflandre & Fert, 1954) Hay & Towe, 1962

Pl. 4, figs 29–32

*Blackites stilus* Bown, 2005

Pl. 4, figs 26, 27

*Blackites subtilis*? Bown & Newsam, 2017

Pl. 4, figs 35, 36

**Remarks:** The identification of this specimen was questionable because it appears to taper at both ends; according to the description in Bown and Newsam (2017), this species does not taper at the ends. However, the tapering may be due to the oblique angle causing a distorted view.

*Blackites tenuis* (Bramlette & Sullivan, 1961) Sherwood, 1974

Pl. 4, fig. 28

*Blackites tortilis* Bown & Dunkley Jones, 2006

Pl. 4, fig. 24

Order SYRACOSPHAERALES Hay, 1977

emend. Young et al., 2003

Family CALCIOSOLENIACEAE Kamptner, 1927

*Calciosolenia alternans* Bown & Dunkley Jones, 2006

Pl. 4, figs 37, 38

Family SYRACOSPHAERACEAE Lemmermann, 1908

*Syracosphaera tanzanensis* Bown, 2005

Pl. 4, figs 39, 40

### 3.6.3 HOLOCOCOLITHS

Family CALYPTROSPHAERACEAE Boudreaux & Hay, 1967

*Holodiscolithus minolettii* Bown, 2005

Pl. 5, figs 5–7

*Orthozygus aureus* (Stradner, 1962) Bramlette & Wilcoxon, 1967

Pl. 5, figs 13–16

*Lanternithus minutus* Stradner, 1962

Pl. 5, figs 1–4

*Zygrhablithus bijugatus* subsp. *bijugatus* (Deflandre in Deflandre & Fert, 1954) Deflandre,  
1959

Pl. 5, figs 19–24

*Clathrolithus ellipticus* Deflandre in Deflandre & Fert, 1954

Pl. 5, figs 17, 18

### 3.6.4 EXTANT NANNOLITHS

Order BRAARUDOSPHAERALES Aubry, 2013

Family BRAARUDOSPHAERACEAE Deflandre, 1947

*Braarudosphaera bigelowii* (Gran & Braarud, 1935) Deflandre, 1947

Pl. 5, figs 25, 26

### 3.6.5 EXTINCT NANNOLITHS

*Micrantholithus astrum?* Bown, 2005

Pl. 5, fig. 27

*Pemma basquense* (Martini, 1959) Báldi-Beke, 1971

Pl. 5, figs 28, 29

*Pemma papillatum* Martini, 1959

Pl. 5, figs 30–32

*Pemma triquetra* Bown & Dunkley Jones, 2006

Pl. 5, figs 33, 34

Unknown nannolith

Pl. 5, figs 35, 36

**Description:** A form resembling a pinwheel, with five visible rays, although we suspected there were six rays in total, inferring that this nannolith possesses three pairs of triangular, overlapping segments. One segment in each pair goes extinct when rotated to 45°, revealing the segment division. At 0°, all the segments are bright. A small, circular central node is present, but has no outstanding features. **Occurrence:** CNO3 (NP23).

Order DISCOASTERALES Hay, 1977

emend. Bown, 2010

Family DISCOASTERACEAE Tan Sin Hok, 1927

**Remarks:** The overall preservation of this genus was not very good, making species identification problematic.

*Discoaster barbadiensis* Tan Sin Hok, 1927

Pl. 6, figs 2, 3, 6

*Discoaster distinctus* Martini, 1958

Pl. 5, figs 37, 38, 41

*Discoaster nodifer* (Bramlette & Riedel, 1954) Bukry, 1973

Pl. 5, figs 39, 40

*Discoaster saipanensis* Bramlette & Riedel, 1954

Pl. 6, fig. 1

*Discoaster septemradiatus?* (Klumpp, 1953) Martini, 1958

Pl. 5, fig. 42

**Remarks:** The rays appear to curve proximally. There was a possible underlying disc.

*Discoaster tanii* Bramlette & Riedel, 1954

Pl. 5, fig. 45

*Discoaster tanii* subsp. *ornatus* Bramlette & Wilcoxon, 1967

Pl. 5, figs 43, 44

Family SPHENOLITHACEAE Deflandre, 1952

*Sphenolithus moriformis* group

Pl. 6, figs 9–18

*Sphenolithus conicus* Bukry, 1971

Pl. 6, figs 9–16

**Remarks:** Small forms of this species were first documented in Upper Eocene sample NKK/1-54A (72.44 mbgl) in CNE19 (NP19/20), with larger forms appearing above, in the Lower Oligocene.

*Sphenolithus moriformis* (Brönnimann & Stradner, 1960) Bramlette & Wilcoxon, 1967

Pl. 6, figs 17, 18

*Sphenolithus predistentus* group

Pl. 6, figs 25–44

*Sphenolithus akropodus* de Kaenel & Villa, 1996

Pl. 6, figs 39–44

**Remarks:** The base of common *S. akropodus* was very close to the base of the Oligocene in CNO1 (NP21).

*Sphenolithus obtusus* Bukry, 1971

Pl. 6, figs 25–30

*Sphenolithus predistentus* Bramlette & Wilcoxon, 1967

Pl. 6, figs 31–34

**Remarks:** A great variation in the shape of the spine and in the size were observed. The specimens ranged from small to large, with spines that diverged distally.

*Sphenolithus tribulosus* Roth, 1970

Pl. 6, figs 35–38

*Sphenolithus radians* group

Pl. 6, figs 19–24

*Sphenolithus radians* Deflandre *in* Grassé, 1952

Pl. 6, figs 19–22

*Sphenolithus pseudoradians* Bramlette & Wilcoxon, 1967

Pl. 6, figs 23, 24

### **Nannoliths incertae sedis**

*Triquetrorhabdulus carinatus* Martini, 1965

Pl. 6, figs 4, 5, 7, 8

**Remarks:** Occurred sporadically in both the Upper Eocene and Lower Oligocene sediments.



Plate 3.1

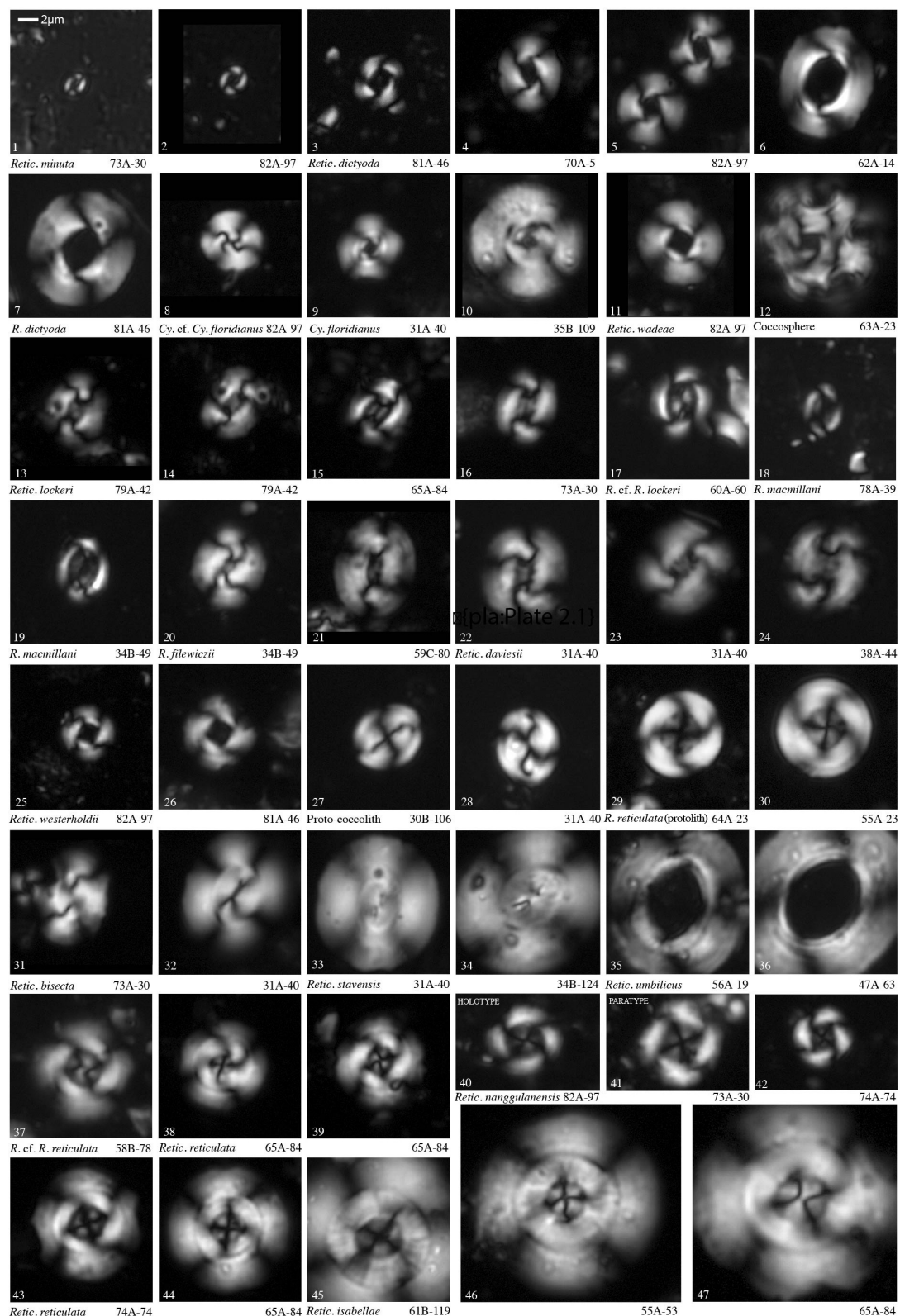


Plate 3.2

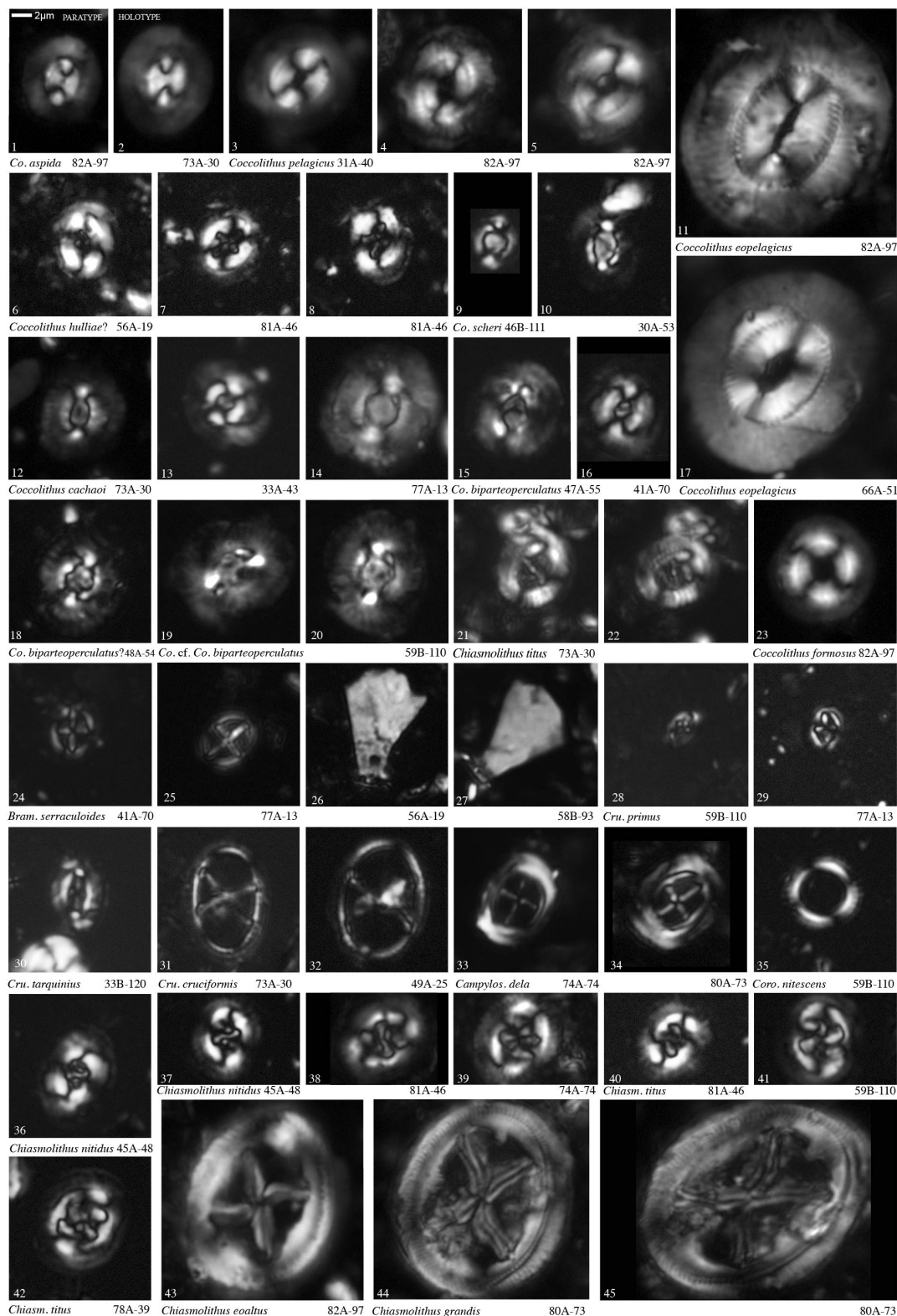


Plate 3.3

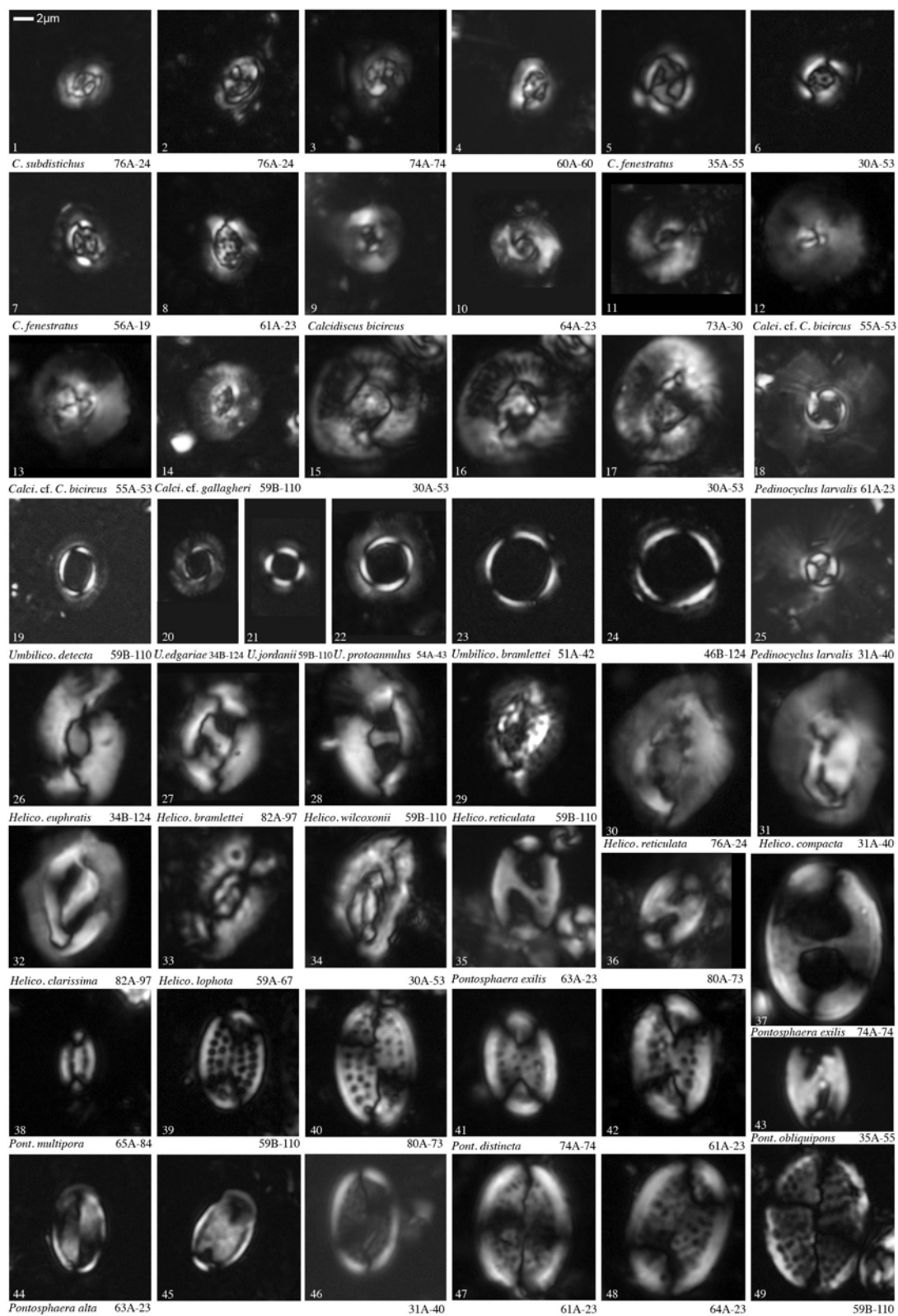


Plate 3.4

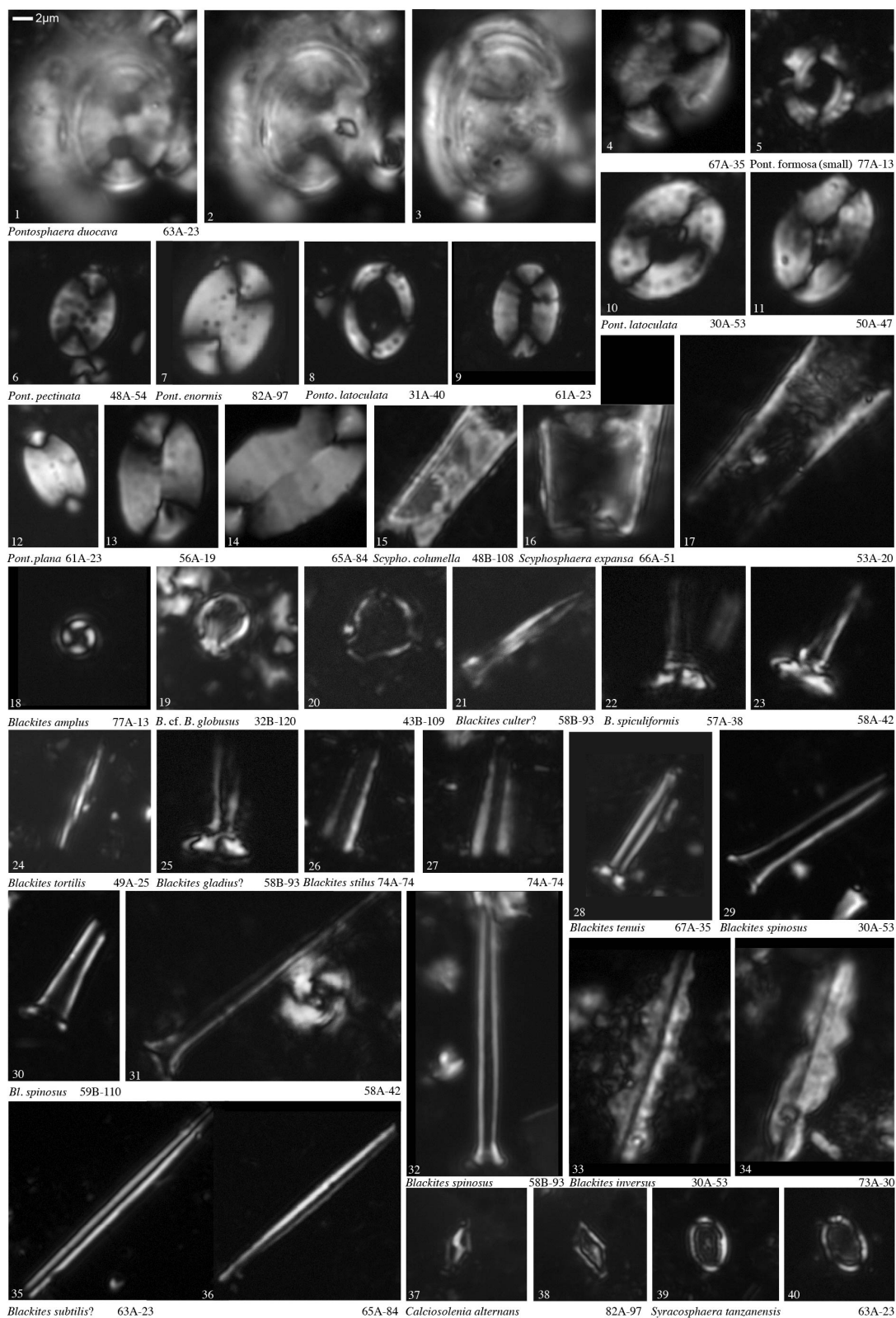


Plate 3.5

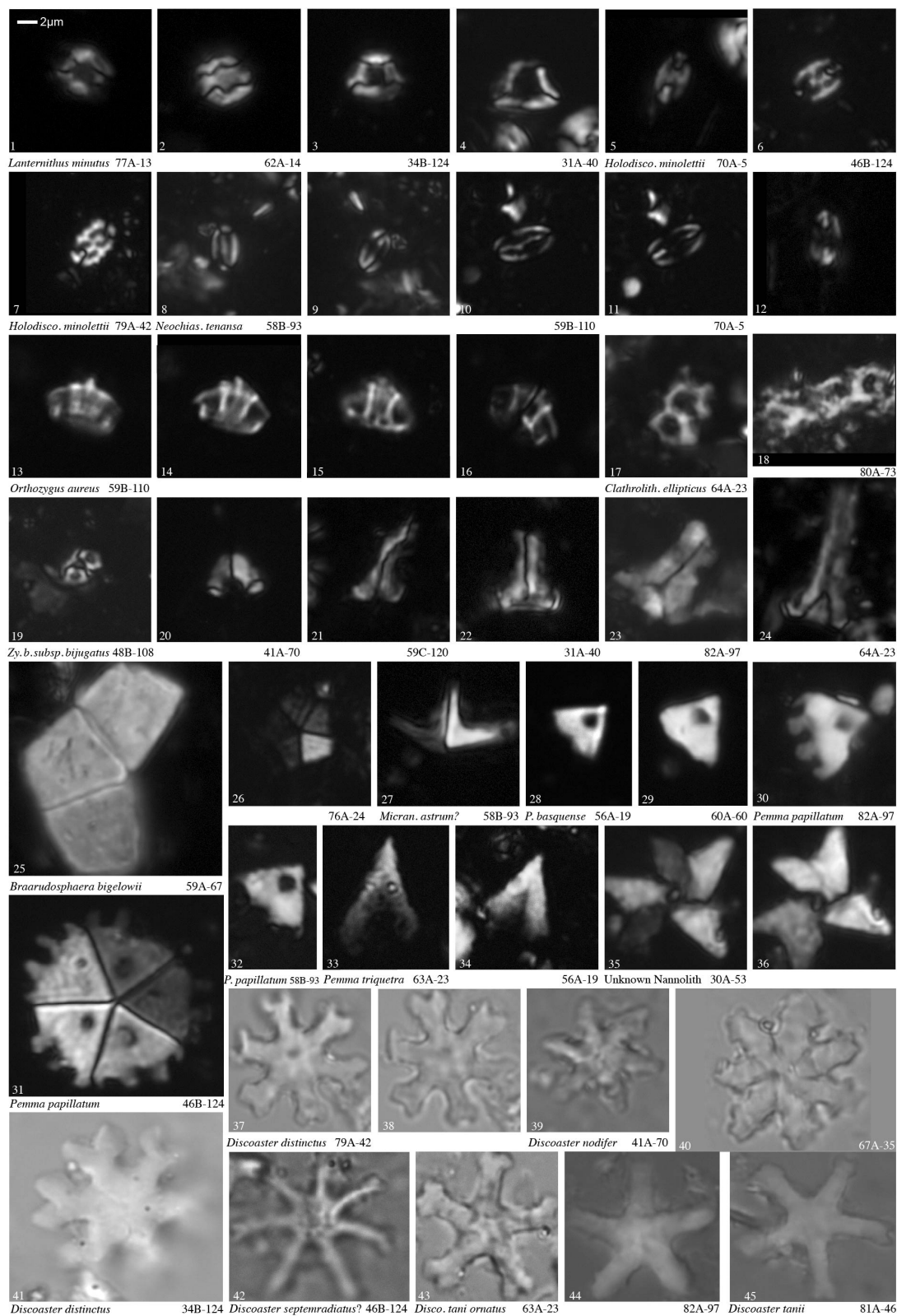
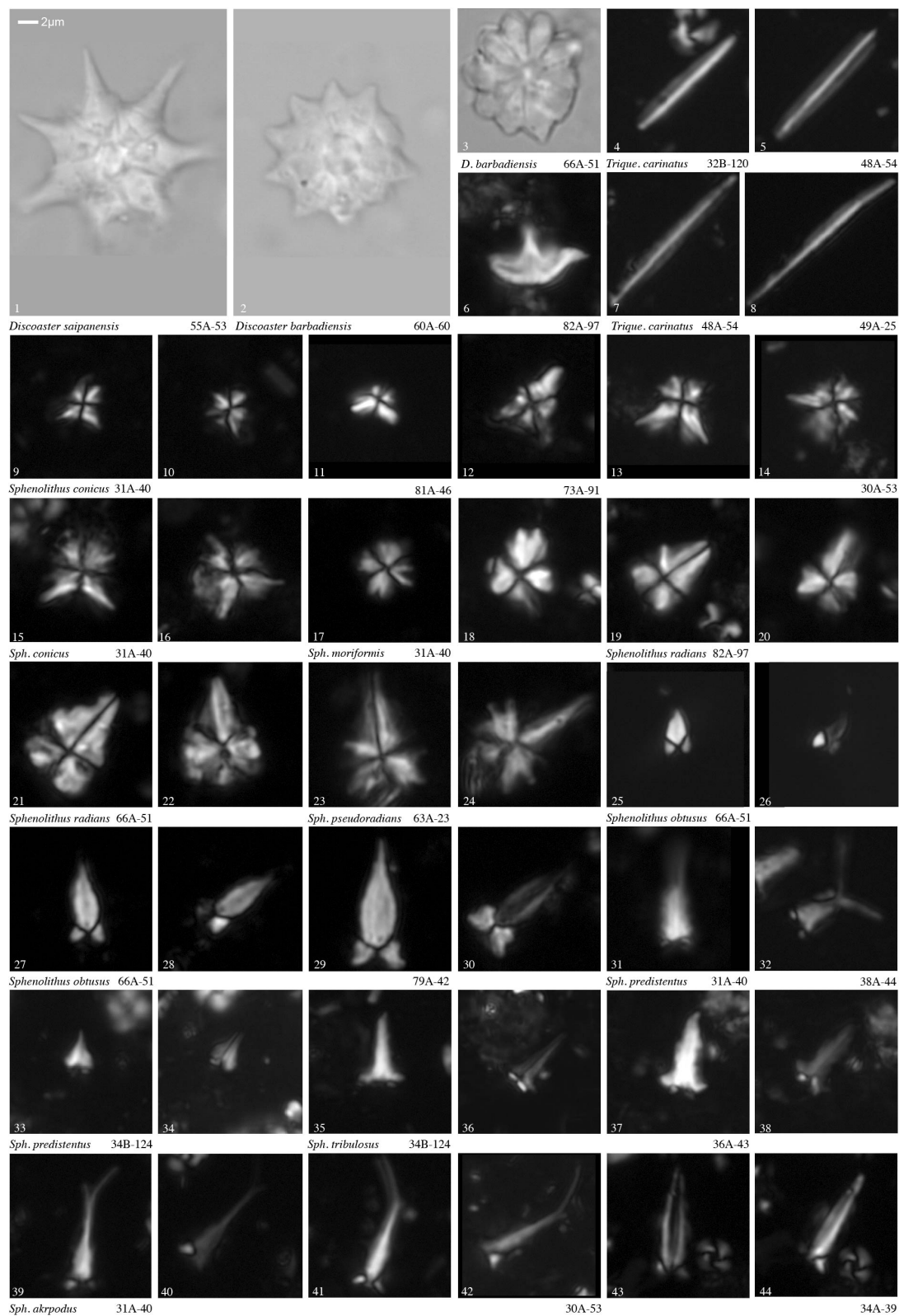




Plate 3.6





# 4 | DRIVERS OF NEOGENE COCCOLITHOPHORE MACROEVOLUTION

## 4.1 INTRODUCTION

Coccolithophores are haptophyte algae and the dominant marine calcifying phytoplankton in modern oceans. The Cenozoic fossil record of coccolithophores – in the form of species-diagnostic calcium carbonate cell covering plates, or coccoliths, preserved in marine sediments – is excellent. Fossil coccolith (or calcareous nannofossil) assemblages have been used to document a coupling between diversity, coccolithophore cell size and community structure, and global-scale climate change throughout the Cenozoic (Dunkley Jones et al. 2008, Gibbs et al. 2013, Lowery et al. 2020, Villa et al. 2008, 2013). On long timescales, calcareous nannofossil species diversity has decreased from a Cenozoic peak in the middle Eocene through to the Recent, despite a temporary increase during the late Miocene (Bown et al. 2004, Lowery et al. 2020). Nannoplankton diversity decline is generally attributed to atmospheric CO<sub>2</sub>-driven global climate cooling, through associated changes in the water column structure, cold polar water masses, the rise in siliceous plankton and ocean circulation, such climatic changes therefore impact numerous nannoplankton taxa and prompt diversity decline (Bown et al. 2004, Lowery et al. 2020, Šupraha and Henderiks 2020).

Through the Neogene, strong trends towards reduced coccolithophore cell and coccolith size across multiple groups - *Helicosphaera* (Šupraha and Henderiks 2020), *Gephyrocapsa* (Bendif et al. 2019) and *Calcidiscus* (Knappertsbusch 2000) – have been related to declining atmospheric CO<sub>2</sub> and surface ocean dissolved inorganic carbon (DIC) concentrations. Carbon limitation between 7-5 Ma is supported by coccolith carbon isotope vital effects and suggest a physiological response in coccolithophores involving the active re-allocation of carbon from calcification to photosynthesis (Bolton et al. 2013). Such relationship between decreasing



CO<sub>2</sub> and ocean alkalinity is also supported by the degree of coccolith calcification in the Noelaerhabdaceae lineage and *Helicosphaera*, showing progressively thinner coccoliths and less calcification over the past 15 million years (Bolton et al. 2016, McClelland et al. 2016, Rae et al. 2021, Šupraha and Henderiks 2020).

Recent studies, have proposed an additional driver of microplankton macroevolution through the Neogene involving a temperature-dependent biological carbon pump (Boscolo-Galazzo et al. 2018, 2021). Planktic foraminiferal isotopic records and biogeochemical modelling show a clear decrease in surface water remineralisation of particulate organic carbon (POC) over the past 15 Ma, driven by ocean and climate cooling, ultimately increasing the efficiency of the biological pump (Boscolo-Galazzo et al. 2021, Boscolo-Galazzo et al., *in review*). The increased transfer of nutrients and carbon from the ocean mixed-layer to greater depths drove the late Neogene diversification of deep-dwelling planktic foraminifera triggering the development of a new twilight-zone habitat (Boscolo-Galazzo et al. 2021). The implication that cooling-driven changes in the efficiency of the biological pump and the nutricline had a major impact on late Neogene microplankton are more in line with the inferred drivers of long-term Cenozoic macroevolutionary trends in the coccolithophore algae (Boscolo-Galazzo et al. 2021, Bown et al. 2004, Lowery et al. 2020). The late Neogene is thus a period when declining atmospheric CO<sub>2</sub> is potentially exerting both “direct” – through cellular carbon limitation – and “indirect” – through ocean cooling and nutrient dynamics – selective pressures on coccolithophore macroevolution. Whilst research has largely focused on carbon-limitation in recent years (Bolton and Stoll 2013, Bolton et al. 2016), the new framework provided by Boscolo-Galazzo et al. (2021) provides scope to re-examine the role different drivers – atmospheric CO<sub>2</sub> and ocean cooling associated with changes in nutricline – had on late Neogene coccolithophore evolution. Understanding the combined impact of direct CO<sub>2</sub> “fertilization” and temperature-dependent nutrient dynamics in past warm oceans will inform predictions of the future responses of phytoplankton communities that are heavily adapted for the ice-house climate states of the Pleistocene glacial age.

We present new nannofossil diversity and assemblage composition data through the Neogene from two datasets. The first follows the same time series from globally distributed sites as used in Boscolo-Galazzo et al. (2021) including nine Deep Sea Drilling Project (DSDP), Ocean Drilling Program (ODP) and Integrated Ocean Drilling Program (IODP) sites span-

ning the last 15 Ma at low resolution ( $\sim 2.5$  Ma sample intervals; Figure 4.1). The second dataset adds higher-resolution (200 ka sample intervals) data from IODP Site U1482 on the north-west Australian margin across the critical late Miocene to early Pleistocene interval (7.7 Ma-1.7 Ma). Site U1482 has good to very good coccolithophore preservation and can be used to represent peak tropical diversity through this key interval (Rosenthal et al. 2018). By combining these two datasets we provide a picture of global coccolithophore diversity and assemblage composition patterns that enable a direct comparison between model and data reconstructions of ocean structure and atmospheric  $\text{CO}_2$  concentrations. Using these datasets, we aim to reveal the drivers of the observed evolutionary changes in Neogene coccolithophore communities.

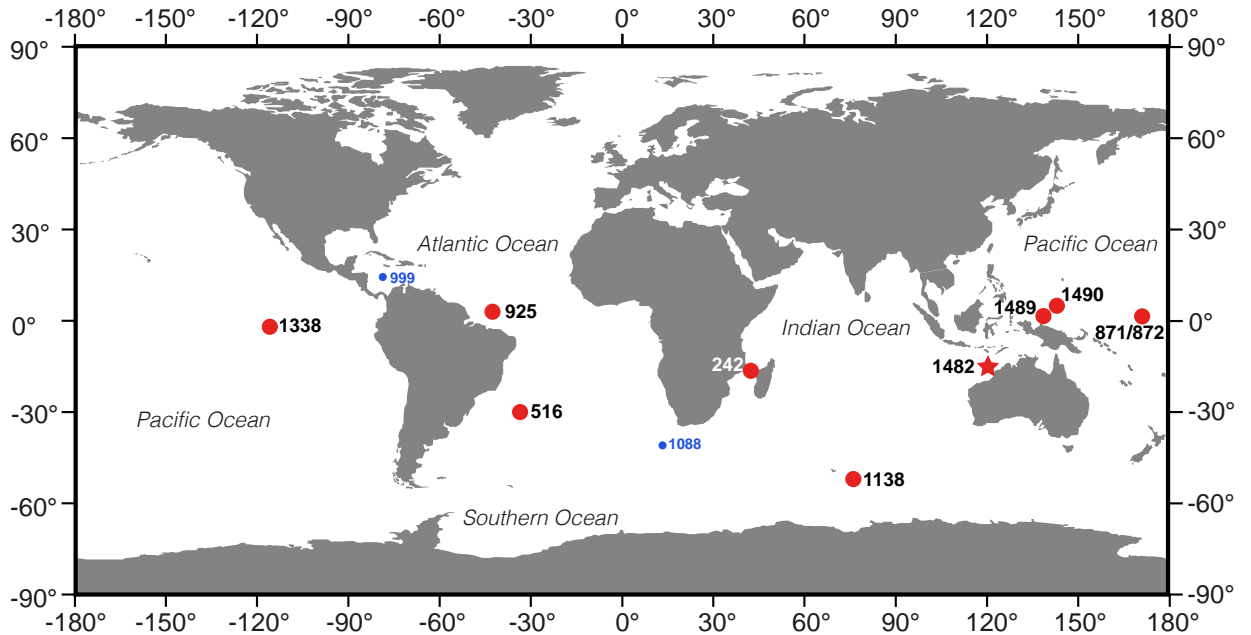


Figure 4.1: A modern-day world map displaying the locations of DSDP, ODP and IODP Sites (red) used in this study. Star represents Site U1482 sediments which were analysed at both high and low resolution. Sites 999 and 1088 (blue) after Bolton et al. (2013) are also included for reference (see Figure 4.5).

## 4.2 METHODS

### 4.2.1 COUNTS

Quantitative calcareous nannoplankton data were collected with a cascading count technique implemented to maximise nannofossil diversity recovery and quantification of low abundance species (Styzen 1997). Nannoplankton were counted per field of view (FOV) until a

minimum of 400 specimens were achieved for each sample (standard count technique; Bown and Young 1998*a*). However, if a high abundance species exceeded an average of 25 specimens per FOV, it was excluded from subsequent counts in that sample, but its abundance was scaled-up based on its average abundance and the total numbers of FOV counted. All taxa recorded contributed to the 400 specimens counted per sample, however, those taxa that were cascaded (i.e abundant cascaded taxa) in samples were added subsequently to the total count. For example, if one dominant taxa had a count of 30 in one FOV, it was not recorded further in that sample, but instead, scaled-up once the total count of 400 was achieved; should the sample have reached 5 FOV of non-abundant taxa, the total count of for that sample would be 550. This total count proxy calculation was used for relative abundance calculations (Figure 4.5). The number of FOV in which a dominant taxon reached or exceeded 25 specimens, and therefore were scaled-up, varied between samples, the sample age and the site studied. Further, an additional scan of two slide transects for every sample were undertaken to record rare species not observed during the extended count and are included in the total species richness analyses.

Samples were prepared for nannofossil analysis using the smear slide technique (Bown and Young 1998*b*) and observed using plane-polarised (PPL) and cross-polarised light (XPL) using a Zeiss Axioscope light-microscope (at x1000 magnification).

#### **4.2.2 TAXONOMY**

Taxonomy follows Young et al. (1997), and the higher taxonomic classification is based on (Young and Bown 1997) for extinct taxa and (Young 2003) for extant taxa. The taxonomy aims to be consistent with recent extensive systematic studies of Neogene calcareous nannofossils (Ciummelli et al. 2016, Bergen et al. 2017, Blair et al. 2017, Boesiger et al. 2017, Browning et al. 2017).

#### **4.2.3 SPECIES RICHNESS**

Global compiled species richness considers all combined taxonomic data from all nine of our DSDP, ODP and IODP sites (Figure 4.1) at each time slice, whereby the number of species across all sites, at each age interval, were measured. Species were quantitatively recorded for all samples, but to obtain a compiled species richness we based the taxonomic data on each

species' presence / absence across all sites. Therefore, if one particular taxon was present at one or multiple sites for a specific age interval, it was included in that intervals species richness total. If a taxon was not recorded at any sites for a specific age interval, despite being present in the preceding or proceeding sample, it was not included in the compiled species richness total. This method required every sample's species list for each time slice to be examined, establishing a low resolution "global" representation of species richness. We include all species and species morphotypes within this species richness, to showcase variety and abundance of species globally present (see appendices A and B for full count data; Figure 4.4).

#### 4.2.4 DIVERSITY

Shannon's diversity ( $H'$ ) was incorporated in Figure 4.4 as boxplots to demonstrate another measure of global species diversity from the Miocene to Holocene while taking both the abundance and evenness, with respect to the species present, into account across all studied low resolution localities (each individual grey point represents data from each of the nine sites per time slice). Raw count data of species from all samples and across all time intervals were converted into relative abundances and those with values greater than 0 were then log transformed, to reduce the skew of the original data, all species log data were summed and finally, multiplied by  $-1$ . The vertical whiskers of each boxplot correspond the the age of the time slice it is representing, rather than the width of the boxplot itself. All boxplots were generated in the R Software, version 4.1.1 (R Core Team 2020) using the ggplot package (`geom_boxplot`); all median, minimum and maximum values, inter-quartile ranges, whiskers and outliers were generated using this package.

Compiled Range Through Diversity (Compiled RTD; Figure 4.4) was a continued analysis from the compiled species richness data, as it was implemented to generate the compiled global RTD. The compiled RTD was calculated by recording species "expected" presence, where it was not recorded within the observed count, e.g. a specific taxon is documented at 0 Ma and 4.5 Ma, but not 2.5 Ma in the count, therefore, its presence is assumed and included within the RTD total count for each age interval.

### 4.2.5 PRESERVATION

The preservation observed across all sites in this study differed dramatically, not only with each locality but through time (Table 4.1). High resolution samples from Site U1482 in the Indian Ocean (7.7-1.7 Ma) revealed preservation that varied between moderate/poor and good/very good, and at low resolution (7.5-0 Ma), however, revealed good to very good preservation. On a similar latitude and also in the Indian Ocean, Site 242 (15-0 Ma) additionally exhibited good to very good preservation. Equatorial Pacific Ocean sites, 871/872 (15-10 Ma and 4.5-2.5 Ma) presented moderate to good preservation; Site U1489 (15-0 Ma) yielded poor to very good preservation; Site 1338 (15-0 Ma) had poor to good preservation; and Site U1490 (15-12.5 Ma and 7.5-0 Ma) presented poor to moderate preservation. Site 925 (10-2.5 Ma) in the Atlantic Ocean ranged between poor and very good preservation. Mid latitude Site 516 (15-10 Ma and 4.5-2.5 Ma) in the Atlantic Ocean varied between moderate/good and good with preservation improving towards the Holocene. Site 1138 (15-7.5 Ma) was our only high latitude locality and presented poor to good preservation, samples at this site at 4.5 and 2.5 Ma were inspected for calcareous nannofossil content, however, they were too siliceous to accurately obtain any count data from.

Calcareous nannofossil preservation was determined for all samples using a standard semi-quantitative scale: VG - very good (no dissolution or recrystallisation, primary morphological characteristics unaltered, specimens identifiable to species level), G – good (little/no dissolution and/or recrystallisation, primary morphological characteristics slightly altered, specimens identifiable to species level), M – moderate (minimal etching and/or recrystallisation, primary morphological characteristics somewhat altered, most specimens identifiable to species level), P – poor (badly etched/overgrown, primary morphological characteristics mostly destroyed, with fragmentation and specimens not identifiable to species/genus level)(Table 4.1). Quantitative calcareous nannofossil data were collected from the same samples as used for planktonic foraminiferal analysis (Supplementary Table 1; Bosocolo Galazzo et al. *in review*), in some cases, this was not possible, due to either, high siliceous content or that samples were barren ("X" indicates such samples in Table 4.1).

Age	Sample	Preservation
15Ma	871A-8H-1-W 0/1cm	G/M
12.5Ma	871B 5H-1 12/14cm	G/M
10Ma	872C 5H-4-W 83/85cm	G
4.5Ma	872C 3H-5-W 113/115cm	G
2.5Ma	872A 2H-2-W 120/121cm	G
0Ma	X	
15Ma	242 7R-6-W 144/145cm	VG
12.5Ma	242 7R-6-W 13/15cm	VG
7.5Ma	242 6R-3-W 3/5cm	VG
4.5Ma	242 3R-1-W 100/102cm	VG
2.5Ma	242 2R-3-W 50/51cm	G
0Ma	242 1R-2-W 143/144cm	G
15Ma	1138A 22R-1-W 19/20cm	G
12.5Ma	1138A 20R-1-W 40/42cm	G
10Ma	1138A 16R-2-W 30/32cm	M
7.5Ma	1138A 14R-2-W 140/142cm	P
4.5Ma	X	
2.5Ma	X	
0Ma	X	
15Ma	516Z 17H-4-W 2/3.5cm	M/P
7.5Ma	516Z 14H-1-W 71/72.5cm	M
4.5Ma	516Z 8H-2-W 8/9.5cm	M
2.5Ma	516Z 3H-3-W 38/40cm	G
0Ma	516Z 1H-1-W 50/52cm	G/M
15Ma	1338B 38H-4-W 52/54cm	M/G
12.5Ma	1338B 32H-3-W 67/69cm	G
10Ma	1338A 25H-6-W 66/68cm	M
7.5Ma	1338B 17H-4-W 12/14cm	P
4.5Ma	1338C 7H-4-W 60/62cm	M/G
2.5Ma	1338C 4H-4-W 60/62cm	P
0Ma	1338B 1H-1-W 5/7cm	P
15Ma	X	
12.5Ma	1489C 38X-3, 25/27cm	M
10Ma	1489C 33X-2, 104/106cm	P
7.5Ma	1489C 25H-4, 15/17cm	M/G
4.5Ma	1489B 12H-1, 5/7cm	VG
2.5Ma	1489B 6H-6, 85/87cm	G
0Ma	1489B 1H-1, 5/7cm	G
7.5Ma	1482A 40F-1, 106/108cm	VG
4.5Ma	1482A 24H-6, 5/7cm	G/VG
2.5Ma	1482A 11H-2, 105/107cm	G/VG
0Ma	1482A 1H-1, 7/9cm	G
15Ma	1490B 26F-1, 45/47cm	M/P
12.5Ma	X	
7.5Ma	1490C 18H-2, 45/47cm	P
4.5Ma	1490A 10H-2, 5/7cm	P
2.5Ma	1490A 4H-7, 35/37cm	M
0Ma	1490A 1H-1, 5/7cm	M

Table 4.1: List of samples, their ages and preservation recorded in all nine low resolution dataset localities. X - no sample used, VG - very good, G - good, M - moderate, P - poor.

### 4.2.6 TIME SLICES AND AGE MODEL

Our dataset from the nine ODP, DSDP and IODP localities focused on seven target ages (15 Ma, 12.5 Ma, 10 Ma, 7.5 Ma, 4.5 Ma, 2.5 Ma, 0 Ma; after Boscolo-Galazzo et al. (2021)) to present a global set of ocean sites and calcareous nannofossil response at low sampling resolution during key climatic events. Sample ages were determined based on planktic foraminifera biostratigraphic analysis (Boscolo-Galazzo et al. *in review*) following the biozonation scheme by Wade et al. (2011). Planktic foraminifera biostratigraphic age assignments were further confirmed during calcareous nannofossil data collection. Planktic foraminifera and calcareous nannoplankton abundance, biogeography, stable isotope and depth habitat reconstructions spanning the last 15 million years has also been collected and is currently in review (Boscolo-Galazzo et al., *Biogeosciences*), however, this study only considers the calcareous nannofossil abundances from the nine localities global dataset.

The age model for U1482 was taken from the Exp. 363 shipboard foraminifera and calcareous nannofossil biostratigraphy and magnetostratigraphy (Appendices B.2 and Figure 4.2; Rosenthal et al. (2018)).

## 4.3 RESULTS

### 4.3.1 DIVERSITY

The Range Through Diversity (RTD) and species richness (S) are shown for both our low resolution global dataset and for the high resolution U1482 record (Figure 4.3). The RTD of the global compiled sites is a proxy for “global species diversity”, which it should approach with an increased number of sample sites. Given the geographic spread and general quality of our study sites (see also Boscolo-Galazzo et al., *in review*), this is a good metric for global species richness. Our global compiled S for the Miocene to Holocene is higher than previous studies (Bown et al. 2004, Lowery et al. 2020), however, we consider all taxa and morphotypes seen within all samples studied. Diversity rose through the Miocene steadily from 72 species (15 Ma) until a peak for both S and RTD at 4.5 Ma with 121 and 135 species respectively. S and RTD subsequently falls in the mid-Pliocene reaching 62 species in the Holocene.

The RTD of Site U1482 is a good representation of tropical species richness through time, and will always be greater than or equal to in-sample S. The S and RTD of the the single

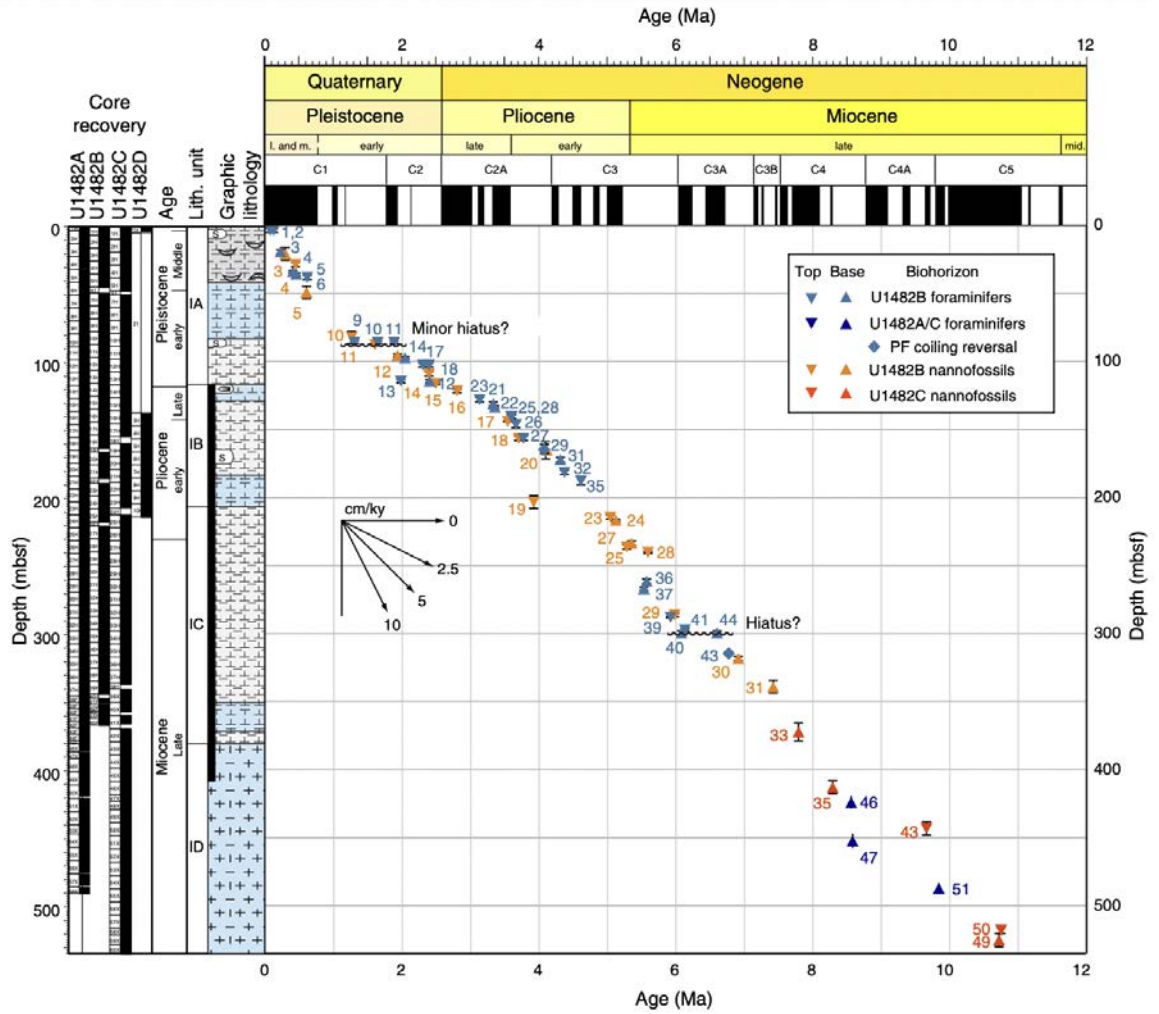


Figure 4.2: IODP Expedition 363 Shipboard Age Model for Site U1482, Holes A-D with Foraminifera (blues) and Calcareous Nannofossil (oranges) biohorizons. Lithostratigraphy, core recovery, Age and units are included on the y-axis and Period, Epoch and magnetostratigraphy displayed on the x-axis. From (Rosenthal et al. 2018).

tropical Site U1482 is lower than the global RTD, indicating significant biogeographic and/or ecological differentiation across late Neogene coccolithophore species. The S of U1482 is at its highest during the Messinian (late Miocene; 6.9 Ma) at 73 species, which then falls continuously into the early-Pliocene. A transient S and RTD recovery is noted at 4.1 Ma with 65 species. Consequently, the S and RTD declines to 31 species at 1.7 Ma (early Pleistocene).



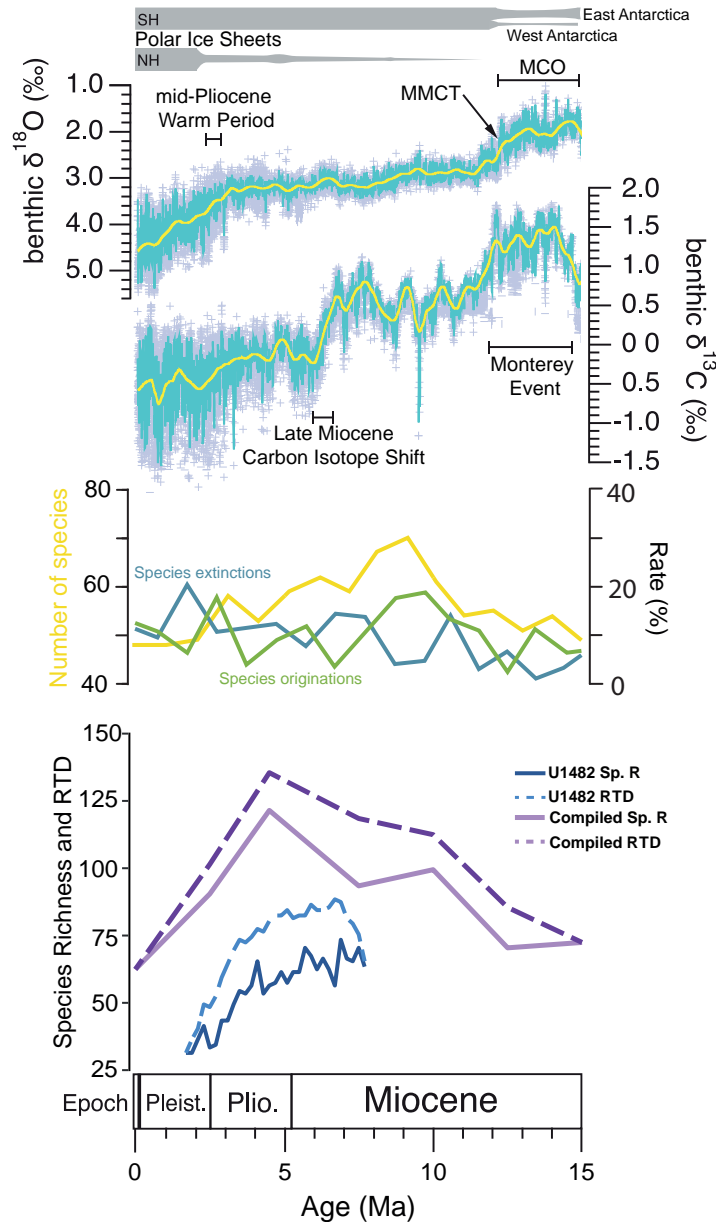


Figure 4.3: Calcareous nannoplankton diversity records through the Neogene from this study and after Lowery et al. (2020). Top panel: benthic  $\delta^{18}\text{O}$  and benthic  $\delta^{13}\text{C}$  curves, edited after Westerhold et al. (2020). Middle panel: nannofossil species number, extinction and origination rates, modified after Lowery et al. (2020). Bottom panel: Compiled global low resolution sample data (purples) and U1482 high resolution sample data (blues) - solid lines represent species richness data and dashed lines indicate Range Through Diversity (RTD).

### 4.3.2 RELATIVE ABUNDANCE

Relative abundance and richness data from multiple, geographically widespread sampling locations are integrated into a single standardised representation shown as boxplots for each time bin (Figure 4.4 and Figure 4.5). They are useful in showing the distribution and spread of data at each time slice between sites and, for relative abundance data, can be taken as a

measure of cosmopolitanism. A cosmopolitan distribution of any group would be expected to show reduced inter-site variation (constrained box plot), whereas groups with a pronounced biogeographic distribution will show the greatest range, with potential exclusion (minimum value of zero) at some locations. Abundance data for all the main groups (*Reticulofenestra* spp., *Florisphaera profunda*, *Gephyrocapsa* spp., and *Discoaster* spp.) are shown in Figure 4.5. The very small reticulofenestrid group (Retic.  $<3\ \mu\text{m}$ ), comprises *Reticulofenestra minuta* and *R. parvula*; the small reticulofenestrid group (Retic.  $3\text{--}5\ \mu\text{m}$ ) includes *Reticulofenestra haqii*, *R. minutula*, *R. producta* and any *Reticulofenestra* specimens within a  $3\text{--}5\ \mu\text{m}$  size range that could not be identified to species level. The medium to large reticulofenestrids group (Retic.  $>5\ \mu\text{m}$ ) contains *Reticulofenestra perplexa*, *R. pseudumbilicus* and *R. rotaria*. *Gephyrocapsa* spp. comprises *Gephyrocapsa caribbeanica*, *G. ericsonii*, *G. muellerae*, *G. oceanica*, *G. omega* and *Gephyrocapsa* “small” spp. The high-resolution U1482 data is plotted with these box plots to illustrate the more continuous background trends in sub-tropical nannofossil assemblages in comparison to global records.

The Retic.  $<3\ \mu\text{m}$  mean abundance declines through late Miocene from 62% to 19% before recovering in the Pliocene (Figure 4.5). The mean abundance trends are mirrored for Site U1482 during the Pliocene, but the group ultimately falls to near zero ( $<1\%$ ) at all sites in the Holocene. Low relative abundance in the Holocene consists of one of the last remaining species, *Reticulofenestra parvula*, which is uncommon and miniscule in size.

The Retic.  $3\text{--}5\ \mu\text{m}$  group (Figure 4.5) shows low median abundance ( $<10\%$ ) in the mid Miocene rising to peak abundances across the late Miocene and Pliocene (7.5 Ma to 4.5 Ma; maximum abundance of 29% at 7.5 Ma; Figure 4.5). Again, the group declines in abundance through Plio-Pleistocene and by the Holocene falls to their lowest median values ( $<1\%$ ).

The largest Retic.  $>5\ \mu\text{m}$  group, reaches peak median abundance in the mid Miocene and shows a maximum single-site relative abundance value (76%) of all reticulofenestrid groups. However, by the late Miocene (7.5 Ma) the group drops to a median abundance of  $\sim 1\%$  (Figure 4.5) in proximity to the “*pseudumbilicus* gap” between 8.8 to  $\sim 7.1$  Ma (biozones CNM15 – CNM17; Agnini et al. 2017, Backman et al. 2012, Raffi et al. 2016). This signal is a proposed global near absence of *Reticulofenestra pseudumbilicus* (coccoliths  $\geq 5\ \mu\text{m}$ ) and is consistent with the majority of our sites. An outlier for the Retic.  $>5\ \mu\text{m}$  group lies within this “gap” at Site 1138 (74% relative abundance) a high latitude site of the Southern Ocean,

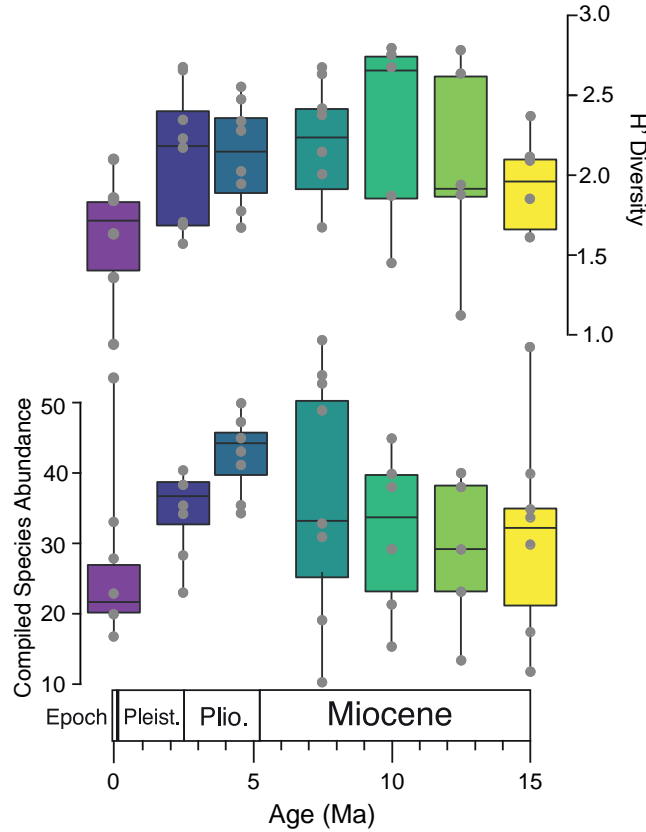


Figure 4.4: Boxplots of H' diversity and Compiled Species Abundance from our nine global dataset low resolution samples used in this study, across the Miocene to Recent. These plots show median values, interquartile range and maximum and minimum values.

suggesting this signal is not truly global. In the Pliocene, similar to the Retic.  $<3 \mu\text{m}$  and  $3\text{--}5 \mu\text{m}$ , there is a small recovery in Retic.  $>5 \mu\text{m}$  abundance, but they then disappear by the end Pliocene. Our high-resolution data from U1482 are consistent with the global trends for this group.

*Gephyrocapsa* spp. are first recorded in the late Miocene (6.1 Ma; Plates 4.1 and 4.3) with low abundance ( $<1\%$ ) and increase in abundance henceforth (Figure 4.5). Subsequently, into the Pliocene, the lineage becomes more established with species diversification and increased cosmopolitanism as this group proliferates rapidly. From the Pleistocene to Holocene the median relative abundance of this group increases from  $\sim 7\%$  at 2.5 Ma to  $24\%$  at 0 Ma. The U1482 data is consistent with the global trend for *Gephyrocapsa* spp., with a latest Miocene appearance followed by a late Pliocene abundance rise, becoming the dominant reticulofenestrid group as the other groups decline across the Plio-Pleistocene transition.

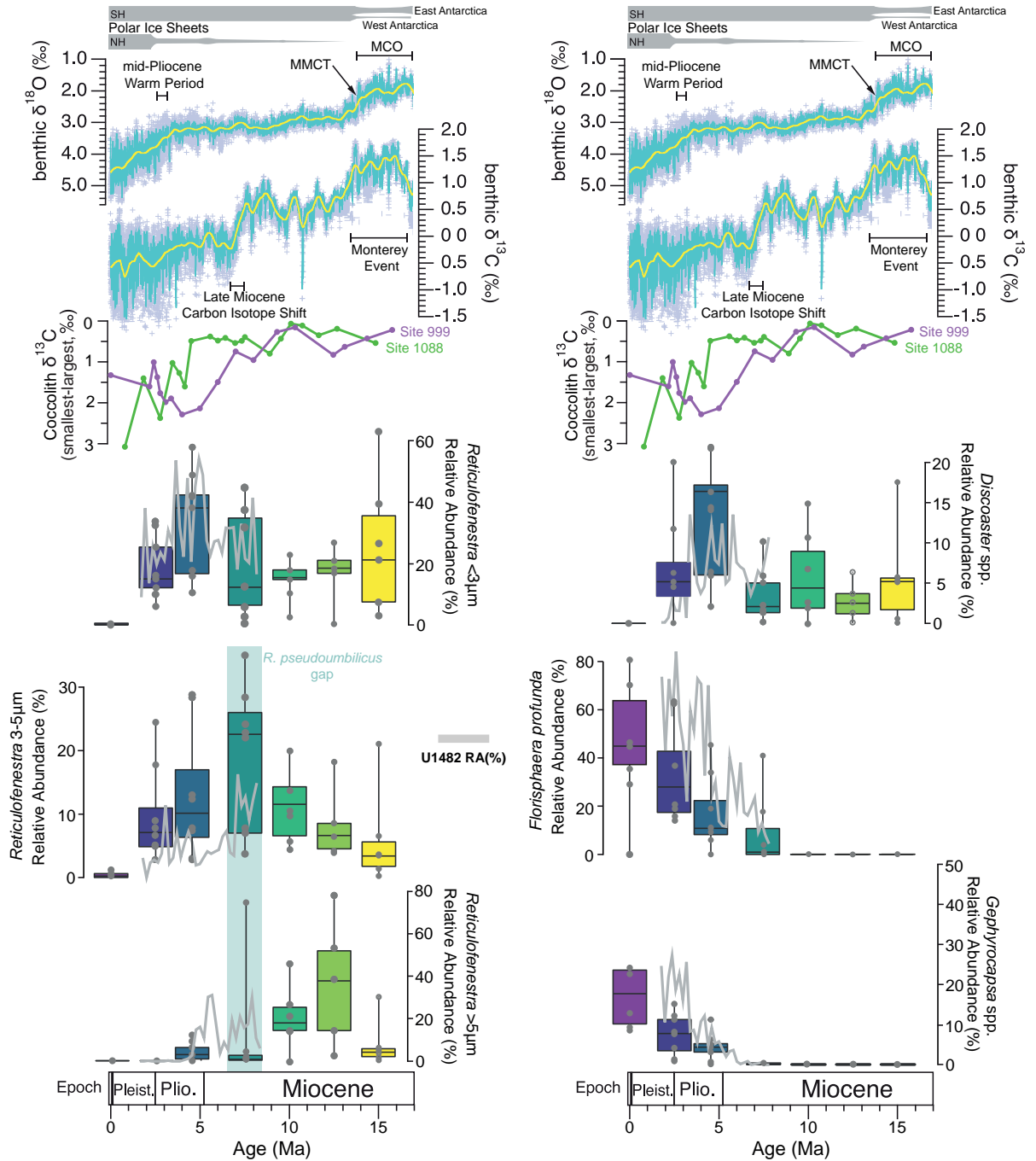


Figure 4.5: From top to bottom: Horizontal grey bars show the extent of the northern hemisphere (NH) and southern hemisphere (SH) polar ice sheets through time. Benthic  $\delta^{18}\text{O}$  and benthic  $\delta^{13}\text{C}$  portraying significant palaeoceanographic events over the past 17 Ma; edited after Westerhold et al. (2020) Cenozoic Global Reference benthic foraminifer carbon and oxygen Isotope Dataset (CENOGRID). Coccolith  $\delta^{13}\text{C}$  after Bolton and Stoll (2013) ranging from 16 Ma to recent; green plot indicates Site 1088 and purple plot is Site 999. Boxplots represent the relative abundance of the main calcareous nannofossil groups at each time slice of this study, with dark grey dots depicting the abundance of species across all sites at each particular time slice. Light grey line plots represent high resolution nannofossil data from U1482. Pale green vertical line portrays the *Reticulofenestra pseudumbilicus* gap.

The first appearance of *Florisphaera profunda* occurs in the Miocene ( $\sim 7.7$  Ma) (Figure 4.5; Plate 4.4). From the early late Miocene to the Pleistocene, this species relative abundance increases with time reaching it's maximum relative abundance at a single site (U1489) of 79% at 0 Ma (Figure 4.5). Strong variation in *F. profunda* relative abundance exists between sites but this taxa becomes increasingly established with time, displaying the largest and quickest rise in abundance of all the groups.

The abundance of the *Discoaster* spp. group remains relatively stable from the mid to late Miocene, (Figure 4.5) but at 4.5 Ma, in the Pliocene, the groups median abundance rises in both the global (to  $\sim 16\%$ ) and the U1482 data ( $\sim 14\%$ ). The relative abundance of this group then falls sharply in the late Pliocene prior to the *Discoaster* global extinction at 1.9 Ma (Bown et al. 2004, Bown 2005a).

Upper Euphotic	Lower Euphotic	Sub Euphotic
<i>Discoaster</i> spp. <i>Gephyrocapsa</i> spp. <i>Rhabdosphaera xiphos</i> <i>Reticulofenestra</i> spp. ( $<3\mu\text{m}$ ) <i>Reticulofenestra</i> spp. ( $3-5\mu\text{m}$ ) <i>Reticulofenestra</i> spp. ( $>5\mu\text{m}$ )	<i>Ceratolithus</i> spp. <i>Emiliana huxleyi</i> <i>Gephyrocapsa ericonsii</i> <i>Rhabdosphaera clavigera</i> <i>Syracosphaera</i> spp.	<i>Calciosolenia murrayi</i> <i>Florisphaera profunda</i> <i>Gladiolithus flabellatus</i>

Figure 4.6: List of calcareous nannofossil species depth habitat preferences as used in Boscolo-Galazzo et al. (2021). Upper Euphotic,  $>10\%$  surface irradiance, Lower Euphotic,  $10-1\%$  surface irradiance and Sub Euphotic Zone,  $<1\%$  surface irradiance after Poulton et al. (2017).

### 4.3.3 CALCAREOUS NANNOPLANKTON ECOGROUPS

Coccolithophores inhabit the water column at differing depths depending on their ecological preferences and photosynthetic requirements. Such zones include the Upper Euphotic Zone (UEZ), Lower Euphotic Zone (LEZ) and Sub Euphotic Zone (SEZ) and are defined based on surface irradiance measurements in the water column (Poulton et al. 2017) (Figure 4.6).

Calcareous nannoplankton show variations in abundance through time between the Upper Euphotic (UEZ) and Sub Euphotic zone (SEZ) ecogroups with both revealing long-term trends towards increased abundance of SEZ ecotypes towards the Holocene. Calcareous nannofossil assemblages are dominated by the UEZ ecogroup from 15 to 10 Ma. By 7.5 Ma the SEZ begins to rise and by 2.5 Ma is almost at equal abundance with the UEZ ecogroup. At the same time the Lower Euphotic Zone (LEZ) ecogroup emerges, but at dramatically lower

values ( $<0.1$ - $1.3\%$ ). At 0 Ma the SEZ becomes the dominant ecogroup ( $72\%$ ) while the UEZ ecogroup falls to  $27\%$  (Figure 4.7).

The number of UEZ ecogroup species recorded shows a rise from the Miocene to the Pliocene, followed by a vast decline by the Holocene. Conversely, the number of SEZ and LEZ ecogroup species shows little change, with both ecogroups establishing at 10 Ma (Figure 4.7). Yet, the SEZ ecogroup abundance increases dramatically in time despite fewer species being recorded than the LEZ and UEZ ecogroups.

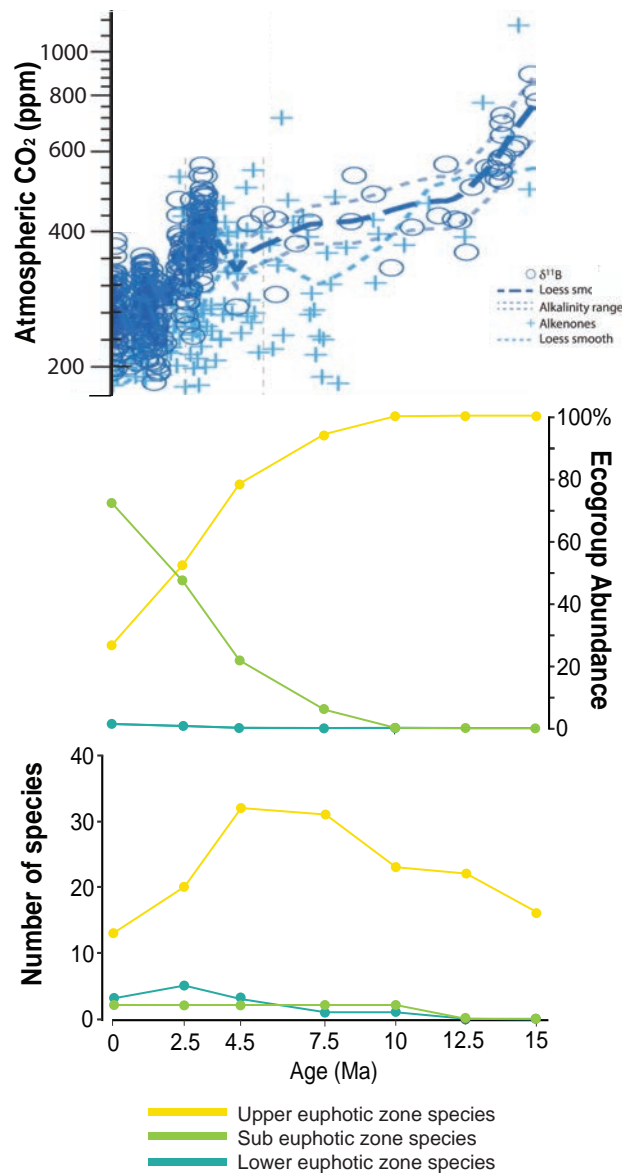


Figure 4.7: Global compiled calcareous nannofossil ecogroup abundance and number of species plotted with atmospheric CO<sub>2</sub> over the last 15 Ma. Ecogroup abundance and number of species data modified after Boscolo-Galazzo et al., (*in review*), atmospheric CO<sub>2</sub> data modified after Rae et al. (2021).

## 4.4 DISCUSSION

After the middle Miocene Climatic Optimum (MCO; 16.9 – 14.7 Ma), the warmest interval of the Neogene (Diester-Haass et al. 2009, Super et al. 2018), considerable global cooling led to the formation of modern ice-house conditions (Westerhold et al. 2020). From our data it is clear that this is also a time of major restructuring of coccolithophore assemblages – from the larger reticulofenestrid assemblages of the mid- to late-Miocene to the modern dominance of *Gephyrocapsa-Florisphaera* – with an associated decline in species richness and absolute (S) diversity (Figure 4.4). There is good evidence that marked changes in coccolithophore cell size, calcification and carbon allocation mechanisms are coupled to declining CO<sub>2</sub> through the Neogene (Bolton and Stoll 2013, Bolton et al. 2016). Progressively decreasing coccolithophore calcification (thinner coccoliths) in the Noelaerhabdaceae lineage is attributed to decreasing CO<sub>2</sub> and ocean alkalinity over the past 15 Ma (Bolton et al. 2016, McClelland et al. 2016, Rae et al. 2021, Šupraha and Henderiks 2020). Although this CO<sub>2</sub>-driver tallies with, and can potentially explain, the shift we observe from large to small reticulofenestrid assemblages in the Mio-Pliocene, it does not offer an immediate explanation of the Plio-Pleistocene loss of diversity and progressive dominance of lower photic zone specialist phytoplankton. Recent studies, have, however proposed a new consideration of temperature-dependent nutricline depth as an additional driver of macroevolution within the microplankton through the late Neogene (Boscolo-Galazzo et al. 2021). Below we explore these two potential drivers of the late Neogene trends in our calcareous nannoplankton assemblage and diversity compilation.

### 4.4.1 SPECIES RICHNESS

The compiled species richness and RTD from our nine global sites, when compared with calcareous nannofossil number of species after Lowery et al. (2020) is far greater (Figure 4.3). Similarly, our high resolution (200 ka) sample data from Site U1482 is higher than that of Lowery et al. (2020). These results consider all species and species morphotypes within calculated richness measurements, and therefore explains the higher records seen in this comparison. The peak in global compiled species richness and RTD (purple line plots; Figure 4.3) occurs during the mid-Pliocene can be deduced to be due to the large number of *Discoaster* morphotypes seen during this interval. Some of these morphotypes are currently not recognised

as new species, however, recently Fernando et al. (2020) described *Discoaster alyssae* (Plate 4.2, Fig. 17) and other variants from IODP Expedition 363, as used in this study; consequently, including these morphotypes in the species richness results seemed logical. However, we recognise that these species richness and RTD are therefore excessive. Despite this, the trends of U1482 species richness and RTD (blue line plots; Figure 4.3) follow similar trends to that of Lowery et al. (2020), overall declining from the mid-Miocene to the Pleistocene, displaying this sites potential as a diversity hotspot in the Indo-Pacific Warm Pool during the Neogene.

#### 4.4.2 LITH SIZE vs $p\text{CO}_2$

A decrease in coccolith size – and from that inferred cell size - within both the reticulofenestrids (Bolton et al. 2016) and *Helicosphaera* (Šupraha and Henderiks 2020) has been associated with cellular carbon limitation driven by declining atmospheric  $\text{CO}_2$  (Bolton et al. 2016, Imai et al. 2015, Suchéras-Marx and Henderiks 2014, Young 1990). The Retic.  $>5\ \mu\text{m}$  and  $3\text{--}5\ \mu\text{m}$  groups during the middle Miocene (15–12.5 Ma) suggest a post-MCO abundance increase but display biogeographical variability across globally compiled sampled sites. The ecological prominence of *Reticulofenestra* is noted across all latitudes coupled with abundance variability across all size groups through the Miocene (Figure 4.5). Henderiks et al. (2020) presents data from the Atlantic Ocean showing increased abundances of medium to large size *Reticulofenestra* (coccoliths  $3\text{--}7\ \mu\text{m}$ ) during the MCO followed by a post-MMCT (middle Miocene Climate transition; 14.7–13.8 Ma) proposed to be driven via a diversification in coccolith morphology and relative abundance increase. This is observed in our results too, as the smallest reticulofenestrids (Retic.  $<3\ \mu\text{m}$  group) are less consistent in abundance while the Retic.  $3\text{--}5\ \mu\text{m}$  abundance increases (Haq 1980, Henderiks et al. 2020).

Assemblage data from the middle to late Miocene (12.5–7.5 Ma) indicate strong directional change within the reticulofenestrid groups, with a marked decline of large *Reticulofenestra* species continuing up to the “*R. pseudoumbilicus* gap” (Young et al. (1998) or “*R. pseudoumbilicus* paracme”; Gibbs et al. (2005)) a pronounced event noted across multiple ocean basins (Rio et al. 1990, Gartner 1992, Takayama 1993, Young 1990, Raffi et al. 1995, 2003). Data from U1482 mirrors a decline in the Retic.  $>5\ \mu\text{m}$  group, but at the end of the event (Figure 4.5). However, both the  $<3\ \mu\text{m}$  and  $3\text{--}5\ \mu\text{m}$  group abundance increases greatly during the *R.*



*psuedoumbilicus* gap, consistent with an overall mean cell size decrease with declining  $p\text{CO}_2$  (Henderiks et al. 2020). The decline in relative abundance for the largest *Reticulofenestra* group begins at 12.5 Ma and likely corresponds with the late Miocene Carbon Isotope Shift (LMCIS) (Westerhold et al. 2020). The LMCIS is a  $-1\text{‰}$  shift in oceanic  $\delta^{13}\text{C}$  and represents the last important carbon cycle shift seen globally in ocean basins (Drury et al. 2017). Atmospheric  $\text{CO}_2$  displays no significant change through this interval but remains on a long-term declining path. The calcification of coccolithophores decreased across 6-4 Ma, partly driven by declining  $\text{CO}_2$  via reduced cellular bicarbonate allocation to calcification (Bolton et al. 2016). The loss of large *Reticulofenestra* species therefore suggests selective pressures (e.g. cooling climate via declining  $\text{CO}_2$ ) favour the smaller, opportunistic reticulofenestrid morphotypes.

An abundance increase in *Gephyrocapsa* spp. is documented across all sites from the mid-Pliocene (4.5 Ma), coinciding with a decrease in abundance of the Retic.  $<3\text{ }\mu\text{m}$  and 3-5  $\mu\text{m}$  group. A similar shift is noted in the Indian Ocean from IODP Exp 356 (NW Australian Shelf) where the small reticulofenestrids recorded at 4.5 Ma show an abundance decrease and a pronounced increase in *Gephyrocapsa* spp. develops by 4.42 Ma (Karatsolis et al. 2020). Almost exactly the same signal is recorded in our data from U1482, where the Retic.  $>5\text{ }\mu\text{m}$  group declines to very low levels at  $\sim 4\text{ Ma}$  with a corresponding rise in the abundance of *Gephyrocapsa* spp. These events preceed the onset of the mid-Pliocene Warm Period ( $\sim 3\text{ Ma}$ ; mPWP), a transient warm interval and high-resolution data from U1482 depicts *Reticulofenestra* abundance declines regardless through the mPWP, therefore suggesting, new evolutionary forces are likely controlling nanoplankton communities. These trends continue across the Plio-Pleistocene such that almost all the Retic. groups have disappeared or been reduced to very low abundances in the Holocene samples, to be replaced by rising *Gephyrocapsa* spp. abundance.

#### 4.4.3 NUTRICLINE

*Florisphaera profunda* is an extant SEZ species (Poulton et al. 2017, Takahashi and Okada 2000) that inhabits depths below the deep chlorophyll maximum ( $\sim 60\text{-}200\text{ m}$ ) within tropical and subtropical surface-waters (Hernández-Almeida et al. 2019, Okada 1983). The artichoke-shape of a *Florisphaera* coccosphere, like other coccospheres, disarticulates after death and the individual liths become preserved in sediments. Therefore, despite it's high relative abundance

from the Pliocene onwards, (Figure 4.5) this may be due to its higher concentration of liths on its coccosphere compared to other taxa e.g. *Gephyrocapsa* spp. The proliferation of *F. profunda* initiates at ~7.7 Ma at Site U1482, and then at all tropical and sub-tropical locations through the Pliocene to Holocene subsequently, indicating a long-term shift of coccolithophore biomass into SEZ habitats over the past ~7 Ma. This shift correlates with a decline of all reticulofenestrid size groups – starting with the largest cell sizes – and a switch in dominance to gephyrocapsids in the Pliocene. The late Neogene decrease in Noelaerhabdaceae coccolith size has been ascribed to carbon limitation with declining CO<sub>2</sub> (see above), but cell-size constraints do not explain the rise of the *Gephyrocapsa* lineage (including *Gephyrocapsa huxleyi* following Bendif et al. 2019) through the Plio-Pleistocene, as coccolith – and inferred cell sizes – overlap with those of the small reticulofenestrids. Instead the ecological replacement of the closely related *Reticulofenestra* by *Gephyrocapsa* strongly implies an adaptive advantage of *Gephyrocapsa* spp. within the Plio-Pleistocene oceans. This suggests a mechanism that explains the coupled shift towards *Gephyrocapsa*- and *Florisphaera*-dominated assemblages within the context of the recently documented deepening of the nutricline through the late Neogene (Boscolo-Galazzo et al. 2021).

A deepening nutricline in non-upwelling tropical and sub-tropical locations is clearly consistent with the great increase in the abundance of specialist SEZ coccolithophores since the late Miocene. These specialist SEZ taxa show clear adaptations to deep, low-light environments (Hernández-Almeida et al. 2019, Bown et al. 2009) where macro-nutrient concentrations are higher than overlying oligotrophic surface waters (Poulton et al. 2017). Such adaptations, that allow a shift in depth-habitat, are one possible response to increasing nutrient limitation in the mixed-layer. Another adaptive strategy would be to become more efficient in nutrient utilization at the expense of maximum growth rates (Zhao et al. 2015). In the modern oceans, this exactly the strategy of the bloom-forming *Gephyrocapsa huxleyi*, which is highly efficient in nutrient use, out-competing diatoms under nutrient limitation (Zhao et al. 2015). Modern *Gephyrocapsa oceanica* behaves in a similar manner, but with a higher optimal growth temperature than *Gephyrocapsa huxleyi* and explains much of the modern biogeography of these two closely related species (Gafar and Schulz 2018). In this context, the Plio-Pleistocene shift to a “*Gephyrocapsa*-*Florisphaera* world” is consistent with a deepening nutricline driven by a temperature-dependent reduction in the efficiency of nutrient recycling (Boscolo-Galazzo

et al. 2021). The reponse of *Florisphaera* is to go deep, whilst *Gephyrocapsa* becomes more efficient in nutrient utilisation than it's ancestral reticulofenestrads.

Alongside *Florisphaera*, *Gephyrocapsa* and other reticulofenestrads, data also shows the abundance of *Discoaster* spp. across sites from the mid-Miocene to Recent. The ecology and early Pleistocene extinction of the *Discoaster* group remains unclear (Chapman and Chepstow-Lusty 1997, Raffi et al. 2006, Schueth and Bralower 2015) but evidence suggests a change in productivity and water column-stratification with the onset of Northern Hemisphere glaciation played a role in the groups extinction (Tangunan et al. 2018, Schueth and Bralower 2015). Previous studies have argued that the discoasters have a similar deep-photoc zone ecology to *F. profunda*, mostly on the basis of their clear preference for warm-water, open ocean tropical water masses (Tangunan et al. 2018, Schueth and Bralower 2015). Our long-term view, however, suggests an ecology quite distinct from *F. profunda* – a group that rises to dominance through the Pliocene to early Pleistocene interval when the final Neogene *Discoaster* species are going extinct (Chapman and Chepstow-Lusty 1997, Raffi et al. 2006). In the framework we present, the Plio-Pleistocene *Discoaster* extinctions should be seen in the context of a deepening nutricline, the rise of specialist SEZ taxa and the dominance of the highly nutrient-efficient *Gephyrocapsa* lineage across mixed layer environments. In this context, an ecology of relatively high optimum growth temperatures and light and nutrient demands would be one poorly suited to the Pliocene-to-Recent oceans. Although the discoasters are routinely used as a marker for oligotrophic conditions palaeoecological studies (Bralower 2002, Bukry 1973, Wei and Wise 1990), these interpretations are of a relative oligotrophic preference; relative to contemporaneous placolith-bearing species. We suggest that instead of a Plio-Pleistocene eutrophication of sub-tropical and tropical oceans driving the loss of these iconic nannolith groups (Tangunan et al. 2018, Schueth and Bralower 2015), their extinction is actually driven by the progressive loss of nutrients from these mixed layers. This alternate hypothesis is more consistent with the long-term coccolithophore macroevolutionary trend to smaller, more efficient cells dominating the mixed layers and the occupation of the SEZ, as well as biogeochemical modelling and direct reconstructions of a deepening nutricline through the late Neogene (Boscolo-Galazzo et al. 2021).

## 4.5 CONCLUSION

This study offers a global deep-time perspective into macroevolutionary drivers that have influenced coccolithophore communities during long-term cooling of the Neogene for the last 15 Ma and provides insight to selective pressures endured by ancestral lineages, leading to the establishment modern coccolithophore communities.  $p\text{CO}_2$  played an important role in influencing certain calcareous nannofossils, such as the Noelaerhabdaceae family, due to a direct correlation with declining atmospheric  $\text{CO}_2$  and decline in *Reticulofenestra* coccolith size (Bolton et al. 2016). Factors associated with the Neogene long-term global cooling and carbon limitation, creates selective pressures on coccolithophore lineages, leading to diversity and size decline (Bolton et al. 2016, Finkel et al. 2007, Hannisdal et al. 2012, Šupraha and Henderiks 2020). However, despite the decline of the reticulofenestrids since the late Miocene, small *Gephyrocapsa* spp. abundance increases from the mid-Pliocene suggesting that  $p\text{CO}_2$  could not be the sole controlling driver of community change. Modern UEZ coccolithophores e.g., members of *Gephyrocapsa* spp., have adapted to nutrient depleted surface waters and are more eurythermal and eurytrophic (Henderiks et al. 2020). Moreover, evidence for a deepened nutricline, which developed through the Late Neogene, due to enhanced nutrient recycling at greater depth likely influenced nannofossil communities more than  $p\text{CO}_2$  alone as these changes occur across multiple nannofossil lineages, for example, the extinction of *Discoaster* at  $\sim 2.3$  Ma and the demise of *Reticulofenestra* groups; both UEZ species and the prolific increase of SEZ species *Florisphaera profunda*.

Plate 4.1

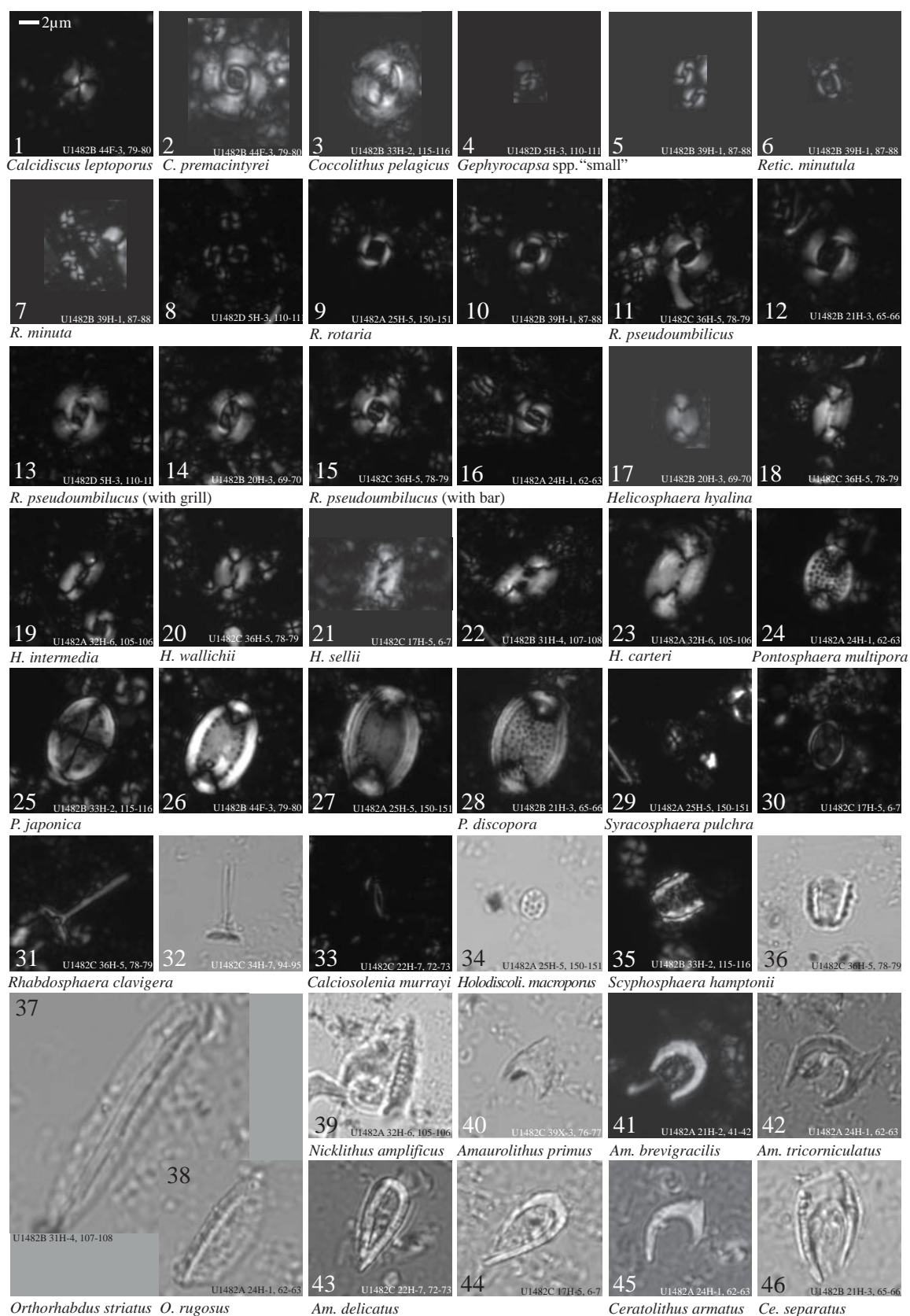


Plate 4.2

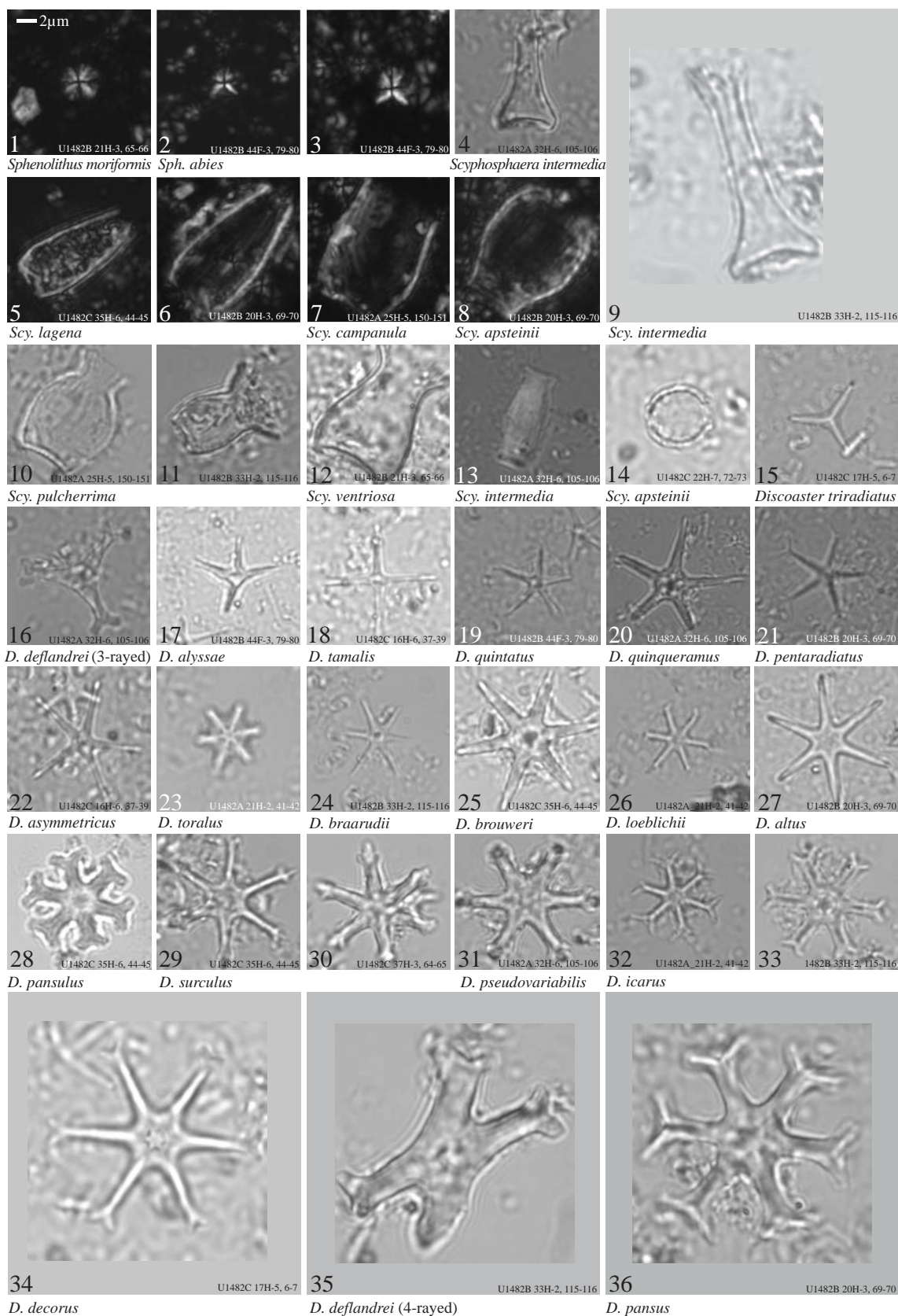




Plate 4.3

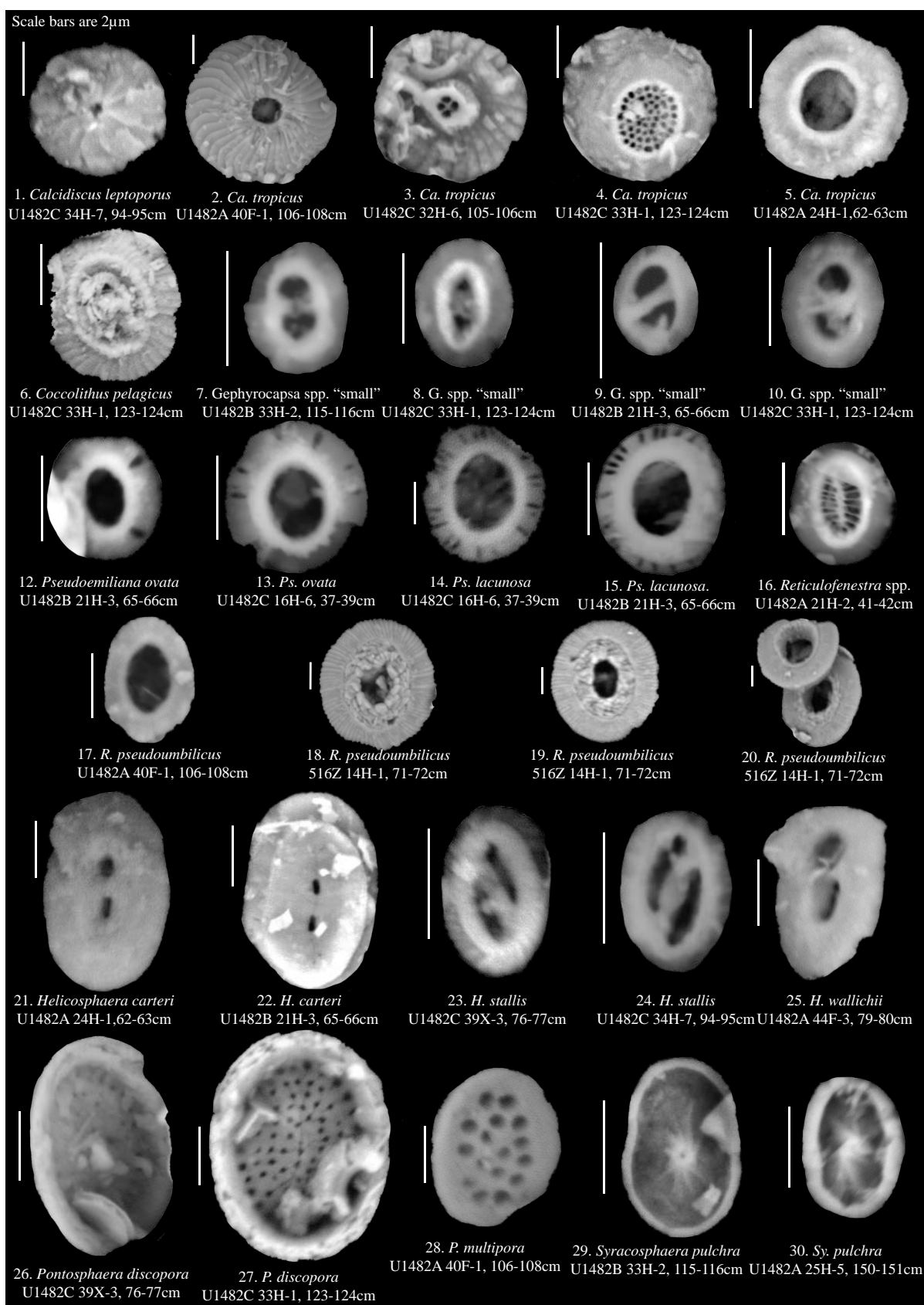


Plate 4.4

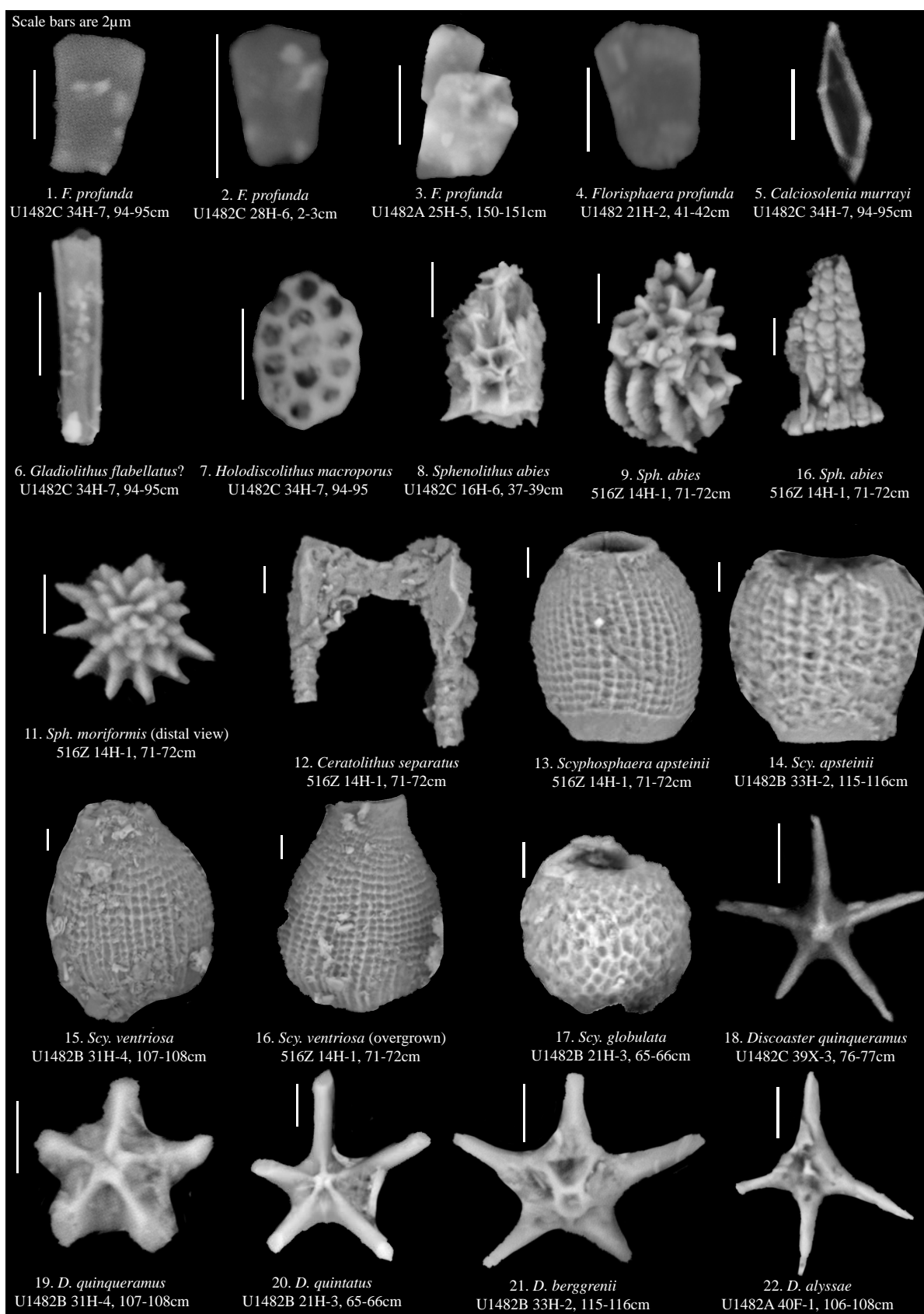
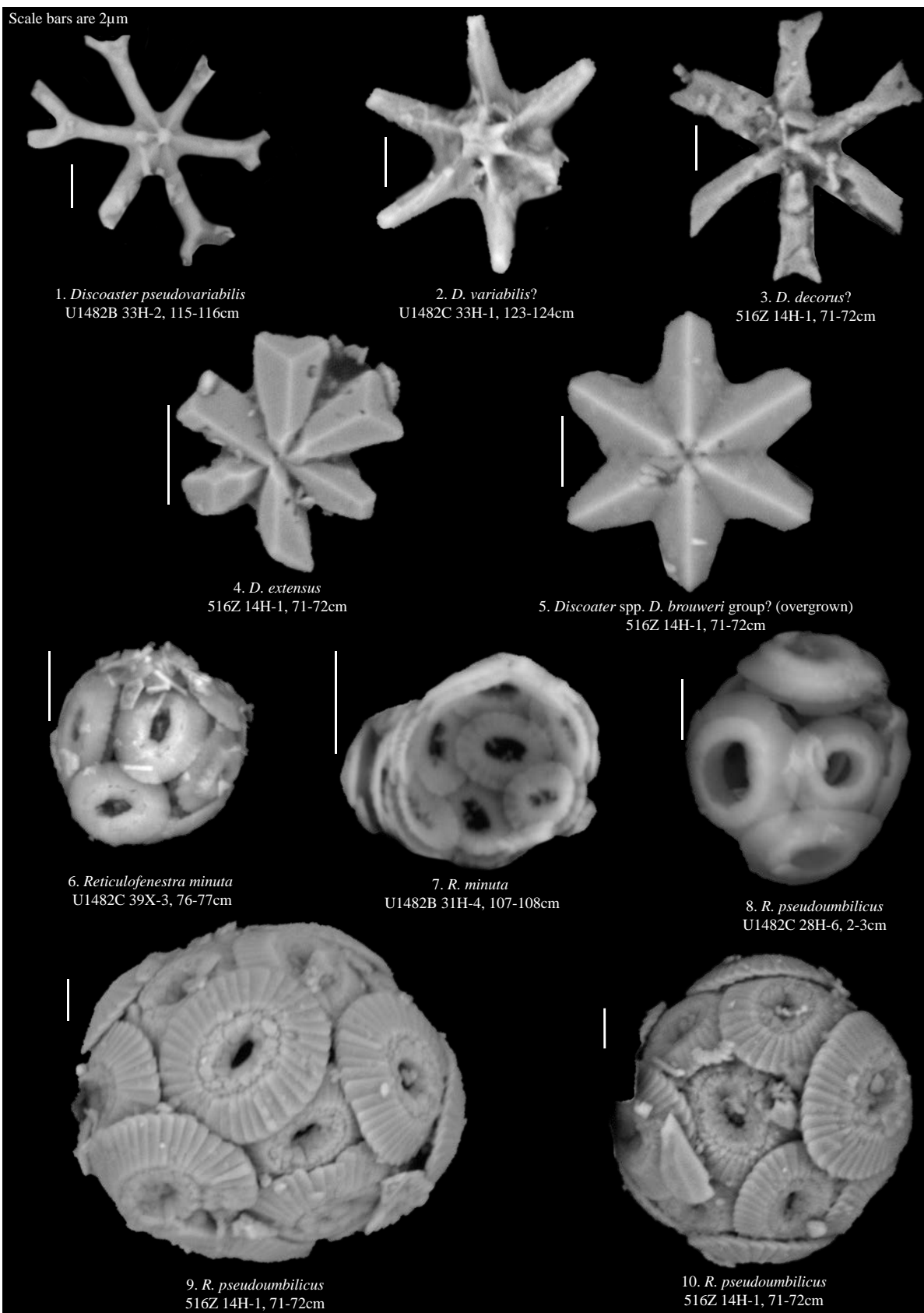




Plate 4.5





## 5 | CONCLUSIONS

### 5.1 SUMMARY

The principal objectives of this thesis were to record the nannoplankton assemblage response during two of the most significant cooling periods of the Cenozoic; across the Eocene-Oligocene Transition (EOT) and the Neogene to Recent, including an exploration of the selective pressures that influence coccolithophore macroevolution over the past 15 Ma. New on-shore drilling material from a single core, NKK1 of the Nanggulan Formation, Java, Indonesia, yielded a near-continuous succession of Eocene-Oligocene (E-O) marine clays and claystones, which documented the crucial EOT event, expressing good recovery and good to excellent preservation of nannofossils. High resolution nannofossil assemblage records were achieved for this stratigraphic sequence, furthering our understanding of tropical coccolithophore response through a climatically dramatic period of Earth's history. Detailed analysis of nannoplankton taxonomy, ecology, community restructuring, diversity and coccolith size were undertaken to address two of the key aims of this thesis, namely, to constrain the loss of calcareous nannoplankton diversity, and the wider ecological response of tropical calcareous phytoplankton to progressive global cooling across the middle Eocene to late Eocene and EOT.

Calcareous nannoplankton assemblage data from multiple deep-sea locations record the long-term cooling of the Neogene, documenting assemblage restructuring and species diversity over the last 15 Ma. Two datasets were collected, first high-resolution tropical site U1482 and second, "time-slice" reconstructions from nine additional global sites from varying latitudes. Data from U1482 served as a new illustrative high-diversity, low-latitude succession within the Indo-Pacific Warm Pool (IPWP) region with a continuous record through the key late Miocene to early Pleistocene interval. The compilation of these high-resolution and time-slice datasets address this theses' final aim; investigating late Neogene macroevolutionary drivers

and the origin of the “modern flora” as well as providing a more detailed picture of late Neogene trends in global coccolithophore diversity, coccolith size and communities.

### 5.1.1 THE EOCENE-OLIGOCENE TRANSITION

The EOT marks the culmination of a critical point in Earth history, the transition from greenhouse to icehouse conditions. High-resolution records from NKK1 provided the first recorded account of IPWP calcareous phytoplankton communities from the late middle Eocene to early Oligocene (Chapter 2). The biostratigraphy and detailed accounts of taxonomy of these assemblages were assessed and determined a new age model for the succession and indicated that some key bioevents before the E-O were potentially diachronous between the mid-latitudes and IPWP (Chapter 3). Together, this data provided a detailed account of calcareous nannofossil response to the EOT within a representative low-latitude locality and is a valuable archive in identifying calcareous nannofossil ecology, biogeography and community restructuring, diversity patterns and biostratigraphy.

Assemblages show a progressive decline in species diversity through the EOT interval and is interpreted as a direct response to enhanced supply of nutrients to low-latitude surface waters from Southern Ocean-sourced subthermocline waters (Chapter 2). The extinction of the rosette-shaped discoasters, *D. barbadiensis* and *D. saipanensis* signifies the point at which community restructuring and extinctions of nannofossils were most intense - at ~34.44 Ma. The timing and nature of these changes in assemblages have consistent features between globally distributed locations; the extinction of warm-water oligotrophs and increased dominance of eutrophic taxa and/or those species with temperate- and cool-water associations. The *Discoaster* Extinction Event (DEE) represents the earliest biotic response to the large-scale environmental changes expressed during the EOT. We record calcareous nannofossil responses substantially prior to that of other plankton groups, including planktic and benthic foraminifera, whose extinctions lie at the Eocene-Oligocene Boundary (EOB). Conversely, calcareous nannofossils show little change at the EOB despite distinct community restructuring at the DEE. Calcareous nannofossils show that reticulofenestrid coccolith size mean and 95%<sub>tile</sub> increased across the EOT interval. There is a pronounced loss of smaller reticulofenestrid morphotypes over the DEE with a rapid switch in the dominance of larger reticulofenestrid cell size. We interpret this dominance switch as a signal of no obvious or

significant  $p\text{CO}_2$  limitation on cell size in NKK1 through the EOT and that instead, a longer-term  $p\text{CO}_2$  control exists through the Paleogene.

The taxonomy of calcareous nannofossils in NKK1 (Chapter 3) were documented and addressed the question of latitudinal and spatial diversity gradients of phytoplankton in the middle and late Eocene. Detailed biostratigraphic records test the nature of nannoplankton community restructuring, diversity loss and extinction diachroneity during the EOT within the IPWP. Recently developed biostratigraphic zonation schemes for mid-latitudes (Agnini et al. 2014) were tested for NKK1 assemblages to assess the bioevents utilisation at low-latitudes. Assemblages indicate the IPWP region is a key location in coccolithophore speciation as younger Oligocene taxa, *Sphenolithus concicus* and *Triquetrorhabdus carinatus* were identified in middle to upper Eocene sediments and two new species were identified and described; *Coccolithus aspida* and *Reticulofenestra nanggulanensis*.

The NKK1 age model, with nannofossil and planktic foraminifera bioevents, tested the application of the Agnini et al. (2014) biozonation scheme and showed consistent results. The use of both Agnini et al. (2014) and Martini (1971) schemes improves overall stratigraphic subdivision of the upper Eocene due to an increased number of biohorizons found at mid- and low latitudes. In the late Eocene, the calibrated ages of bioevents from Agnini et al. (2014) provided a consistent age model for NKK1 and is coherent with planktic foraminifera ages. The synchronous extinction of *Reticulofenestra reticulata* and *R. isabellae* is documented at  $\sim 34.5$  Ma in NKK1, proving that the last occurrence of *R. reticulata* is diachronous across latitudes as this species is  $\sim 0.7$ - $0.8$  Ma younger in NKK1 compared with the Agnini et al. (2014) biozonation scheme. Due to an unconformity between the upper Jetis Beds and lower Tegalsari Marls (88.02–86.85 mbgl; CNE17–CNE18 and NP18) the boundary between middle and upper Eocene was not present, therefore, biostratigraphic assessment of these zones were not possible.

### 5.1.2 DRIVERS OF MACROEVOLUTION IN NANNOPLANKTON DURING THE LATE NEOGENE

Several calcareous phytoplankton groups clearly show long-term macroevolutionary morphological change in response to long-term directional evolution of global climate through the late Neogene. Declining atmospheric  $\text{CO}_2$  is thought to be the driver of long-term cooling and

deepening global ice-house conditions from the mid Miocene to Recent and can be correlated with a reduction in coccolithophore cell size and diversity through time. The global compilation of sites compared with tropical Site U1482, provide a new perspective into whether the macroevolutionary drivers of change were purely driven by the direct impacts of declining CO<sub>2</sub>, or also involved the impact of cooling on ocean structure and biogeochemistry over the last 15 Ma. This study facilitated the understanding of the selective pressures experienced by ancestral nanoplankton taxa which ultimately led to the establishment of modern communities.

Selective pressures on coccolithophore lineages were created due to factors associated with the long-term cooling of the Neogene and carbon limitation and resulted in a diversity and coccolith size decline.  $p\text{CO}_2$  had a significant role in affecting specific calcareous nanoplankton taxa, especially the Noelaerhabdaceae, as a direct correlation between declining atmospheric CO<sub>2</sub> and coccolith size decrease across the *Reticulofenestra* since the late Miocene was observed (Henderiks et al. 2020). In the Plio-Pleistocene the abundance of small *Gephyrocapsa* spp. increased at the expense of similar sized small reticulofenestrids, showing that there are multiple controlling factors were forcing community change, rather than solely a  $p\text{CO}_2$  control on cell size. Extant upper euphotic zone (UEZ) coccolithophores, e.g. *Gephyrocapsa* spp., are adapted to environments where surface ocean conditions are nutrient depleted (Henderiks et al. 2020). We present evidence that a deepening nutricline through the late Neogene influenced nanoplankton communities due greater nutrient recycling at depth and reduced nutrient availability in surface waters. A deeper nutricline over  $p\text{CO}_2$  alone, is consistent with the remarkable rise of sub-euphotic zone taxa through the same time interval, especially *Florisphaera profunda* and may be an explanation for the extinction (*Discoaster* spp.) or decline (*Reticulofenestra* groups) of UEZ group taxa.

## 5.2 FUTURE WORK

The EOT remains a key research area in palaeoceanography and palaeoclimatology, in both the terrestrial and marine realms (Colwyn and Hren 2019, Hutchinson et al. 2019, 2021, Kennedy-Asser et al. 2019, Sibert et al. 2020). Timing of Southern Ocean gateways (Huck et al. 2017, Houben et al. 2019), biotic overturning (Sibert et al. 2020) and EOT model-data comparisons (Kennedy-Asser et al. 2019, Hutchinson et al. 2021) are still debated. Research

remains somewhat focused on high-latitude localities, therefore, more assemblage data, including that of other plankton groups, at new or existing tropical localities would be of benefit.

The research in this thesis demonstrates the importance of low latitude tropical sites with regards to plankton communities, diversity, and oceanographic changes. Supplementary research could further underpin species-climate relationships over regional and potentially global scales during the EOT. It is understood, however, that there are limited low-latitude EOT localities at present due to continuous sedimentary records for the interval being uncommon which presents a limitation on the potential for future work, unless new localities are discovered and drilled.

Research on IODP Exp. 363, U1482 remains an ongoing project and further proxy data produced from the expedition's shipboard and shore-based scientists will strengthen results and interpretations for this site and therefore, this thesis. Yet, future research on long-term macroevolutionary drivers in coccolithophores would benefit from further insights into the coupling between morphological changes observed within specific genera and climate intervals during the Neogene. Higher-resolution assemblage records, from low latitude localities in addition to those presented in this thesis, would aid the identification of selective pressures, either climatic, environmental, or other, which may be influencing coccolithophore macroevolution. Although, finding continuous sedimentary records across numerous localities that can recover the same or similar age intervals and concurrently able to yield good nannofossil preservation may present challenges. Additionally, valid correlations in coccolithophore morphology and physiology only emerge when closely related taxa are pooled together, therefore, short-term physiological responses may not translate with long-term evolution of coccolithophores within the fossil record due to more complex selective pressures across longer time scales relating to numerous biotic and/or abiotic factors (Šupraha and Henderiks 2020).

# A | GLOBAL CALCAREOUS NANNOFOSSIL COUNT DATA (LOW RESOLUTION SAMPLING)



A.1 SITE U1482

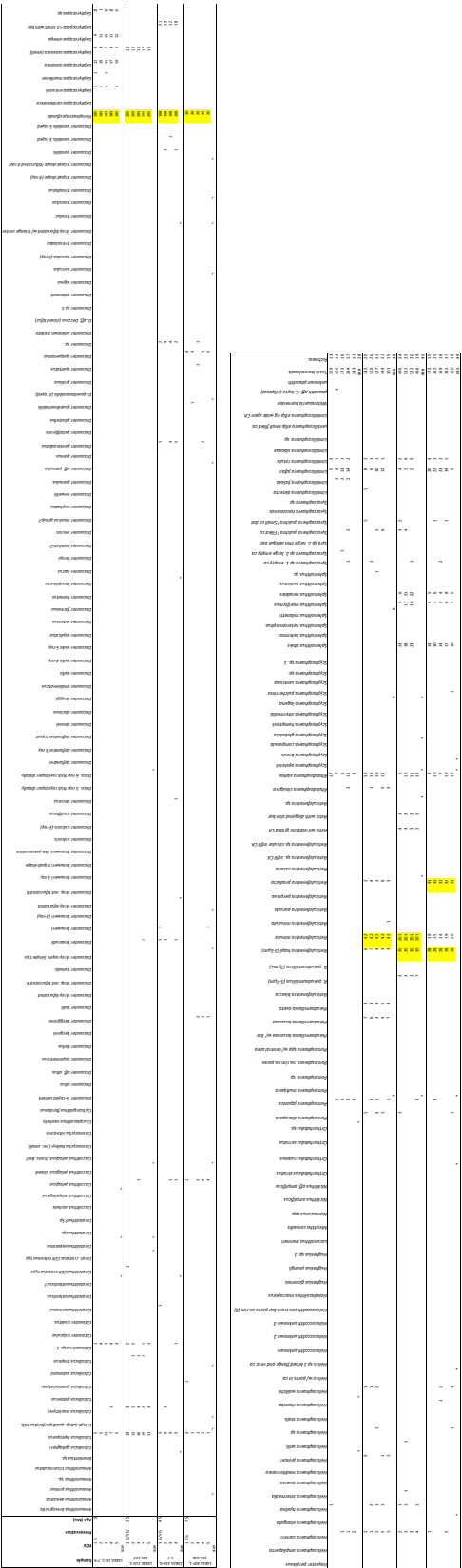


Figure A.1: Low resolution sampling count data for Site 1482

A.2 SITE U1489

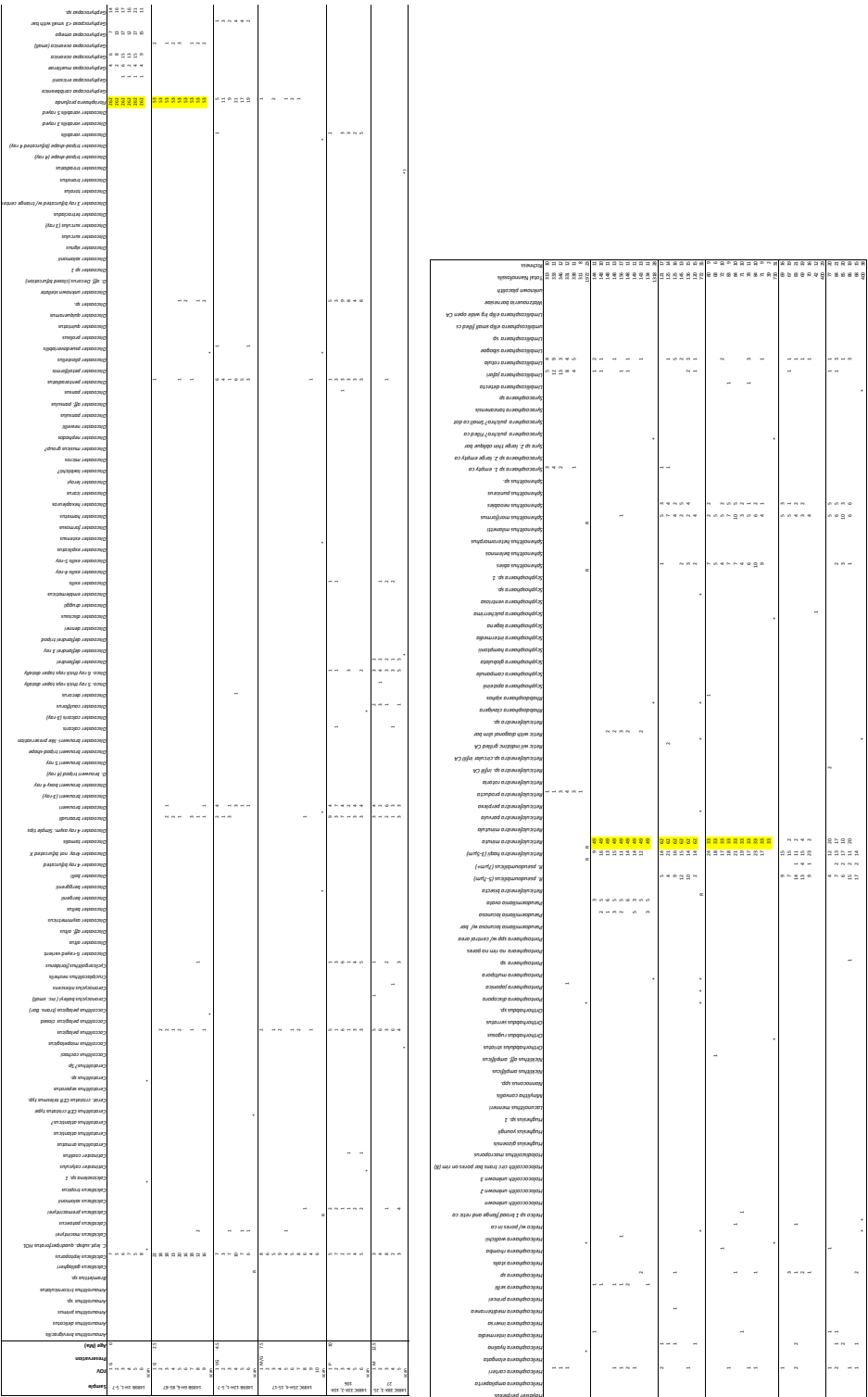


Figure A.2: Low resolution sampling count data for Site 1489

A.3 SITE U1490

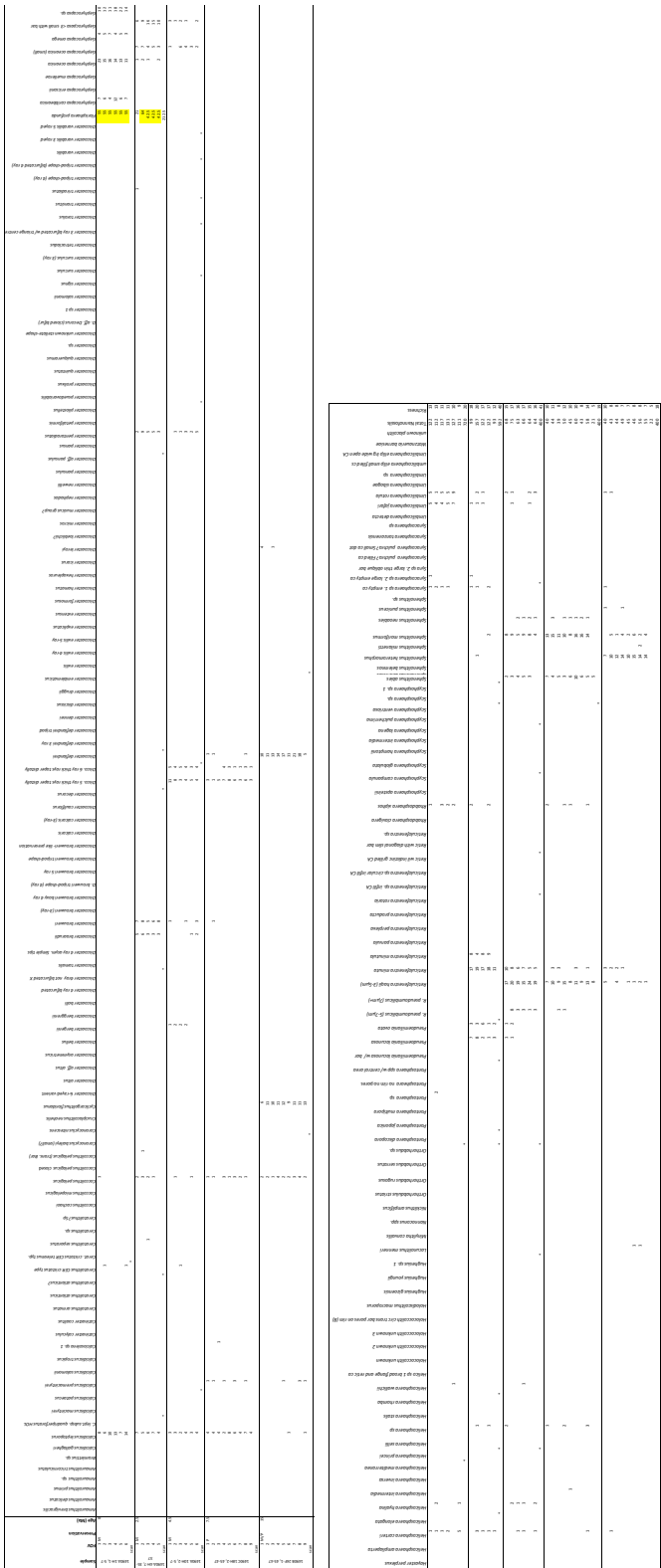
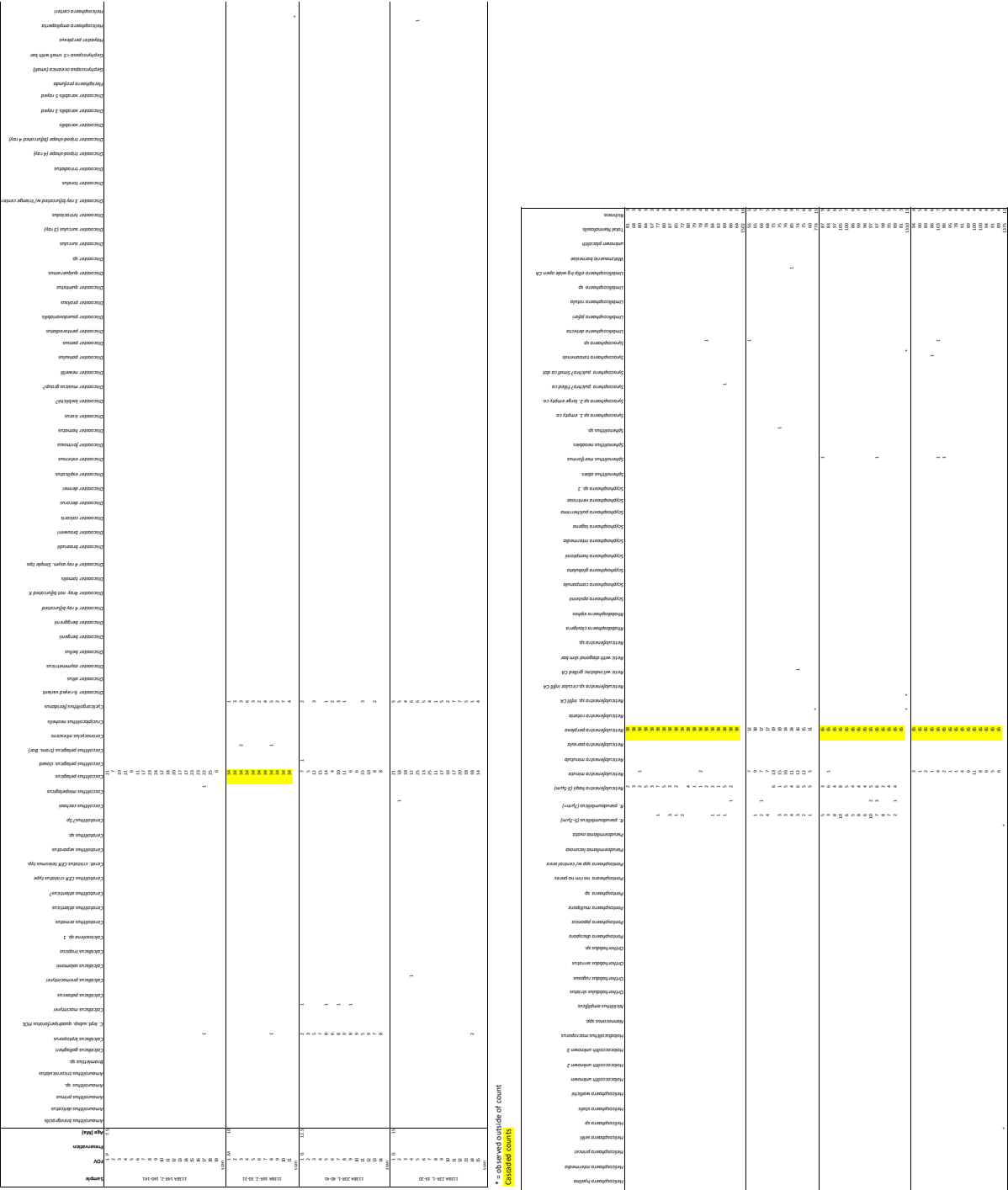


Figure A.3: Low resolution sampling count data for Site 1490

A.4 SITE 1138



## A.5 SITE 242

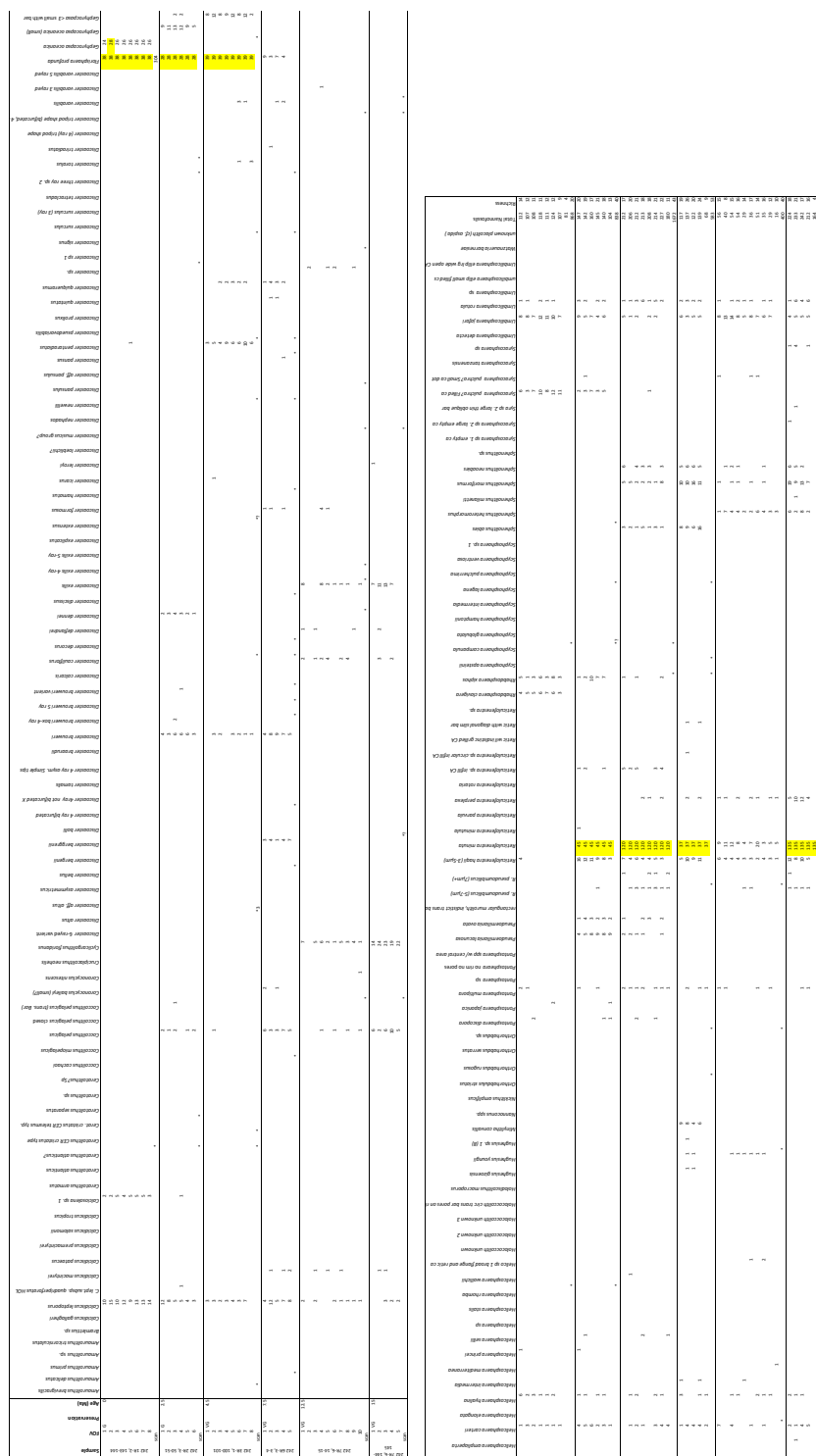


Figure A.5: Low resolution sampling count data for Site 242

## A.6 SITE 1338

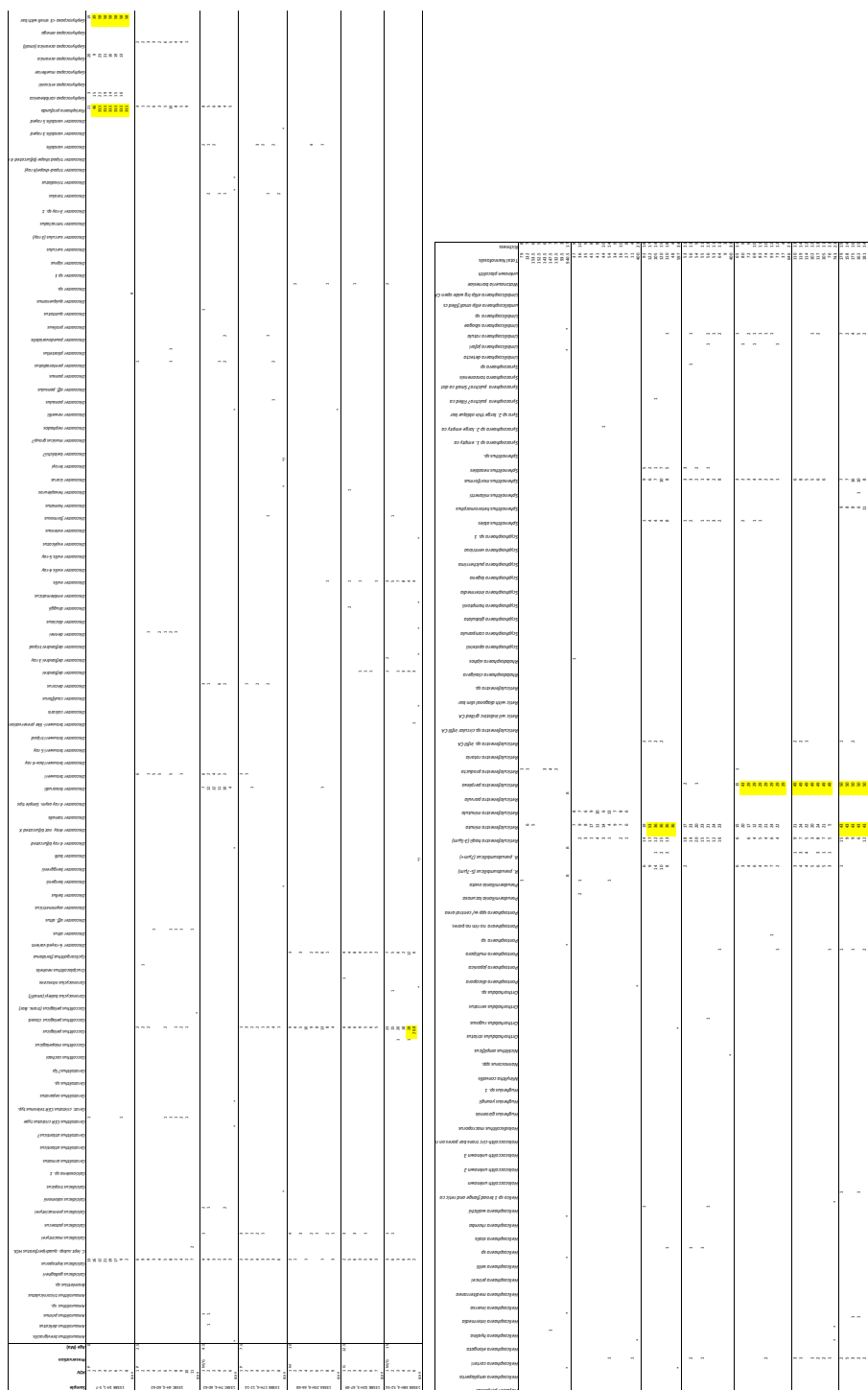


Figure A.6: Low resolution sampling count data for Site 1338



## A.8 SITE 871/872

[illegible]

Figure A.8: Low resolution sampling count data for Site 871/872





## A.10 DIVERSITY METRICS

### A.10.1 H' DIVERSITY, SPECIES RICHNESS AND RTD

Site	Age (Ma)	H' Diversity	Species Richness	RTD
516Z 1H-1, 50-52	0	2.06937618	33	50
1482A 1H-1, 7-9	0	1.33136753	28	52
1489B 1H-1, 5-7	0	0.92145578	23	52
1490A 1H-1, 5-7	0	1.83098806	20	52
1338B 1H-1, 5-7	0	1.60916697	17	52
242 1R-2, 143-144	0	1.81291587	20	52
516Z 3H-3, 38-40	2.5	2.6493276	35	84
925C 8H-6, 32-33.5	2.5	1.66088097	34	84
1482A 11H-2, 105-107	2.5	1.5434992	38	84
1489B 6H-6, 85-87	2.5	1.68718447	28	84
1490A 4H-7, 35-37	2.5	2.15301196	40	84
872A 2H-2, 120-121	2.5	2.61887103	38	85
1338C 4H-4, 60-62	2.5	2.19666237	23	86
242 2R-3, 50-51	2.5	2.31583447	40	84
516Z 8H-2, 8-9.5	4.5	2.46058676	50	117
925C 21H-5, 127-128.5	4.5	2.01159476	47	118
1482A 24H-6, 5-7	4.5	1.75984014	45	118
1489B 12H-1, 5-7	4.5	1.9239299	35	116
1490A 10H-2, 5-7	4.5	2.53108296	41	116
872C 3H-5, 113-115	4.5	2.31161999	45	116
1338C 7H-4, 60-62	4.5	2.26866314	34	116
242 3R-1, 100-101	4.5	1.66713163	43	117
925C 31H-5, 72-74	7.5	2.56676251	53	115
1482A 40F-1, 106-108	7.5	2.35156264	48	113
1489C 25H-4, 15-17	7.5	2.32669879	31	115
1490C 18H-2, 45-47	7.5	1.67002923	19	113
1338B 17H-4, 12-14	7.5	2.12980921	33	113
242 6R-3, 3-4	7.5	1.98577093	52	114
1138A 14R-2, 140-141	7.5	0.74424151	10	112
516Z 14H-1, 71-72.5	10	2.59353456	44	98
925C 35X-2, 7-9	10	2.64469167	38	97
1489C 33X-2, 104-106	10	2.73104636	29	97
872C 5H-4, 83-85	10	2.7594296	40	98
1338A 25H-6, 66-68	10	1.84857335	21	97
1138A 16R-2, 30-31	10	1.43632841	15	97
1489C 38X-3, 25-27	12.5	2.75203588	38	84
871B 5H-1, 12-14	12.5	1.90903411	29	84
1338B 32H-3, 67-69	12.5	1.85985366	23	84
242 7R-6, 14-15	12.5	1.1090787	40	84
1138A 20R-1, 40-41	12.5	2.60751152	13	83
516Z 17H-4, 2-3.5	15	2.34509887	40	69
1490B 26F-1, 45-47	15	1.83988816	18	68
871A 8H-1, 0-1	15	2.06899121	30	68
1338B 38H-4, 52-54	15	2.09879256	34	68
242 7R-6, 144-145	15	0.89086112	35	68
1138A 22R-1, 19-20	15	1.59520727	12	68

Figure A.10: H' diversity, species richness (abundance) and RTD values from all global sites used in Figure 4.4, Chapter 4

---

Age	Compiled Species Richness	Compiled RTD
0	62	62
2.5	90	101
4.5	121	135
7.5	92	117
10	98	111
12.5	70	85
15	72	72

Figure A.11: Compiled species richness and RTD values from Figure 4.4,Chapter 4

## A.10.2 ABSOLUTE AND RELATIVE ABUNDANCE

Site	Age	Retic. spp. (<3)	Retic. spp. (3-5)	Retic. spp. (>5)	<i>F. profunda</i>	<i>Gephyrocapsa</i> spp.	<i>Discoaster</i> spp.
516Z 1H-1, 50-52	0	5	0	0	315	66	0
1482A 1H-1, 7-9	0	0	0	0	925	171	0
1489B 1H-1, 5-7	0	0	13	0	1572	173	0
1490A 1H-1, 5-7	0	0	0	0	330	162	0
1338B 1H-1, 5-7	0	11	11	0	268	457	0
242 1R-2, 143-144	0	0	4	0	304	208	0
516Z 3H-3, 38-40	2.5	39	26	0	73	48	0
925C 8H-6, 32-33.5	2.5	66	51	0	700	15	18
1482A 11H-2, 105-107	2.5	210	42	0	1025	68	1
1489B 6H-6, 85-87	2.5	441	115	0	477	13	21
1490A 4H-7, 35-37	2.5	82	29	0	212.5	88	79
872A 2H-2, 120-121	2.5	64	70	0	60	44	25
1338C 4H-4, 60-62	2.5	92	97	0	53	32	38
242 2R-3, 50-51	2.5	270	64	1	168	63	46
516Z 8H-2, 8-9.5	4.5	80	150	63	57	23	70
925C 21H-5, 127-128.5	4.5	245	106	0	640	70	68
1482A 24H-6, 5-7	4.5	804	55	15	672	70	29
1489B 12H-1, 5-7	4.5	372	96	42	82	16	45
1490A 10H-2, 5-7	4.5	41	114	18	0	25	87
872C 3H-5, 113-115	4.5	270	52	6	60	75	86
1338C 7H-4, 60-62	4.5	216	78	52	36	0	102
242 3R-1, 100-101	4.5	960	52	22	312	71	81
925C 31H-5, 72-74	7.5	87	295	0	150	0	20
1482A 40F-1, 106-108	7.5	148	90	47	492	4	30
1489C 25H-4, 15-17	7.5	330	174	0	7	0	9
1490C 18H-2, 45-47	7.5	10	90	2	0	0	59
1338B 17H-4, 12-14	7.5	151	112	5	0	0	23
242 6R-3, 3-4	7.5	185	38	4	23	0	72
1138A 14R-2, 140-141	7.5	3	50	1113	0	0	0
516Z 14H-1, 71-72.5	10	64	58	97	0	0	25
925C 35X-2, 7-9	10	74	54	0	0	0	28
1489C 33X-2, 104-106	10	10	79	58	0	0	130
872C 5H-4, 83-85	10	59	38	85	0	0	59
1338A 25H-6, 66-68	10	154	36	296	0	0	10
1138A 16R-2, 30-31	10	114	33	206	0	0	0
1489C 38X-3, 25-27	12.5	67	69	57	0	0	73
871B 5H-1, 12-14	12.5	107	17	151	0	0	8
1338B 32H-3, 67-69	12.5	137	49	386	0	0	10
242 7R-6, 14-15	12.5	84	34	11	0	0	52
1138A 20R-1, 40-41	12.5	1	59	1001	0	0	0
516Z 17H-4, 2-3.5	15	66	5	24	0	0	4
1490B 26F-1, 45-47	15	8	14	0	0	0	125
871A 8H-1, 0-1	15	155	83	6	0	0	23
1338B 38H-4, 52-54	15	258	63	301	0	0	48
242 7R-6, 144-145	15	675	35	36	0	0	46
1138A 22R-1, 19-20	15	61	0	65	0	0	0

Figure A.12: Global main species groups absolute abundance values

Site	Age	Retic. spp. (<3)	Retic. spp. (3-5)	Retic. spp. (>5)	<i>F. profunda</i>	<i>Gephyrocapsa</i> spp.	<i>Discoaster</i> spp.
516Z 1H-1, 50-52	0	0.699300699	0	0	44.0559441	9.230769231	0
1482A 1H-1, 7-9	0	0	0	0	69.8113208	12.90566038	0
1489B 1H-1, 5-7	0	0	0.659229209	0	79.7160243	8.772819473	0
1490A 1H-1, 5-7	0	0	0	0	45.8333333	22.5	0
1338B 1H-1, 5-7	0	1.169590643	1.169590643	0	28.4954811	48.59117491	0
242 1R-2, 143-144	0	0	0.460829493	0	35.0230415	23.96313364	0
516Z 3H-3, 38-40	2.5	9.75	6.5	0	18.25	12	0
925C 8H-6, 32-33.5	2.5	6	4.636363636	0	63.6363636	1.363636364	4.5
1482A 11H-2, 105-107	2.5	12.8440367	2.568807339	0	62.6911315	4.159021407	0.049603175
1489B 6H-6, 85-87	2.5	33.45978756	8.725341426	0	36.1911988	0.986342944	5.25
1490A 4H-7, 35-37	2.5	13.86306002	4.902789518	0	35.9256128	14.87743026	19.75
872A 2H-2, 120-121	2.5	16	17.5	0	15	11	6.25
1338C 4H-4, 60-62	2.5	23	24.25	0	13.25	8	5.114401077
242 2R-3, 50-51	2.5	32.21957041	7.637231504	0.119331742	20.0477327	7.517899761	11.5
516Z 8H-2, 8-9.5	4.5	15.44401544	28.95752896	12.16216216	11.003861	4.44015444	13.51351351
925C 21H-5, 127-128.5	4.5	17.07317073	7.386759582	0	44.5993031	4.87804878	5.619834711
1482A 24H-6, 5-7	4.5	39.88095238	2.728174603	0.744047619	33.3333333	3.472222222	1.773700306
1489B 12H-1, 5-7	4.5	48.1865285	12.43523316	5.440414508	10.6217617	2.07253886	6.164383562
1490A 10H-2, 5-7	4.5	10.25	28.5	4.5	0	6.25	21.75
872C 3H-5, 113-115	4.5	40.29850746	7.76119403	0.895522388	8.95522388	11.19402985	21.5
1338C 7H-4, 60-62	4.5	36.18090452	13.06532663	8.710217755	6.03015075	0	15.78947368
242 3R-1, 100-101	4.5	57.41626794	3.110047847	1.315789474	18.6602871	4.246411483	13.89365352
925C 31H-5, 72-74	7.5	12.23140496	7.438016529	3.884297521	40.661157	0.330578512	2.090592334
1482A 40F-1, 106-108	7.5	10.29585799	34.9112426	0	17.7514793	0	1.509433962
1489C 25H-4, 15-17	7.5	45.20547945	23.83561644	0	0.95890411	0	1.165803109
1490C 18H-2, 45-47	7.5	2.5	22.5	0.5	0	0	9.974640744
1338B 17H-4, 12-14	7.5	37.75	28	1.25	0	0	5.75
242 6R-3, 3-4	7.5	31.73241852	6.518010292	0.686106346	3.94511149	0	4.306220096
1138A 14R-2, 140-141	7.5	0.199733688	3.328894807	74.1011984	0	0	0
516Z 14H-1, 71-72.5	10	16	14.5	24.25	0	0	0
925C 35X-2, 7-9	10	18.5	13.5	0	0	0	2.545454545
1489C 33X-2, 104-106	10	2.5	19.75	14.5	0	0	9.863429439
872C 5H-4, 83-85	10	14.75	9.5	21.25	0	0	14.75
1338A 25H-6, 66-68	10	23.83900929	5.572755418	45.82043344	0	0	1.675041876
1138A 16R-2, 30-31	10	14.72868217	4.263565891	26.61498708	0	0	0
1489C 38X-3, 25-27	12.5	16.75	17.25	14.25	0	0	3.701825558
871B 5H-1, 12-14	12.5	26.75	4.25	37.75	0	0	1.194029851
1338B 32H-3, 67-69	12.5	18.43876178	6.594885599	51.95154778	0	0	2.5
242 7R-6, 14-15	12.5	21	8.5	2.75	0	0	6.205250597
1138A 20R-1, 40-41	12.5	0.076335878	4.503816794	76.41221374	0	0	0
516Z 17H-4, 2-3.5	15	16.5	1.25	6	0	0	0.559440559
1490B 26F-1, 45-47	15	2	3.5	0	0	0	17.36111111
871A 8H-1, 0-1	15	38.75	20.75	1.5	0	0	5.75
1338B 38H-4, 52-54	15	25.75364344	6.288680375	30.04591735	0	0	5.103668262
242 7R-6, 144-145	15	62.79069767	3.255813953	3.348837209	0	0	5.299539171
1138A 22R-1, 19-20	15	4.436363636	0	4.727272727	0	0	0

Figure A.13: Global main species groups relative abundance values used in Figure 4.5

Age	Retic. spp. (<3µm)	Retic. spp. (3-5µm)	Retic. spp. (>5µm)	<i>F. produnda</i>	<i>Gephyrocapsa</i> spp.	<i>Discoaster</i> spp.
0	16	28	0	3714	1237	0
2.5	1264	494	1	2768.5	371	228
4.5	2988	703	218	1859	350	568
7.5	914	849	1171	672	4	213
10	475	298	742	0	0	252
12.5	396	228	1606	0	0	143
15	1223	200	432	0	0	246

Age	Retic. spp. (<3µm)	Retic. spp. (3-5µm)	Retic. spp. (>5µm)	<i>F. produnda</i>	<i>Gephyrocapsa</i> spp.	<i>Discoaster</i> spp.
0	0.244629615	0.428101827	0	56.78464949	18.91292715	0
2.5	18.91507669	7.392442948	0.014964459	41.42910587	5.551814441	3.411896745
4.5	36.98019802	8.70049505	2.698019802	23.00742574	4.331683168	7.02970297
7.5	16.11992945	14.97354497	20.65255732	11.85185185	0.070546737	3.756613757
10	15.72847682	9.867549669	24.56953642	0	0	8.344370861
12.5	12.17337842	7.008914848	49.36981248	0	0	4.395942207
15	26.29089815	4.299410981	9.286727718	0	0	5.288275506

Figure A.14: Compiled main species absolute and relative abundances

## A.10.3 ECOGROUP ABUNDANCE

Age	Upper Euphotic	Lower euphtotic	Sub euphotic
15	2108	0	0
12.5	2373	0	0
10	1620	1	2
7.5	2877	0	181
4.5	4404	5	1221
2.5	2317	30	2081.5
0	1402	69	3770

Figure A.15: Compiled ecogroup absolute abundance values

Age	Upper Euphotic	Lower euphtotic	Sub euphotic
15	100	0	0
12.5	100	0	0
10	99.81515712	0.061614295	0.123228589
7.5	94.08109876	0	5.918901243
4.5	78.22380107	0.088809947	21.68738899
2.5	52.32019871	0.677430281	47.00237101
0	26.75062011	1.316542645	71.93283724

Figure A.16: Compiled ecogroup relative abundance values used in Figure of Chapter 4

## B | U1482 DATA (HIGH RESOLUTION SAMPLING)

### B.1 COUNT DATA







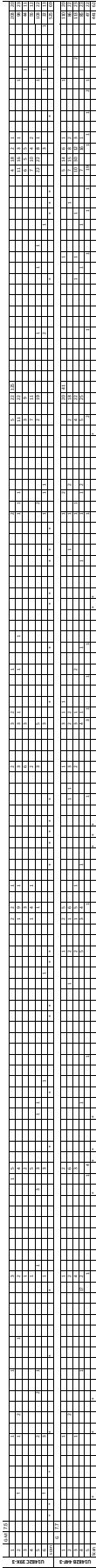


Figure B.1: Site U1482 high resolution sampling count data

### B.1.1 RANGE THROUGH DIVERSITY AND SPECIES RICHNESS

Sample	Age	RTD	Species Richness
U1482A 10H-1, 2-3cm	1.7	31	31
U1482B 11H-3, 88-89cm	1.9	36	31
U1482A 11H-3, 8-9cm	2.1	40	36
U1482A 12H-1, 125-126cm	2.3	49	41
U1482A 12H-6, 123-124cm	2.5	48	33
U1482A 13H-4, 148-149cm	2.7	52	34
U1482C 14H-5, 139-140cm	2.9	59	43
U1482C 15H-3, 20-21cm	3.1	64	43
U1482B 16H-1, 87-88cm	3.3	69	49
U1482C 16H-6, 37-38cm	3.5	73	54
U1482C 17H-5, 6-7cm	3.7	72	53
U1482D 5H-3, 110-111cm	3.9	74	56
U1482B 20H-3, 69-70cm	4.1	77	65
U1482B 21H-3, 65-66cm	4.3	76	53
U1482A 21H-2, 41-42cm	4.5	80	56
U1482C 22H-7, 72-73cm	4.7	82	57
U1482A 23H-1, 16-17cm	4.9	82	61
U1482A 24H-1, 62-63cm	5.1	84	57
U1482A 25H-5, 150-151cm	5.3	81	61
U1482C 28H-6, 2-3cm	5.5	82	61
U1482B 31H-4, 107-108cm	5.7	82	70
U1482B 33H-2, 115-116cm	5.9	86	67
U1482C 33H-1, 123-124cm	6.1	83	62
U1482A 32H-6, 105-106cm	6.3	83	65
U1482C 34H-7, 94-95cm	6.5	84	61
U1482C 35H-6, 44-45cm	6.7	87	56
U1482C 36H-6, 78-79cm	6.9	86	72
U1482C 37H-3, 64-65cm	7.1	80	65

U1482B 39H-1, 87-88cm	7.3	78	64
U1482C 39X-3, 76-77cm	7.5	75	69
U1482B 44F-3, 79-80cm	7.7	65	62

Table B.1: Site U1482 RTD and species richness data as used in Figure 4.3

## B.1.2 RELATIVE ABUNDANCE

Sample	Age	<i>F. profunda</i>	<i>Gephyrocapsa</i> spp.	<i>Discoaster</i> spp.	<i>Retic.</i> spp. (<3µm)	<i>Retic.</i> spp. (3-5µm)	<i>Retic.</i> spp. (>5µm)
U1482A 10H-1, 2-3cm	1.7	35.47523427	28.91566265	0.133868809	4.953145917	4.016064257	0
U1482B 11H-3, 88-89cm	1.9	20.4638472	12.41473397	0.136425648	21.82810368	0	0
U1482A 11H-3, 8-9cm	2.1	34.9799733	25.63417891	0.934579439	7.610146862	3.070761015	0.133511348
U1482A 12H-1, 125-126cm	2.3	27.40471869	31.94192377	3.811252269	14.51905626	3.629764065	0
U1482A 12H-6, 123-124cm	2.5	40.63647491	21.90942472	2.080783354	11.13831089	3.05997552	0
U1482A 13H-4, 148-149cm	2.7	26.44067797	26.44067797	2.033898305	13.38983051	4.915254237	0
U1482C 14H-5, 139-140cm	2.9	21.63636364	18.90909091	7.454545455	12	14.72727273	0
U1482C 15H-3, 20-21cm	3.1	9.963768116	30.07246377	0.905797101	17.57246377	2.898550725	0.18115942
U1482B 16H-1, 87-88cm	3.3	28.57142857	9.706959707	17.76556777	15.2014652	4.029304029	0
U1482C 16H-6, 37-38cm	3.5	24.52619844	10.14492754	11.81716834	30.88071349	9.030100334	0
U1482C 17H-5, 6-7cm	3.7	35.0310559	6.459627329	6.583850932	18.26086957	4.099378882	0
U1482D 5H-3, 110-111cm	3.9	33.99374348	12.6173097	4.900938478	12.6173097	6.986444213	0.31282586
U1482B 20H-3, 69-70cm	4.1	15.31223268	14.28571429	5.988023952	27.54491018	9.324208725	0.598802395
U1482B 21H-3, 65-66cm	4.3	33.72513562	5.605786618	11.12115732	11.6636528	7.233273056	1.356238698
U1482A 21H-2, 41-42cm	4.5	11.18110236	10.86614173	16.06299213	25.82677165	2.519685039	7.244094488
U1482C 22H-7, 72-73cm	4.7	13.93617021	6.170212766	10.31914894	31.17021277	2.765957447	7.872340426
U1482A 23H-1, 16-17cm	4.9	5.9375	6.770833333	9.6875	28.125	4.0625	5.3125
U1482A 24H-1, 62-63cm	5.1	5.023547881	4.552590267	16.32653061	15.69858713	5.337519623	14.7566719
U1482A 25H-5, 150-151cm	5.3	4.873646209	2.346570397	6.498194946	12.99638989	4.873646209	15.16245487
U1482C 28H-6, 2-3cm	5.5	19.11262799	3.924914676	7.167235495	15.52901024	5.290102389	8.532423208
U1482B 31H-4, 107-108cm	5.7	14.85451761	4.287901991	17.76416539	15.77335375	5.666156202	1.837672282
U1482B 33H-2, 115-116cm	5.9	9.222423146	0.904159132	9.945750452	13.38155515	8.318264014	4.339963834
U1482C 33H-1, 123-124cm	6.1	17.90744467	0.201207243	9.255533199	18.10865191	9.456740443	2.615694165
U1482A 32H-6, 105-106cm	6.3	7.786885246	0	8.81147541	18.03278689	5.12295082	9.426229508
U1482C 34H-7, 94-95cm	6.5	7.157464213	0	6.952965235	18.200409	4.498977505	5.316973415
U1482C 35H-6, 44-45cm	6.7	8.869179601	0	4.65631929	10.19555654	21.06430155	10.19955654
U1482C 36H-6, 78-79cm	6.9	10.7505071	0	6.288032454	18.86409736	14.60446247	7.707910751
U1482C 37H-3, 64-65cm	7.1	3.719912473	0	8.533916849	12.25382932	16.41137856	8.533916849
U1482B 39H-1, 87-88cm	7.3	5.530973451	0	7.743362832	11.50442478	11.72566372	14.60176991
U1482C 39X-3, 76-77cm	7.5	3.047619048	0	10.66666667	23.80952381	15.80952381	5.333333333

Figure B.2: Site U1482 relative abundance data of the main species and groups used in Figure 4.5 (grey line plots) in Chapter 4

## **B.2 U1482 AGE MODEL DATA TABLES**

**(FROM IODP EXP. 363 SHIPBOARD DATA)**

### **B.2.1 CALCAREOUS NANNOFOSSILS**

Marker species	Age (Ma)	Base (sub) zone	Core, Section, interval (cm)		Depth CSF-A	
			Top	Bottom	Top	Bottom
			363-U1482A-			
<i>B Emiliana huxleyi</i>	0.29	NN21	3H-CC	4H-2, 75	22.12	23.14
<i>T Pseudoemiliana lacunosa</i>	0.44	NN20	4H-4, 75	4H-6, 75	27.15	28.65
<i>B ac Gephyrocapsa caribbeanica</i>	0.6		5H-CC	6H-2, 75	40.97	42.06
<i>T Helicosphaera selii</i>	1.26		8H-4, 75	8H-6, 75	65.15	66.66
<i>T Calcidiscus macintyreii</i>	1.6		9H-CC	10H-2, 75	79.25	80.20
<i>T Discoaster brouweri</i>	1.93	NN19	11H-CC	12H-2, 75	98.07	99.12
<i>Bc Discoaster triradiatus</i>	2.22		12H-6, 75	12H-CC	106.19	106.99
<i>T Discoaster pentaradiatus</i>	2.39	NN18	12H-CC	13H-2, 75	107.79	108.72
<i>T Discoaster surculus</i>	2.49	NN17	14H-2, 75	14H-4, 75	119.15	120.66
<b>Pliocene / Pleistocene boundary</b>						
<i>T Discoaster tamalis</i>	2.58		14H-CC	15H-CC	126.82	131.51
<i>T Sphenolithus spp.</i>	3.54		16H-CC	17H-2, 75	145.90	146.78
<i>T Reticulofenestra pseudoumbilicus</i>	3.7	NN16	17H-6, 75	17H-CC	153.69	154.51
<i>T Amaurolithus tricorniculatus (/delicatus)</i>	3.92	NN15	22H-4, 75	22H-6, 75	198.19	199.70
<i>Bc Discoaster brouweri</i>	4.12		18H-CC	19H-CC	164.76	169.53
<i>T Ceratolithus armatus</i>	5.04		23H-2, 75	23H-4, 75	204.65	206.16
<i>B Ceratolithus cristatus</i>	5.12	NN13-14	23H-4, 75	23H-6, 75	207.66	209.17
<i>T Orthostylus rugosus</i>	5.28		23H-CC	24H-CC	212.47	217.17
<b>Miocene / Pliocene boundary</b>						
<i>B Ceratolithus armatus</i>	5.33		25H-CC	26H-CC	231.48	236.20
<i>T Discoaster quinqueramus</i>	5.35		25H-CC	26H-CC	231.48	236.20
<i>Tc Nicklithus amplifiscus</i>	5.59	NN12	30H-4,	30H-6,	274.15	275.69
<i>B Nicklithus amplifiscus</i>	5.98		32H-CC	33H-CC	297.72	302.71
<i>B Amaurolithus spp.</i>	6.91		36H-CC	37H-CC	335.02	340.13
<i>Bc Discoaster surculus</i>	7.42		44F-CC	45F-CC	362.20	370.05
<i>B Discoaster berggrenii</i>	7.79		49X-CC	50X-CC	410.80	414.85
<i>T Catinaster coalitus</i>	8.29	NN11	53CC	54X-2, 75	448.43	448.62
	9.66					0.19



Biohorizon		Marker species	Age (Ma)	Base (sub) zone	Core, Section, interval (cm)		Depth CSF-A			
Number					Top	Bottom	Top	Bottom	Midpoint ±	
					363-U1482B-					
3	B	<i>Emiliana huxleyi</i>	0.29	NN21	2H-CC	3H-CC	16.09	25.42	20.76	4.67
4	T	<i>Pseudoemiliana lacunosa</i>	0.44	NN20	4H-2, 50	4H-4, 50	27.10	30.10	28.60	1.50
5	B	<i>ac Gephyrocapsa caribbeanica</i>	0.6		5H-CC	7H-4, 50	44.54	53.60	49.07	4.53
9	T	<i>Helicosphaera selii</i>	1.26		9H-CC	10H-CC	77.64	86.79	82.22	4.58
10	T	<i>Calcidiscus macintyreii</i>	1.6		10H-CC	11H-2, 50	86.79	88.56	87.68	0.88
11	T	<i>Discoaster brouweri</i>	1.93	NN19	11H-6, 50	11H-CC	94.43	96.38	95.41	0.97
12	B	<i>Discoaster triradiatus</i>	2.22							
14	T	<i>Discoaster pentaradiatus</i>	2.39	NN18	13H-2, 51	13H-4, 51	107.57	110.46	109.02	1.45
15	T	<i>Discoaster surculus</i>	2.49	NN17	13H-CC	14H-2, 51	115.52	117.07	116.30	0.77
<b>Pliocene / Pleistocene boundary</b>										
<b>2.58</b>										
16	T	<i>Discoaster tamalis</i>	2.8		14H-4, 51	14H-6, 51	120.00	122.92	121.46	1.46
17	T	<i>Sphenolithus</i> spp.	3.54		16H-CC	17H-1, 51	144.09	144.10	144.10	0.00
18	T	<i>Reticulofenestra pseudoumbilicus</i>	3.7	NN16	18H-2	18H-4	155.11	158.03	156.57	1.46
19	T	<i>Amaurolithus tricorniculatus (delicatus)</i>	3.92	NN15	23H-CC	24H-CC	198.63	208.01	203.32	4.69
20	B	<i>Discoaster brouweri</i>	4.12							
23	T	<i>Ceratolithus armatus</i>	5.04		25H-4, 50/52	25H-6, 50/52	212.91	215.76	214.34	1.43
24	B	<i>Ceratolithus cristatus</i>	5.12	NN13-14	25H-6, 50/52	25H-CC	215.76	217.38	216.57	0.81
25	T	<i>Orthostylus rugosus</i>	5.28		28H-4, 51	28H-6, 51	234.90	237.76	236.33	1.43
<b>Miococene / Pliocene boundary</b>										
<b>5.33</b>										
27	B	<i>Ceratolithus armatus</i>	5.35		28H-2, 51	28H-4, 51	232.02	234.90	233.46	1.44
28	T	<i>Discoaster quinqueramus</i>	5.59	NN12	28H-CC	29H-2, 50	239.66	241.02	240.34	0.68
29	T	<i>Nicklithus amplifiscus</i>	5.98		33H-6, 50	33H-CC	284.93	287.52	286.23	1.29
30	B	<i>Nicklithus amplifiscus</i>	6.91		37H-2,	37H-4,	317.01	319.67	318.34	1.33
31	B	<i>Amaurolithus</i> spp.	7.42		38H-CC	39H-CC	334.47	343.81	339.14	4.67
33	B	<i>Discoaster surculus</i>	7.79							
35	B	<i>Discoaster berggrenii</i>	8.29	NN11						
43	T	<i>Catinaster coalitus</i>	9.66							
49	B	<i>Helicosphaera stalis</i>	10.72							
50	T	<i>Helicosphaera walbersdorffensis</i>	10.75							
51	B	<i>Discoaster brouweri</i>								

Biohorizon	Age	Base	Core, Section, interval (cm)		Depth CSF-A	
Number	(Ma)	(sub) zone	Top	Bottom	Top	Bottom Midpoint ±
363-U1482C-						
3	0.29	NN21	2H-CC	3H-CC	19.02	28.54 23.78 4.76
4	0.44	NN20	3H-CC	4H-CC	28.54	38.04 33.29 4.75
5	0.6		4H-CC	5H-CC	38.04	47.44 42.74 4.70
9	1.26		8H-CC	9H-CC	69.34	78.88 74.11 4.77
10	1.6		11H-3, 14	11H-3, 75	90.86	91.47 91.17 0.31
11	1.93	NN19	12H-2, 75	12H-3, 75	99.56	100.98 100.27 0.71
12	2.22					
14	2.39	NN18	12H-CC	13H-CC	107.41	116.91 112.16 4.75
15	2.49	NN17	13H-CC	14H-CC	116.91	125.97 121.44 4.53
Pliocene / Pleistocene boundary						
2.58						
16	2.8		13H-CC	14H-CC	116.91	125.97 121.44 4.53
17	3.54		15H-CC	17H-CC	135.70	154.72 145.21 9.51
18	3.7	NN16	17H-CC	19H-CC	154.72	169.24 161.98 7.26
19	3.92	NN15	22H-CC	23H-CC	197.80	206.90 202.35 4.55
20	4.12		19H-CC	20H-CC	169.24	178.73 173.99 4.74
23	5.04		22H-CC	23H-CC	197.75	206.85 202.30 4.55
24	5.12	NN13-14	23H-CC	25H-CC	206.85	221.88 214.37 7.52
25	5.28		22H-CC	23H-CC	197.75	206.85 202.30 4.55
Miocene / Pliocene boundary						
5.33						
27	5.35		23H-CC	25H-CC	206.85	221.88 214.37 7.52
28	5.59	NN12	26H-CC	27H-CC	231.35	240.74 236.05 4.70
29	5.98		31H-CC	32H-CC	279.28	288.59 283.94 4.66
30	6.91		34H-CC	35H-CC	307.50	317.29 312.40 4.90
31	7.42		37H-CC	39X-CC	336.35	349.68 343.02 6.66
33	7.79		41X-CC	42X-CC	365.65	378.80 372.23 6.58
35	8.29	NN11	45X-CC	46X-CC	408.15	417.68 412.915 4.8
43	9.66		49X-CC	50X-CC	438.38	448.11 443.245 4.9
49	10.72		58X-CC	59X-cc	520.33	530.3 525.315 5
50	10.75		57X-CC	58X-CC	515.88	520.33 518.105 2.2
51						

Notes: B = bottom, T = top, Bc = bottom common, Tc = top common, T ac = top acme, X = abundance cross-over

## **B.2.2 FORAMINIFERA**

Marker species	Age (Ma)	(Sub) zone base	Core, Section, interval (cm)		Depth CSF-A (m)		Midpoint	±
			Top	Bottom	Top	Bottom		
			363-U1482A-		363-U1482A-			
T <i>Globigerinoides ruber</i> (pink)	0.12		1H-CC	2H-CC	2.93	12.70	7.82	4.89
B <i>Globigerinella calida</i>	0.22		2H-CC	3H-CC	12.70	22.12	17.41	4.71
T <i>Globorotalia tosaensis</i>	0.61	Pt1b	3H-CC	4H-CC	22.12	30.64	26.38	4.26
T <i>Globigerinoidesella fistulosa</i>	1.88	Pt1a	10H-CC	11H-CC	88.19	98.07	93.13	4.94
B <i>Globorotalia truncatulinoides</i>	2.40*		10H-CC	11H-CC	88.91	98.07	93.49	4.58
B <i>Pulleniatina finalis</i>	2.04		10H-CC	11H-CC	88.91	98.07	93.49	4.58
T <i>Globorotalia pseudomiocenica</i>	2.30	PL6	10H-CC	11H-CC	88.91	98.07	93.49	4.58
T <i>Globorotalia limbata</i>	2.39		10H-CC	11H-CC	88.91	98.07	93.49	4.58
<b>Pliocene / Pleistocene boundary</b>								
T <i>Dentoglobigerina altispira</i>	2.58							
B <i>Globigerinoidesella fistulosa</i>	3.13**	PL5	14H-CC	15H-CC	126.82	136.20	131.51	4.69
B <i>Globorotalia tosaensis</i>	3.33		14H-CC	15H-CC	126.82	136.20	131.51	4.69
B <i>Globorotalia tosaensis</i>	3.35		14H-CC	15H-CC	126.82	136.20	131.51	4.69
T <i>Sphaeroidinellopsis seminulina</i>	3.59	PL4	15H-CC	16H-CC	136.20	145.90	141.05	4.85
T <i>Globorotalia margaritae</i> *	3.60***	PL3	15H-CC	16H-CC	136.20	145.90	141.05	4.85
X <i>Pulleniatina colling s-d</i> ('L9')	4.08		17H-CC	19H-CC	155.32	174.34	164.83	9.51
B <i>Sphaeroidinella dehiscens</i> s.l.	5.53		26H-CC	27H-CC	240.92	250.40	245.66	4.74
B <i>Globorotalia tumida</i>	5.57	PL1	27H-CC	28H-CC	250.40	259.78	255.09	4.69
<b>Miocene / Pliocene boundary</b>								
T <i>Globorotalia linguaensis</i>	5.33							
B <i>Neoglobobadrina humerosa</i>	6.13	M14	29H-CC	30H-CC	269.53	278.63	274.08	4.55
B <i>Globorotalia plesiotumida</i>	8.56	M13b	50X-CC	51X-CC	418.92	429.35	424.14	5.21
	8.58	M13a	53X-CC	54X-CC	448.38	456.47	452.43	4.05

[illegible]





## REFERENCES

- Agnini, C., Fornaciari, E., Raffi, I., Catanzariti, R., Pälike, H., Backman, J. and Rio, D. (2014), ‘Biozonation and biochronology of Paleogene calcareous nannofossils from low and middle latitudes’, *Newsletters on Stratigraphy* **47**(2), 131–181.
- Agnini, C., Monechi, S. and Raffi, I. (2017), ‘Calcareous nannofossil biostratigraphy: historical background and application in Cenozoic chronostratigraphy’, *Lethaia* **50**(3), 447–463.
- Aubry, M.-P. (1992*a*), Late Paleogene Calcareous Nannoplankton Evolution: A Tale of Climatic Deterioration, *in* D. Prothero and W. A. Berggren, eds, ‘Eocene-Oligocene Climatic and Biotic Evolution’, Princeton University Press, pp. 272–309.
- Aubry, M. P. (1992*b*), ‘Paleogene calcareous nannofossils from the Kerguelen Plateau, Leg 120’, *Proceedings of the Ocean Drilling Program, Scientific Results* **120**, 471–491.
- Backman, J. (1987), ‘Quantitative Calcareous Nannofossil Biochronology of Middle Eocene through Early Oligocene Sediment from DSDP Sites 522 and 523’, *Abhandlungen der Geologischen Bundesanstalt* **39**, 21–31.
- Backman, J., Raffi, I., Rio, D., Fornaciari, E. and Pälike, H. (2012), ‘Biozonation and biochronology of miocene through pleistocene calcareous nannofossils from low and middle latitudes’, *Newsletters on Stratigraphy* **45**(3), 221–244.
- Badger, M. P., Lear, C. H., Pancost, R. D., Foster, G. L., Bailey, T. R., Leng, M. J. and Abels, H. A. (2013), ‘CO<sub>2</sub> drawdown following the middle Miocene expansion of the Antarctic Ice Sheet’, *Paleoceanography* **28**(1), 42–53.
- Baldauf, J. (1992), Middle Eocene through Early Miocene diatom floral turnover, *in* D. R. Prothero and W. A. Berggren, eds, ‘Eocene-Oligocene Climatic and Biotic Evolution’, Princeton University Press, Princeton, pp. 310–326.



- Baumann, K.-H., Čeppek, M. and Kinkel, H. (1999), Coccolithophores as Indicators of Ocean Water Masses, Surface-Water Temperature, and Paleoproductivity — Examples from the South Atlantic, *in* ‘Use of Proxies in Paleoceanography’, Springer Berlin Heidelberg, Berlin, Heidelberg, pp. 117–144.
- Beaufort, L., Probert, I., de Garidel-Thoron, T., Bendif, E. M., Ruiz-Pino, D., Metzl, N., Goyet, C., Buchet, N., Coupel, P., Grelaud, M., Rost, B., Rickaby, R. E. M. and de Vargas, C. (2011), ‘Sensitivity of coccolithophores to carbonate chemistry and ocean acidification’, *Nature* **476**(7358), 80–83.
- Beerling, D. J. and Royer, D. L. (2011), ‘Convergent Cenozoic CO<sub>2</sub> history’, *Nature Geoscience* **4**(7), 418–420.
- Bendif, E. M., Nevado, B., Wong, E. L., Hagino, K., Probert, I., Young, J. R., Rickaby, R. E. and Filatov, D. A. (2019), ‘Repeated species radiations in the recent evolution of the key marine phytoplankton lineage *Gephyrocapsa*’, *Nature Communications* **10**(1), 1–9.
- Bergen, J. A., de Kaenel, E., Blair, S. A., Boesiger, T. M. and Browning, E. (2017), ‘Oligocene-Pliocene taxonomy and stratigraphy of the genus *Sphenolithus* in the circum North Atlantic Basin: Gulf of Mexico and ODP Leg 154.’, *Journal of Nannoplankton Research* **37**(2-3), 77–112.
- Berggren, W. A., Kent, D. V., Swisher, C. C. I. and Aubry, M. P. (1995), A revised Cenozoic geochronology and chronostratigraphy, *in* W. Berggren, D. V. Kent, M. Aubry and J. Hardenbol, eds, ‘Geochronology, time scales and global stratigraphic correlation: A unified temporal framework for an historical geology’, number 54, Society for Sedimentary Geology, pp. 129–212.
- Blair, S. A., Bergen, J. A., de Kaenel, E., Browning, E. and Boesiger, T. M. (2017), ‘Upper Miocene-Lower Pliocene taxonomy and stratigraphy in the circum North Atlantic Basin: radiation and extinction of *Amauroliths*, *Ceratoliths* and the *D. quinqueramus* lineage’, *Journal of Nannoplankton Research* **37**(2-3), 113–144.
- Blaj, T., Backman, J. and Raffi, I. (2009), ‘Late Eocene To Oligocene Preservation History and Biochronology of Calcareous Nannofossils From Paleo-Equatorial Pacific Ocean Sediments’, *Rivista Italiana di Paleontologia e Stratigrafia* **115**(1), 67.

- Boesiger, T. M., de Kaenel, E., Bergen, J. A., Browning, E. and Blair, S. A. (2017), ‘Oligocene to Pleistocene taxonomy and stratigraphy of the genus *Helicosphaera* and other placolith taxa in the circum North Atlantic Basin’, *Journal of Nannoplankton Research* **37**(2-3), 145–175.
- Bohaty, S. M., Zachos, J. C. and Delaney, M. L. (2012), ‘Foraminiferal Mg/Ca evidence for Southern Ocean cooling across the Eocene-Oligocene transition’, *Earth and Planetary Science Letters* **317-318**, 251–261.
- Bolton, C. T., Chang, L., Clemens, S. C., Kodama, K., Ikehara, M., Medina-Elizalde, M., Paterson, G. A., Roberts, A. P., Rohling, E. J., Yamamoto, Y. and Zhao, X. (2013), ‘A 500,000 year record of Indian summer monsoon dynamics recorded by eastern equatorial Indian Ocean upper water-column structure’, *Quaternary Science Reviews* **77**, 167–180.
- Bolton, C. T., Hernández-Sánchez, M. T., Fuertes, M. Á., González-Lemos, S., Abrevaya, L., Mendez-Vicente, A., Flores, J. A., Probert, I., Giosan, L., Johnson, J. and Stoll, H. M. (2016), ‘Decrease in coccolithophore calcification and CO<sub>2</sub> since the middle Miocene’, *Nature Communications* **7**, 10284.
- Bolton, C. T. and Stoll, H. M. (2013), ‘Late Miocene threshold response of marine algae to carbon dioxide limitation’, *Nature* **500**(7464), 558–562.
- Bolton, C. T., Stoll, H. M. and Mendez-Vicente, A. (2012), ‘Vital effects in coccolith calcite: Cenozoic climate-pCO<sub>2</sub> drove the diversity of carbon acquisition strategies in coccolithophores?’, *Paleoceanography* **27**(4), 1–16.
- Bordiga, M., Henderiks, J., Tori, F., Monechi, S., Fenero, R., Legarda-Lisarri, A. and Thomas, E. (2015), ‘Microfossil evidence for trophic changes during the Eocene-Oligocene transition in the South Atlantic (ODP Site 1263, Walvis Ridge)’, *Climate of the Past* **11**(9), 1249–1270.
- Boscolo-Galazzo, F., Crichton, K. A., Barker, S. and Pearson, P. N. (2018), ‘Temperature dependency of metabolic rates in the upper ocean: A positive feedback to global climate change?’, *Global and Planetary Change* **170**, 201–212.
- Boscolo-Galazzo, F., Crichton, K. A., Ridgwell, A., Mawbey, E. M., Wade, B. S. and Pearson,

- P. N. (2021), ‘Temperature controls carbon cycling and biological evolution in the ocean twilight zone’, *Science* **371**(6534), 1148–1152.
- Boscolo-Galazzo, F., Jones, A. P., Jones, T. D., Crichton, K. A., Wade, B. S. and Pearson, P. N. (n.d.), ‘Evolution and diversification of deep-dwelling plankton’, *Biogeosciences* **in review**, 1–48.
- Bown, P. R. (2005*a*), ‘Calcareous nannoplankton evolution: a tale of two oceans’, *Micropaleontology* **51**(4), 299–308.
- Bown, P. R. (2005*b*), ‘Palaeogene calcareous nannofossils from the Kilwa and Lindi areas of coastal Tanzania (Tanzania Drilling Project 2003-2004)’, *Journal of Nannoplankton Research* **27**(1), 21–95.
- Bown, P. R. and Dunkley Jones, T. (2012), ‘Calcareous nannofossils from the Paleogene equatorial Pacific (IODP Expedition 320 Sites U1331-1334)’, *Journal of Nannoplankton Research* **32**(2), 3–51.
- Bown, P. R., Dunkley Jones, T., Young, J. R. and Randell, R. (2009), ‘A palaeogene record of extant lower photic zone calcareous nannoplankton’, *Palaeontology* **52**(2), 457–469.
- Bown, P. R., Jones, T. D., Lees, J. A., Randell, R. D., Mizzi, J. A., Pearson, P. N., Coxall, H. K., Young, J. R., Nicholas, C. J., Karega, A., Singano, J. and Wade, B. S. (2008), ‘A Paleogene calcareous microfossil Konservat-Lagerstätte from the Kilwa Group of coastal Tanzania’, *Bulletin of the Geological Society of America* **120**(1-2), 3–12.
- Bown, P. R., Jones, T. D. and Young, J. R. (2007), ‘*Umbilicosphaera jordanii* Bown, 2005 from the Paleogene of Tanzania: confirmation of generic assignment and a Paleocene origination for the Family Calcidiscaceae’, *Journal of Nannoplankton Research* **29**(1), 25–30.
- Bown, P. R., Lees, J. A. and Young, J. R. (2004), Calcareous nannoplankton evolution and diversity through time, *in* J. R. Young and H. R. Thierstein, eds, ‘Coccolithophores From Molecular Processes to Global Impacts’, Springer, pp. 481–508.
- Bown, P. R. and Newsam, C. (2017), ‘Calcareous nannofossils from the Eocene North Atlantic Ocean (IODP Expedition 342 Sites U1403–1411)’, *Journal of Nannoplankton Research* **37**(1), 25–60.

- Bown, P. R. and Young, J. R. (1998a), *Calcareous Nannofossil Biostratigraphy*, Springer Netherlands, Dordrecht.
- Bown, P. R. and Young, J. R. (1998b), Techniques, *in* P. R. Bown, ed., ‘Calcareous Nannofossil Biostratigraphy’, Springer, chapter 2, pp. 16–29.
- Bralower, T. J. (2002), ‘Evidence of surface water oligotrophy during the Paleocene-Eocene thermal maximum: Nannofossil assemblage data from Ocean Drilling Program Site 690, Maud Rise, Weddell Sea’, *Paleoceanography* **17**(2), 1–15.
- Bralower, T. J. (2005), ‘Data Report: Paleocene-Early Oligocene Calcareous Nannofossil Biostratigraphy, ODP Leg 198 Sites 1209, 1210, and 1211 (Shatsky Rise, Pacific Ocean)’, *Proceedings of the Ocean Drilling Program, Scientific Results* **198**.
- Browning, E., Bergen, J. A., Blair, S. A., Boesiger, T. M. and de Kaenel, E. (2017), ‘Late Miocene to Late Pliocene taxonomy and stratigraphy of the genus *Discoaster* in the circum North Atlantic Basin: Gulf of Mexico and ODP Leg 154’, *Journal of Nanoplankton Research* **37**(2-3), 189–214.
- Bukry, D. (1971), ‘Cenozoic Calcareous Nannofossils From The Pacific Ocean’, *Transactions of the San Diego Society of Natural History*. **16**, 303–328.
- Bukry, D. (1973), ‘Low-Latitude Coccolith Biostratigraphic Zonation’, *Initial Reports of the Deep Sea Drilling Project* **15**, 685–703.
- Burke, K. D., Williams, J. W., Chandler, M. A., Haywood, A. M., Lunt, D. J. and Otto-Bliesner, B. L. (2018), ‘Pliocene and Eocene provide best analogs for near-future climates’, *Proceedings of the National Academy of Sciences of the United States of America* **115**(52), 13288–13293.
- Chalk, T. B., Hain, M. P., Foster, G. L., Rohling, E. J., Sexton, P. F., Badger, M. P., Cherry, S. G., Hasenfratz, A. P., Haug, G. H., Jaccard, S. L., Martínez-García, A., Pälike, H., Pancost, R. D. and Wilson, P. A. (2017), ‘Causes of ice age intensification across the mid-pleistocene transition’, *Proceedings of the National Academy of Sciences of the United States of America* **114**(50), 13114–13119.

- Chapman, M. R. and Chepstow-Lusty, A. J. (1997), ‘Late Pliocene climatic change and the global extinction of the discoasters: An independent assessment using oxygen isotope records’, *Palaeogeography, Palaeoclimatology, Palaeoecology* **134**(1-4), 109–125.
- Ciummelli, M., Raffi, I. and Backman, J. (2016), ‘Biostratigraphy and evolution of Miocene Discoaster spp. from IODP Site U1338 in the equatorial Pacific Ocean’, *Journal of Micropalaeontology* **36**, 137–152.
- Clark, P. U., Archer, D., Pollard, D., Blum, J. D., Rial, J. A., Brovkin, V., Mix, A. C., Pisias, N. G. and Roy, M. (2006), ‘The middle Pleistocene transition: characteristics, mechanisms, and implications for long-term changes in atmospheric pCO<sub>2</sub>’, *Quaternary Science Reviews* **25**(23-24), 3150–3184.
- Coccioni, R., Monaco, P., Monechi, S., Nocchi, M. and Parisi, G. (1988), Biostratigraphy of the Eocene-Oligocene Boundary at Massignano (Ancona, Italy), in I. Premoli Silva, R. Coccioni and A. Montanari, eds, ‘The Eocene-Oligocene Boundary in the Marche-Umbria Basin (Italy).’, International Subcommission on Paleogene Stratigraphy, pp. 59–80.
- Colwyn, D. A. and Hren, M. T. (2019), ‘An abrupt decrease in Southern Hemisphere terrestrial temperature during the Eocene–Oligocene transition’, *Earth and Planetary Science Letters* **512**, 227–235.
- Coxall, H. K., Dunkley Jones, T., Jones, A. P., Lunt, P., MacMillan, I., Marliyani, G. I., Nicholas, C. J., O’Halloran, A., Piga, E., Sanyoto, P., Rahardjo, W. and Pearson, P. N. (2021), ‘The Eocene-Oligocene Transition in Nanggulan, Java: lithostratigraphy, biostratigraphy and foraminiferal stable isotopes’, *Journal of the Geological Society*.
- Coxall, H. K., Huck, C. E., Huber, M., Lear, C. H., Legarda-Lisarri, A., O’Regan, M., Sliwiska, K. K., Van De Flierdt, T., De Boer, A. M., Zachos, J. C. and Backman, J. (2018), ‘Export of nutrient rich Northern Component Water preceded early Oligocene Antarctic glaciation’, *Nature Geoscience* **11**(3), 190–196.
- Coxall, H. K. and Pearson, P. N. (2006), Taxonomy, biostratigraphy and phylogeny of Hantkeninidae (Clavigerinella, Hantkenina and Cribrohantkenina), in P. N. Pearson, R. K. Olsson, C. Hemleben, B. T. Huber and W. A. Berggren, eds, ‘Atlas of Eocene Planktonic

- Foraminifera Cushman Foundation of Foraminiferal Research, Special Publication no. 41', Allen Press, Lawrence, Kansas, pp. 213–252.
- Coxall, H. K. and Pearson, P. N. (2007), The Eocene-Oligocene transition, *in* M. Williams, A. M. Haywood, J. Gregory and D. N. Schmidt, eds, 'Deep Time Perspectives on Climate Change: Marrying the Signal From Computer Models and Biological Proxies', Geological Society Special Publication, pp. 351–387.
- Coxall, H. K. and Wilson, P. A. (2011), 'Early Oligocene glaciation and productivity in the eastern equatorial Pacific: Insights into global carbon cycling', *Paleoceanography* **26**(2), 1–18.
- Coxall, H. K., Wilson, P. A., Pälike, H., Lear, C. H. and Backman, J. (2005), 'Rapid stepwise onset of Antarctic glaciation and deeper calcite compensation in the Pacific Ocean', *Nature* **433**(7021), 53–57.
- Cramer, B. S., Miller, K. G., Barrett, P. J. and Wright, J. D. (2011), 'Late Cretaceous–Neogene trends in deep ocean temperature and continental ice volume: Reconciling records of benthic foraminiferal geochemistry (d18O and Mg/Ca) with sea level history', *Journal of Geophysical Research* **116**, 1–23.
- Cramwinckel, M. J., Huber, M., Kocken, I. J., Agnini, C., Bijl, P. K., Bohaty, S. M., Frieling, J., Goldner, A., Hilgen, F. J., Kip, E. L., Peterse, F., Van Der Ploeg, R., Röhl, U., Schouten, S. and Sluijs, A. (2018), 'Synchronous tropical and polar temperature evolution in the Eocene letter', *Nature* **559**(7714), 382–386.
- da Gama, R. O. B. P. and Varol, O. (2013), 'New Late Oligocene to Miocene Species', *Journal of Nannoplankton Research* **33**(1), 1–12.
- De Deckker, P. (2016), 'The Indo-Pacific Warm Pool: critical to world oceanography and world climate', *Geoscience Letters* **3**(1).
- de Kaenel, E. and Villa, G. (1996), 'Oligocene-Miocene calcareous nannofossils biostratigraphy and paleoecology from the Iberia Abyssal Plain', *Proceedings of the Ocean Drilling Program, Leg 149 Scientific Results* **149**.

- DeConto, R. M. and Pollard, D. (2003), ‘Rapid Cenozoic glaciation of Antarctica induced by declining atmospheric CO<sub>2</sub>’, *Nature* **421**(6920), 245–249.
- Diester-Haass, L. (1995), ‘Middle Eocene to early Oligocene paleoceanography of the Antarctic Ocean (Maud Rise, ODP Leg 113, Site 689): change from a low to a high productivity ocean’, *Palaeogeography, Palaeoclimatology, Palaeoecology* **113**(2-4), 311–334.
- Diester-Haass, L., Billups, K. and Emeis, K. C. (2006), ‘Late Miocene carbon isotope records and marine biological productivity: Was there a (dusty) link?’, *Paleoceanography* **21**(4), 1–18.
- Diester-Haass, L., Billups, K., Gröcke, D. R., François, L., Lefebvre, V. and Emeis, K. C. (2009), ‘Mid-Miocene paleoproductivity in the Atlantic Ocean and implications for the global carbon cycle’, *Paleoceanography* **24**(1), 1–19.
- Diester-Haass, L. and Zachos, J. C. (2003), The Eocene-Oligocene Transition in the Equatorial Atlantic (ODP Site 925): Palaeoproductivity Increase and Positive  $\delta^{13}\text{C}$  Excursion, in D. Prothero, L. Ivany and E. Nesbitt, eds, ‘From Greenhouse to Icehouse: The Marine Eocene-Oligocene Transition’, Columbia University Press, New York, pp. 397–416.
- Diester-Haass, L. and Zahn, R. (2001), ‘Paleoproductivity increase at the Eocene - Oligocene climatic transition: ODP/DSDP sites 763 and 592’, *Palaeogeography, Palaeoclimatology, Palaeoecology* **172**(1-2), 153–170.
- Drury, A. J., Lee, G. P., Gray, W. R., Lyle, M., Westerhold, T., Shevenell, A. E. and John, C. M. (2018), ‘Deciphering the State of the Late Miocene to Early Pliocene Equatorial Pacific’, *Paleoceanography and Paleoclimatology* **33**(3), 246–263.
- Drury, A. J., Westerhold, T., Frederichs, T., Tian, J., Wilkens, R., Channell, J. E., Evans, H., John, C. M., Lyle, M. and Röhl, U. (2017), ‘Late Miocene climate and time scale reconciliation: Accurate orbital calibration from a deep-sea perspective’, *Earth and Planetary Science Letters* **475**, 254–266.
- Dunkley Jones, T., Bown, P. R. and Pearson, P. N. (2009), ‘Exceptionally well preserved upper Eocene to lower Oligocene calcareous nannofossils (Prymnesiophyceae) from the Pande Formation (Kilwa Group), Tanzania’, *Journal of Systematic Palaeontology* **7**(4), 359–411.

- Dunkley Jones, T., Bown, P. R., Pearson, P. N., Wade, B. S., Coxall, H. K. and Lear, C. H. (2008), ‘Major shifts in calcareous phytoplankton assemblages through the Eocene-Oligocene transition of Tanzania and their implications for low-latitude primary production’, *Paleoceanography* **23**(4), 1–14.
- Egan, K. E., Rickaby, R. E., Hendry, K. R. and Halliday, A. N. (2013), ‘Opening the gateways for diatoms primes Earth for Antarctic glaciation’, *Earth and Planetary Science Letters* **375**, 34–43.
- Elderfield, H., Ferretti, P., Greaves, M., Crowhurst, S., McCave, I. N., Hodell, D. and Piotrowski, A. M. (2012), ‘Evolution of ocean temperature and ice volume through the mid-Pleistocene climate transition’, *Science* **337**(6095), 704–709.
- Elsworth, G., Galbraith, E., Halverson, G. and Yang, S. (2017), ‘Enhanced weathering and CO<sub>2</sub> drawdown caused by latest Eocene strengthening of the Atlantic meridional overturning circulation’, *Nature Geoscience* **10**(3), 213–216.
- Ezard, T. H., Aze, T., Pearson, P. N. and Purvis, A. (2011), ‘Interplay between changing climate and species’ ecology drives macroevolutionary dynamics’, *Science* **332**(6027), 349–351.
- Falkowski, P. G. and Oliver, M. J. (2007), ‘Mix and match: how climate selects phytoplankton. Nature Reviews. Microbiology, 5(10), 813-9’, *Nature Reviews Microbiology* **5**(10), 813–819.
- Fernando, A. G. S., Jones, T. D., Beaufort, L., Kulhanek, D. K., Doyongan, Y. I. L., Binuya, A. M. E., P, J. R. C. and Uy, M. A. C. (2020), ‘Pliocene four-rayed discoasters from IODP Expedition 363 sites in the eastern Indian Ocean and western Pacific Ocean’, *Journal of Nanoplankton Research* **38**(1), 49–55.
- Finkel, Z. V., Sebbo, J., Feist-Burkhardt, S., Irwin, A. J., Katz, M. E., Schofield, O. M., Young, J. R. and Falkowski, P. G. (2007), ‘A universal driver of macroevolutionary change in the size of marine phytoplankton over the Cenozoic’, *Proceedings of the National Academy of Sciences of the United States of America* **104**(51), 20416–20420.
- Fioroni, C., Villa, G., Persico, D. and Jovane, L. (2015), ‘Middle Eocene-Lower Oligocene calcareous nannofossil biostratigraphy and paleoceanographic implications from Site 711 (equatorial Indian Ocean)’, *Marine Micropaleontology* **118**, 50–62.



- Fornaciari, E., Agnini, C., Catanzariti, R., Rio, D., Bolla, E. and Valvasoni, E. (2010), 'Mid-latitude calcareous nannofossil biostratigraphy and biochronology across the middle to late Eocene transition', *Stratigraphy* **7**(4), 229–264.
- Gafar, N. A. and Schulz, K. G. (2018), 'A three-dimensional niche comparison of *Emiliana huxleyi* and *Gephyrocapsa oceanica*: Reconciling observations with projections', *Biogeosciences* **15**(11), 3541–3560.
- Gartner, S. (1992), 'Miocene nannofossil chronology in the North Atlantic, DSDP Site 608', *Marine Micropaleontology* **18**(4).
- Gibbs, S. J., Poulton, A. J., Bown, P. R., Daniels, C. J., Hopkins, J., Young, J. R., Jones, H. L., Thiemann, G. J., O'dea, S. A. and Newsam, C. (2013), 'Species-specific growth response of coccolithophores to Palaeocene-Eocene environmental change', *Nature Geoscience* **6**(3), 218–222.
- Gibbs, S. J., Sheward, R. M., Bown, P. R., Poulton, A. J. and Alvarez, S. A. (2018), 'Warm plankton soup and red herrings: calcareous nanoplankton cellular communities and the Palaeocene–Eocene Thermal Maximum', *Philosophical Transactions of the Royal Society* **376**(20170075), 1–20.
- Gibbs, S. J., Young, J. R., Bralower, T. J. and Shackleton, N. J. (2005), 'Nannofossil evolutionary events in the mid-Pliocene: An assessment of the degree of synchrony in the extinctions of *Reticulofenestra pseudoumbilicus* and *Sphenolithus abies*', *Palaeogeography, Palaeoclimatology, Palaeoecology* **217**(1-2), 155–172.
- Goldner, A., Herold, N. and Huber, M. (2014), 'Antarctic glaciation caused ocean circulation changes at the Eocene-Oligocene transition', *Nature* **511**(7511), 574–577.
- Gradstein, F. M., Ogg, J. G., Schmitz, M. D. and Ogg, G. M. (2012), *The Geologic Time Scale*, Elsevier B.V.
- Hall, R. (2009), 'Southeast Asia's changing palaeogeography', *Blumea - Biodiversity, Evolution and Biogeography of Plants* **54**(1), 148–161.
- Hall, R. (2012), 'Late Jurassic-Cenozoic reconstructions of the Indonesian region and the Indian Ocean', *Tectonophysics* **570-571**, 1–41.

- Hall, R. (2013), 'The palaeogeography of Sundaland and Wallacea since the Late Jurassic', *Journal of Limnology* **72**.
- Hannisdal, B., Henderiks, J. and Liow, L. H. (2012), 'Long-term evolutionary and ecological responses of calcifying phytoplankton to changes in atmospheric CO<sub>2</sub>', *Global Change Biology* **18**(12), 3504–3516.
- Haq, B. U. (1980), 'Biogeographic history of Miocene Calcareous Nannofossils and paleoceanography of the Atlantic Ocean'.
- Henderiks, J., Bartol, M., Pige, N., Karatsolis, B. T. and Lougheed, B. C. (2020), 'Shifts in Phytoplankton Composition and Stepwise Climate Change During the Middle Miocene', *Paleoceanography and Paleoclimatology* **35**(8).
- Henderiks, J. and Pagani, M. (2007), 'Refining ancient carbon dioxide estimates: Significance of coccolithophore cell size for alkenone-based pCO<sub>2</sub> records', *Paleoceanography* **22**(3), 1–12.
- Henderiks, J. and Pagani, M. (2008), 'Coccolithophore cell size and the Paleogene decline in atmospheric CO<sub>2</sub>', *Earth and Planetary Science Letters* **269**(3–4), 576–584.
- Herbert, T. D., Lawrence, K. T., Tzanova, A., Peterson, L. C., Caballero-Gill, R. and Kelly, C. S. (2016), 'Late Miocene global cooling and the rise of modern ecosystems', *Nature Geoscience* **9**(11), 843–847.
- Hernández-Almeida, I., Ausín, B., Saavedra-Pellitero, M., Baumann, K. H. and Stoll, H. M. (2019), 'Quantitative reconstruction of primary productivity in low latitudes during the last glacial maximum and the mid-to-late Holocene from a global *Florisphaera profunda* calibration dataset', *Quaternary Science Reviews* **205**, 166–181.
- Hill, D. J., Haywood, A. M., Hindmarsh, R. C. A. and Valdes, P. J. (2007), 'Characterising ice sheets during the mid Pliocene: evidence from data and models', *Deep time Perspectives on Climate Change Marrying the Signal from Computer Models and Biological Proxies* pp. 517–538.
- Hodell, D. A. and Venz Curtis, K. A. (2006), 'Late neogene history of deepwater ventilation in the Southern Ocean', *Geochemistry, Geophysics, Geosystems* **7**(9), 1–16.

- Holbourn, A. E., Kuhnt, W., Clemens, S. C., Kochhann, K. G., Jöhnck, J., Lübbers, J. and Andersen, N. (2018), ‘Late Miocene climate cooling and intensification of southeast Asian winter monsoon’, *Nature Communications* **9**(1).
- Holbourn, A., Kuhnt, W., Clemens, S., Prell, W. and Andersen, N. (2013), ‘Middle to late Miocene stepwise climate cooling: Evidence from a high-resolution deep water isotope curve spanning 8 million years’, *Paleoceanography* **28**(4), 688–699.
- Holbourn, A., Kuhnt, W., Schulz, M. and Erlenkeuser, H. (2005), ‘Impacts of orbital forcing and atmospheric carbon dioxide on Miocene ice-sheet expansion’, *Nature* **438**(7067), 483–487.
- Holbourn, A., Kuhnt, W., Schulz, M., Flores, J. A. and Andersen, N. (2007), ‘Orbitally-paced climate evolution during the middle Miocene "Monterey" carbon-isotope excursion’, *Earth and Planetary Science Letters* **261**(3-4), 534–550.
- Houben, A. J., Quaijtaal, W., Wade, B. S., Schouten, S. and Brinkhuis, H. (2019), ‘Quantitative organic-walled dinoflagellate cyst stratigraphy across the eocene-oligocene transition in the Gulf of Mexico: A record of climate and sea level change during the onset of antarctic glaciation’, *Newsletters on Stratigraphy* **52**(2), 131–154.
- Huber, M. and Caballero, R. (2011), ‘The early Eocene equable climate problem revisited’, *Climate of the Past* **7**(2), 603–633.
- Huber, M. and Sloan, L. C. (2001), ‘Heat transport , deep waters , and thermal gradients : Coupled simulation of an Eocene Greenhouse Climate’, *Geophysical Research Letters* **28**(18), 3481–3484.
- Huck, C. E., van de Flierdt, T., Bohaty, S. M. and Hammond, S. J. (2017), ‘Antarctic climate, Southern Ocean circulation patterns, and deep water formation during the Eocene’, *Paleoceanography* **32**(7), 674–691.
- Hutchinson, D. K., Coxall, H. K., Lunt, D. J., Steinhorsdottir, M., de Boer, A. M., Baatsen, M., von der Heydt, A., Huber, M., Kennedy-Asser, A. T., Kunzmann, L., Ladant, J.-B., Lear, C. H., Moraweck, K., Pearson, P. N., Piga, E., Pound, M. J., Salzmann, U., Scher, H. D., Sijp, W. P., Śliwińska, K. K., Wilson, P. A. and Zhang, Z. (2021), ‘The

- Eocene–Oligocene transition: a review of marine and terrestrial proxy data, models and model–data comparisons’, *Climate of the Past* **17**(1), 269–315.
- Hutchinson, D. K., Coxall, H. K., O’Regan, M., Nilsson, J., Caballero, R. and de Boer, A. M. (2019), ‘Arctic closure as a trigger for Atlantic overturning at the Eocene-Oligocene Transition’, *Nature Communications* **10**(1), 1–9.
- Hutchinson, D. K., De Boer, A. M., Coxall, H. K., Caballero, R., Nilsson, J. and Baatsen, M. (2018), ‘Climate sensitivity and meridional overturning circulation in the late Eocene using GFDL CM2.1’, *Climate of the Past* **14**(6), 789–810.
- Huybers, P. (2011), ‘Combined obliquity and precession pacing of late Pleistocene deglaciations’, *Nature* **480**(7376), 229–232.
- Imai, R., Farida, M., Sato, T. and Iryu, Y. (2015), ‘Evidence for eutrophication in the north-western Pacific and eastern Indian oceans during the Miocene to Pleistocene based on the nannofossil accumulation rate, Discoaster abundance, and coccolith size distribution of *Reticulofenestra*’, *Marine Micropaleontology* **116**, 15–27.
- Jones, A. P., Dunkley Jones, T., Coxall, H., Pearson, P. N., Nala, D. and Hoggett, M. (2019), ‘Low-Latitude Calcareous Nannofossil Response in the Indo-Pacific Warm Pool Across the Eocene-Oligocene Transition of Java, Indonesia’, *Paleoceanography and Paleoclimatology* **34**(11), 1833–1847.
- Karatsolis, B. T., De Vleeschouwer, D., Groeneveld, J., Christensen, B. and Henderiks, J. (2020), ‘The Late Miocene to Early Pliocene “Humid Interval” on the NW Australian Shelf: Disentangling Climate Forcing From Regional Basin Evolution’, *Paleoceanography and Paleoclimatology* **35**(9).
- Katz, M. E., Miller, K. G., Wright, J. D., Wade, B. S., Browning, J. V., Cramer, B. S. and Rosenthal, Y. (2008), ‘Stepwise transition from the Eocene greenhouse to the Oligocene icehouse’, *Nature Geoscience* **1**(5), 329–334.
- Kennedy-Asser, A. T., Lunt, D. J., Farnsworth, A. and Valdes, P. J. (2019), ‘Assessing Mechanisms and Uncertainty in Modeled Climatic Change at the Eocene-Oligocene Transition’, *Paleoceanography and Paleoclimatology* **34**(1), 16–34.

- Knappertsbusch, M. (2000), ‘Morphologic evolution of the coccolithophorid *Calcidiscus leptoporus* from the early miocene to recent’, *Journal of Paleontology* **74**(4), 712–730.
- Koenig, S. J., Dolan, A. M., De Boer, B., Stone, E. J., Hill, D. J., Deconto, R. M., Abe-Ouchi, A., Lunt, D. J., Pollard, D., Quiquet, A., Saito, F., Savage, J. and Van De Wal, R. (2015), ‘Ice sheet model dependency of the simulated Greenland Ice Sheet in the mid-Pliocene’, *Climate of the Past* **11**(3), 369–381.
- Krumhardt, K. M., Lovenduski, N. S., Iglesias-Rodriguez, M. D. and Kleypas, J. A. (2017), ‘Coccolithophore growth and calcification in a changing ocean’, *Progress in Oceanography* **159**, 276–295.
- Lear, C. H., Bailey, T. R., Pearson, P. N., Coxall, H. K. and Rosenthal, Y. (2008), ‘Cooling and ice growth across the Eocene-Oligocene transition’, *Geology* **36**(3), 251–254.
- Lear, C. H., Rosenthal, Y., Coxall, H. K. and Wilson, P. A. (2004), ‘Late Eocene to early Miocene ice sheet dynamics and the global carbon cycle’, *Paleoceanography* **19**(4), 1–11.
- Liu, H., Sun, J., Wang, D., Zhang, X., Zhang, C., Song, S. and Thangaraj, S. (2018), ‘Distribution of living coccolithophores in eastern Indian Ocean during spring intermonsoon’, *Scientific Reports* **8**(1), 1–12.
- Liu, S., Glass, B., Kyte, F. T. and Bohaty, S. M. (2009), The late Eocene clinopyroxene-bearing spherule layer: New sites, nature of the strewn field, Ir data, and discovery of coesite and shocked quartz, in C. Koeberl and A. Montanari, eds, ‘The Late Eocene Earth—Hothouse, Icehouse, and Impacts’, number Special Paper 452, Geological Society of America, chapter 4, pp. 37–66.
- Lowery, C. M., Bown, P. R., Fraass, A. J. and Hull, P. M. (2020), ‘Ecological Response of Plankton to Environmental Change: Thresholds for Extinction’, *Annual Review of Earth and Planetary Sciences* **48**, 403–429.
- Lunt, D. J., Dunkley Jones, T., Heinemann, M., Huber, M., LeGrande, A., Winguth, A., Loptson, C., Marotzke, J., Roberts, C. D., Tindall, J., Valdes, P. and Winguth, C. (2012), ‘A model–data comparison for a multi-model ensemble of early Eocene atmosphere–ocean simulations: EoMIP’, *Climate of the Past* **8**(5), 1717–1736.

- Lunt, D. J., Farnsworth, A., Loptson, C., L Foster, G., Markwick, P., O'Brien, C. L., Pancost, R. D., Robinson, S. A. and Wrobel, N. (2016), 'Palaeogeographic controls on climate and proxy interpretation', *Climate of the Past* **12**(5), 1181–1198.
- Lyle, A. O. and Lyle, M. W. (2006), 'Missing organic carbon in Eocene marine sediments: Is metabolism the biological feedback that maintains end-member climates?', *Paleoceanography* **21**(2), 1–13.
- Martini, E. (1971), Standard Tertiary and Quaternary calcareous nannoplankton zonation, *in* A. Farinacci, ed., 'Proceedings of the 2nd International Conference Planktonic Microfossils Roma', Edizioni Tecnoscienza, Rome, pp. 739–785.
- McClelland, H. L., Barbarin, N., Beaufort, L., Hermoso, M., Ferretti, P., Greaves, M. and Rickaby, R. E. (2016), 'Calcification response of a key phytoplankton family to millennial-scale environmental change', *Scientific Reports* **6**, 1–11.
- McKinley, C. C., Thomas, D. J., LeVay, L. J. and Rolewicz, Z. (2019), 'Nd isotopic structure of the Pacific Ocean 40–10 Ma, and evidence for the reorganization of deep North Pacific Ocean circulation between 36 and 25 Ma', *Earth and Planetary Science Letters* **521**, 139–149.
- Mejía, L. M., Méndez-Vicente, A., Abrevaya, L., Lawrence, K. T., Ladlow, C., Bolton, C., Cacho, I. and Stoll, H. (2017), 'A diatom record of CO<sub>2</sub> decline since the late Miocene', *Earth and Planetary Science Letters* **479**, 18–33.  
**URL:** <http://dx.doi.org/10.1016/j.epsl.2017.08.034>
- Miller, K. G., Wright, J. D., Katz, M. E., Wade, B. S., Browning, J. V., Cramer, B. S. and Rosenthal, Y. (2009), Climate threshold at the Eocene-Oligocene transition: Antarctic ice sheet influence on ocean circulation, *in* C. Koeberl and A. Montanari, eds, 'The Late Eocene Earth—Hothouse, Icehouse, and Impacts', Geological Society of America.
- Monechi, S. (1986), 'Calcareous nannofossil events around the Eocene-Oligocene boundary in the Umbrian Apennines (Italy).', *Palaeogeography Palaeoclimatology Palaeoecology* **57**, 61–69.
- Naish, T., Powell, R., Levy, R., Wilson, G., Scherer, R., Talarico, F., Krissek, L., Niessen, F., Pompilio, M., Wilson, T., Carter, L., DeConto, R., Huybers, P., McKay, R., Pollard,

- D., Ross, J., Winter, D., Barrett, P., Browne, G., Cody, R., Cowan, E., Crampton, J., Dunbar, G., Dunbar, N., Florindo, F., Gebhardt, C., Graham, I., Hannah, M., Hansaraj, D., Harwood, D., Helling, D., Henrys, S., Hinnov, L., Kuhn, G., Kyle, P., Läufer, A., Maffioli, P., Magens, D., Mandernack, K., McIntosh, W., Millan, C., Morin, R., Ohneiser, C., Paulsen, T., Persico, D., Raine, I., Reed, J., Riesselman, C., Sagnotti, L., Schmitt, D., Sjunneskog, C., Strong, P., Taviani, M., Vogel, S., Wilch, T. and Williams, T. (2009), ‘Obliquity-paced Pliocene West Antarctic ice sheet oscillations’, *Nature* **458**(7236), 322–328.
- Narciso, A., Cachão, M. and De Abreu, L. (2006), ‘Coccolithus pelagicus subsp. pelagicus versus Coccolithus pelagicus subsp. braarudii (Coccolithophore, Haptophyta): A proxy for surface subarctic Atlantic waters off Iberia during the last 200 kyr’, *Marine Micropaleontology* **59**(1), 15–34.
- Newsam, C., Bown, P. R., Wade, B. S. and Jones, H. L. (2017), ‘Muted calcareous nannoplankton response at the Middle/Late Eocene Turnover event in the western North Atlantic Ocean’, *Newsletters on Stratigraphy* **50**(3), 297–309.
- Okada, H. (1983), Modern nannofossil assemblages in sediments of coastal and marginal seas along the Western Pacific Ocean, *in* J. E. Meulenkamp, ed., ‘Utrecht Micropaleontological Bulletins’, Vol. 30, Netherlands, pp. 171–188.
- Pagani, M., Huber, M., Liu, Z., Bohaty, S. M., Henderiks, J., Sijp, W., Krishnan, S. and DeConto, R. M. (2011), ‘The Role of Carbon Dioxide During the Onset of Antarctic Glaciation’, *Science* **334**(6060), 1261–1264.
- Pagani, M., Liu, Z., Larivière, J. and Ravelo, A. C. (2010), ‘High Earth-system climate sensitivity determined from Pliocene carbon dioxide concentrations’, *Nature Geoscience* **3**(1), 27–30.
- Pälike, H., Lyle, M. W., Nishi, H., Raffi, I., Ridgwell, A., Garnage, K., Klaus, A., Acton, G., Anderson, L., Backman, J. and Al., E. (2012), ‘A Cenozoic record of the equatorial Pacific carbonate compensation depth’, *Nature* **488**(7413), 609–614.
- Passchier, S., Ciarletta, D. J., Miriagos, T. E., Bijl, P. K. and Bohaty, S. M. (2017), ‘An

- antarctic stratigraphic record of stepwise ice growth through the eocene-oligocene transition', *Bulletin of the Geological Society of America* **129**(3-4), 318–330.
- Pearson, P. N., Foster, G. L. and Wade, B. S. (2009), 'Atmospheric carbon dioxide through the Eocene-Oligocene climate transition', *Nature* **461**(7267), 1110–1113.
- Pearson, P. N., McMillan, I. K., Wade, B. S., Jones, T. D., Coxall, H. K., Bown, P. R. and Lear, C. H. (2008), 'Extinction and environmental change across the Eocene-Oligocene boundary in Tanzania', *Geology* **36**(2), 179–182.
- Perch-Nielsen, K. (1985), Cenozoic calcareous nannofossils, *in* H. Bolli, J. B. Saunders and K. Perch-Nielsen, eds, 'Plankton Stratigraphy', Cambridge University Press, Cambridge, pp. 427–554.
- Persico, D., Fioroni, C. and Villa, G. (2012), 'A refined calcareous nannofossil biostratigraphy for the middle Eocene-early Oligocene Southern Ocean ODP sites', *Palaeogeography, Palaeoclimatology, Palaeoecology* **335–336**, 12–23.
- Persico, D. and Villa, G. (2004), 'Eocene-Oligocene calcareous nannofossils from Maud Rise and Kerguelen Plateau (Antarctica): Paleoecological and paleoceanographic implications', *Marine Micropaleontology* **52**(1-4), 153–179.
- Pollard, D. and DeConto, R. M. (2009), 'Modelling West Antarctic ice sheet growth and collapse through the past five million years', *Nature* **458**(7236), 329–332.
- Pontes, G. M., Wainer, I., Taschetto, A. S., Sen Gupta, A., Abe-Ouchi, A., Brady, E. C., Chan, W. L., Chandan, D., Contoux, C., Feng, R., Hunter, S. J., Kame, Y., Lohmann, G., Otto-Bliesner, B. L., Peltier, W. R., Stepanek, C., Tindall, J., Tan, N., Zhang, Q. and Zhang, Z. (2020), 'Drier tropical and subtropical Southern Hemisphere in the mid-Pliocene Warm Period', *Scientific Reports* **10**(1), 1–11.
- Poulton, A. J., Adey, T. R., Balch, W. M. and Holligan, P. M. (2007), 'Relating coccolithophore calcification rates to phytoplankton community dynamics: Regional differences and implications for carbon export', *Deep-Sea Research Part II: Topical Studies in Oceanography* **54**(5-7), 538–557.



- Poulton, A. J., Holligan, P. M., Charalampopoulou, A. and Adey, T. R. (2017), ‘Coccolithophore ecology in the tropical and subtropical Atlantic Ocean: New perspectives from the Atlantic meridional transect (AMT) programme’, *Progress in Oceanography* **158**, 150–170.
- Poulton, A. J., Sanders, R., Holligan, P. M., Stinchcombe, M. C., Adey, T. R., Brown, L. and Chamberlain, K. (2006), ‘Phytoplankton mineralization in the tropical and subtropical Atlantic Ocean’, *Global Biogeochemical Cycles* **20**(4), 1–10.
- R Core Team (2020), ‘A Language and Environment for Statistical Computing’.  
**URL:** <http://www.r-project.org>
- Rabosky, D. L. and Sorhannus, U. (2009), ‘Diversity dynamics of marine planktonic diatoms across the Cenozoic’, *Nature* **457**(7226), 183–186.
- Rae, J. W., Zhang, Y. G., Liu, X., Foster, G. L., Stoll, H. M. and Whiteford, R. D. (2021), ‘Atmospheric CO<sub>2</sub> over the Past 66 Million Years from Marine Archives’, *Annual Review of Earth and Planetary Sciences* **49**(609-641).
- Raffi, I., Agnini, C., Backman, J., Catanzariti, R. and Pälike, H. (2016), ‘A Cenozoic calcareous nannofossil biozonation from low and middle latitudes: A synthesis’, *Journal of Nannoplankton Research* **36**(2), 121–132.
- Raffi, I., Backman, J., Fornaciari, E., Pälike, H., Rio, D., Lourens, L. and Hilgen, F. (2006), ‘A review of calcareous nannofossil astrobiochronology encompassing the past 25 million years’, *Quaternary Science Reviews* **25**(23-24), 3113–3137.
- Raffi, I., Mozzato, C., Fornaciari, E., Hilgen, F. J. and Rio, D. (2003), ‘Late Miocene calcareous nannofossil biostratigraphy and astrobiochronology for the Mediterranean region’, *Micropaleontology* **49**(1), 1–26.
- Raffi, I., Rio, D., D’Atri, A., Fornaciari, E. and Rocchetti, S. (1995), ‘Quantitative Distribution Patterns and Biomagnetostratigraphy of Middle and Late Miocene Calcareous Nannofossils from Equatorial Indian and Pacific Oceans (Legs 115, 130, and 138)’, *Proceedings of the Ocean Drilling Program, 138 Scientific Results* **138**.

- Renema, W., Bellwood, D. R., Braga, J. C., Bromfield, K., Hall, R., Johnson, K. G., Lunt, P., Meyer, C. P., McMonagle, L. B., Morley, R. J., O'Dea, A., Todd, J. A., Wesselingh, F. P., Wilson, M. E. J. and Pandolfi, J. M. (2008), 'Hopping Hotspots: Global Shifts in Marine Biodiversity', *Science* **321**(5889), 654–657.
- Rickaby, R. E., Henderiks, J. and Young, J. N. (2010), 'Perturbing phytoplankton: Response and isotopic fractionation with changing carbonate chemistry in two coccolithophore species', *Climate of the Past* **6**(6), 771–785.
- Rio, D., Raffi, I. and Villa, G. (1990), 'Pliocene-Pleistocene Calcareous Nannofossil Distribution Patterns in the Western Mediterranean', *Proceedings of the ODP Scientific Results* **107**, 117–121.
- Rohling, E. J., Foster, G. L., Grant, K. M., Marino, G., Roberts, A. P., Tamisiea, M. E. and Williams, F. (2014), 'Sea-level and deep-sea-temperature variability over the past 5.3 million years', *Nature* **508**(7497), 477–482.
- Rosenthal, Y., Holbourn, A. E., Kulhanek, D. K., Aiello, I. W., Babila, T. W., Bayon, G., Beaufort, L., Bova, S. C., Chun, J. H., Dang, H., Drury, A. J., Dunkley Jones, T., Eichler, P. P. B., Fernando, A. G. S., Gibson, K., Hatfield, R., Johnson, D. L., Kumagai, Y., Li, T., Linsey, B. K., Meinicke, N., Mountain, G. S., Opdyke, B., Pearson, P. N., Poole, C. R., Ravelo, A. C., Sagawa, T., Schmitt, A., Wurtzel, J. B., Xu, J., Yamamoto, M. and Zhang, Y. G. (2018), Site U1482, in Y. Rosenthal, A. Holbourn, D. Kulhanek, Scientists and the Expedition 363, eds, 'Western Pacific Warm Pool', Proceedings of the International Ocean Discovery Program Volume 363, College Station Texas, pp. 1–62.
- Rost, B. and Riebesell, U. (2004), Coccolithophores and the biological pump: responses to environmental changes, in 'Coccolithophores', Springer Berlin Heidelberg, Berlin, Heidelberg, pp. 99–125.
- Roth, P. H. (1994), Distribution of coccoliths in oceanic sediments, in A. Winter and W. Siesser, eds, 'Coccolithophores', Cambridge University Press, Cambridge, pp. 199–218.
- Sahy, D., Condon, D. J., Terry, D. O., Fischer, A. U. and Kuiper, K. F. (2015), 'Synchronizing terrestrial and marine records of environmental change across the Eocene-Oligocene transition', *Earth and Planetary Science Letters* **427**, 171–182.

- Sarmiento, J. L., Gruber, N., Brzezinski, M. A. and Dunne, J. P. (2004), ‘High-latitude controls of thermocline nutrients and low latitude biological productivity’, *Nature* **427**(6969), 56–60.
- Scher, H. D., Bohaty, S. M., Zachos, J. C. and Delaney, M. L. (2011), ‘Two-stepping into the icehouse: East Antarctic weathering during progressive ice-sheet expansion at the Eocene–Oligocene transition’, *Geology* **39**(4), 383–386.
- Schiebel, R. (2002), ‘Planktic foraminiferal sedimentation and the marine calcite budget’, *Global Biogeochemical Cycles* **16**(4), 3–13–21.
- Schueth, J. D. and Bralower, T. J. (2015), ‘The relationship between environmental change and the extinction of the nannoplankton *Discoaster* in the early Pleistocene’, *Paleoceanography* **30**(7), 863–876.
- Seki, O., Foster, G. L., Schmidt, D. N., Mackensen, A., Kawamura, K. and Pancost, R. D. (2010), ‘Alkenone and boron-based Pliocene pCO<sub>2</sub> records’, *Earth and Planetary Science Letters* **292**(1–2), 201–211.
- Self-Trail, J. M., Parker, M., Haynes, J. T., Schultz, A. P. and Huddleston, P. F. (2019), ‘Geology and biostratigraphy of the Upper Floridan aquifer in the greater Savannah region, Georgia and South Carolina’, *Stratigraphy* **16**(1), 41–62.
- Shamrock, J. L. and Watkins, D. K. (2012), ‘Eocene calcareous nannofossil biostratigraphy and community structure from Exmouth Plateau, Eastern Indian Ocean (ODP Site 762)’, *Stratigraphy* **9**(1), 1–54.
- Sibert, E. C., Zill, M. E., Frigyk, E. T. and Norris, R. D. (2020), ‘No state change in pelagic fish production and biodiversity during the Eocene–Oligocene transition’, *Nature Geoscience* **13**(3), 238–242.
- Sijp, W. P., von der Heydt, A. S., Dijkstra, H. A., Flögel, S., Douglas, P. M. and Bijl, P. K. (2014), ‘The role of ocean gateways on cooling climate on long time scales’, *Global and Planetary Change* **119**, 1–22.
- Stoll, H. M., Shimizu, N., Archer, D. and Ziveri, P. (2007), ‘Coccolithophore productiv-

- ity response to greenhouse event of the Paleocene-Eocene Thermal Maximum', *Earth and Planetary Science Letters* **258**(1-2), 192–206.
- Strömberg, C. A. (2011), 'Evolution of grasses and grassland ecosystems', *Annual Review of Earth and Planetary Sciences* **39**, 517–544.
- Styzen, M. J. (1997), 'Cascading counts of nannofossil abundance', *Journal of Nannoplankton Research* **19**(1), 49.
- Suchéras-Marx, B. and Henderiks, J. (2014), 'Downsizing the pelagic carbonate factory: Impacts of calcareous nannoplankton evolution on carbonate burial over the past 17 million years', *Global and Planetary Change* **123**(PA), 97–109.
- Super, J. R., Thomas, E., Pagani, M., Huber, M., O'Brien, C. and Hull, P. M. (2018), 'North Atlantic temperature and pCO<sub>2</sub> coupling in the early-middle Miocene', *Geology* **46**(6), 519–522.
- Šupraha, L. and Henderiks, J. (2020), 'A 15 million-year long record of phenotypic evolution in the heavily calcified coccolithophore *Helicosphaera* and its biogeochemical implications', *Biogeosciences Discussions* pp. 1–26.
- Takahashi, K. and Okada, H. (2000), 'Environmental control on the biogeography of modern coccolithophores in the southeastern Indian Ocean offshore of Western Australia', *Marine Micropaleontology* **39**(1-4), 73–86.
- Takayama, T. (1993), 'Notes on Neogene calcareous nannofossil biostratigraphy of the Ontong Java Plateau and size variations of Reticulofenestra coccoliths', *Proceedings of the Ocean Drilling Program, Scientific Results* **130**, 179–230.
- Tangunan, D. N., Baumann, K. H., Just, J., LeVay, L. J., Barker, S., Brentegani, L., De Vleeschouwer, D., Hall, I. R., Hemming, S. and Norris, R. (2018), 'The last 1 million years of the extinct genus *Discoaster*: Plio–Pleistocene environment and productivity at Site U1476 (Mozambique Channel)', *Palaeogeography, Palaeoclimatology, Palaeoecology* **505**, 187–197.
- Villa, G., Fioroni, C., Pea, L., Bohaty, S. and Persico, D. (2008), 'Middle Eocene-late Oligocene climate variability: Calcareous nannofossil response at Kerguelen Plateau, Site 748', *Marine Micropaleontology* **69**(2), 173–192.

- Villa, G., Fioroni, C., Persico, D., Roberts, A. P. and Florindo, F. (2013), 'Middle Eocene to Late Oligocene Antarctic glaciation / deglaciation and Southern Ocean productivity', *Paleoceanography* **29**, 223–237.
- Wade, B. S. and Bown, P. R. (2006), 'Calcareous nannofossils in extreme environments: The Messinian Salinity Crisis, Polemi Basin, Cyprus', *Palaeogeography, Palaeoclimatology, Palaeoecology* **233**(3-4), 271–286.
- Wade, B. S. and Pearson, P. N. (2008), 'Planktonic foraminiferal turnover, diversity fluctuations and geochemical signals across the Eocene/Oligocene boundary in Tanzania', *Marine Micropaleontology* **68**(3-4), 244–255.
- Wade, B. S., Pearson, P. N., Berggren, W. A. and Pälike, H. (2011), 'Review and revision of Cenozoic tropical planktonic foraminiferal biostratigraphy and calibration to the geomagnetic polarity and astronomical time scale', *Earth-Science Reviews* **104**(1-3), 111–142.
- Wei, W. C. and Wise, S. W. (1990), 'Biogeographic Gradients of Middle Eocene Oligocene Calcareous Nannoplankton in the South-Atlantic Ocean', *Palaeogeography Palaeoclimatology Palaeoecology* **79**(1-2), 29–61.
- Wei, W., Villa, G. and Wise, S. W. (1992), 'Paleoceanographic implications of Eocene-Oligocene calcareous nannofossils from Sites 711 and 748 in the Indian Ocean', *Proceedings of the Ocean Drilling Program, Scientific Results* **120**, 979–999.
- Wei, W. and Wise, S. W. (1992), 'Oligocene-Plesitocene Calcareous Nannofossils from Southern Ocean Sites 747, 748 and 751', *Sites The Journal Of 20Th Century Contemporary French Studies* **120**(1980).
- Westerhold, T., Marwan, N., Drury, A. J., Liebrand, D., Agnini, C., Anagnostou, E., Barnet, J. S., Bohaty, S. M., De Vleeschouwer, D., Florindo, F., Frederichs, T., Hodell, D. A., Holbourn, A. E., Kroon, D., Lauretano, V., Littler, K., Lourens, L. J., Lyle, M., Pälike, H., Röhl, U., Tian, J., Wilkens, R. H., Wilson, P. A. and Zachos, J. C. (2020), 'An astronomically dated record of Earth's climate and its predictability over the last 66 million years', *Science* **369**(6509), 1383–1388.
- Westerhold, T., Röhl, U., Pälike, H., Wilkens, R., Wilson, P. A. and Acton, G. (2014), 'Or-

- bitally tuned timescale and astronomical forcing in the middle Eocene to early Oligocene', *Climate of the Past* **10**, 955–973.
- Winter, A., Jordan, R. W. and Roth, P. H. (1994), Biogeography of living coccolithophores in ocean waters, in A. Winter and W. G. Siesser, eds, 'Coccolithophores', Cambridge University Press, Cambridge, pp. 161–178.
- Young, J. (1990), 'Size variation of Neogene *Reticulofenestra* coccoliths from Indian Ocean DSDP Cores', *Journal of Micropalaeontology* **9**(1), 71–85.
- Young, J. and Bown, P. (1997), 'Higher classification of calcareous nannofossils', *Journal of Nannoplankton Research* **19**(1), 1–56.
- Young, J. R. (2003), 'Biomineralization Within Vesicles: The Calcite of Coccoliths', *Reviews in Mineralogy and Geochemistry* **54**(1), 189–215.
- Young, J. R., Bergen, J. A., Bown, P. R., Burnett, J. A., Fiorentino, A., Jordan, R. W., Kleijne, A., van Niel, B. E., Romein, A. J. T. and von Salis, K. (1997), 'Guidelines for coccolith and calcareous nannofossil terminology', *Palaeontology* **40**, 875–912.
- Young, J. R., Jordan, R. W. and Cros, L. (1998), 'Notes on nannoplankton systematics and life-cycles. *Ceratolithus cristatus*, *Neosphaera coccolithomorpha* and *Umbilicosphaera sibogae*', *Journal of Nannoplankton Research* **20**(2), 89–99.
- Zachos, J. C., Dickens, G. R. and Zeebe, R. E. (2008), 'An early Cenozoic perspective on greenhouse warming and carbon-cycle dynamics', *Nature* **451**(7176), 279–283.
- Zachos, J. C. and Kump, L. R. (2005), 'Carbon cycle feedbacks and the initiation of Antarctic glaciation in the earliest Oligocene', *Global and Planetary Change* **47**(1), 51–66.
- Zachos, J., Pagani, M., Sloan, L., Thomas, E. and Billups, K. (2001), 'Trends, Global Rhythms, Aberrations in Global Climate 65Ma to Present', *Science* **292**(5517), 686–693.
- Zhang, Y. G., Pagani, M., Liu, Z., Bohaty, S. M., Deconto, R. and A, P. T. R. S. (2013), 'A 40-million-year history of atmospheric CO<sub>2</sub>', *Philosophical transactions of the Royal Society of London*. **371**(20130096), 1–20.

- Zhao, Y., Wang, Y. and Quigg, A. (2015), ‘Comparison of population growth and photosynthetic apparatus changes in response to different nutrient status in a diatom and a coccolithophore’, *Journal of Phycology* **51**(5), 872–884.